UNIVERSITY OF KWAZULU-NATAL

Long-term and climatological studies on Sulphur Dioxide (SO_2) using ground-based and space-borne measurements over South Africa

By

Sangeetha Venkataraman
214558728

A thesis submitted in partial fulfilment of the requirements for the degree of

Doctor of Philosophy

College of Agriculture, Engineering and Science
School of Geography and Environmental Sciences,

Supervisor: Dr. Michael Gebreslasie
Co Supervisor: Dr. Caradee Yael Wright

March, 2018

ABSTRACT

Sulphur dioxide (SO_2) is a constant and pervasive element in the atmosphere and is ranked among the key pollutants due to it being produced both by natural and anthropogenic means. SO_2 can cause harm to the environment and cause non-fatal but debilitating human health-effects. Thus, it is necessary to observe its deviations in the atmosphere.

The work performed in this study entailed the exploration of available data from satellite measurements and their applicability to study the variability of SO_2, using both ground-based and space-borne measurements. The aim was to address the use of satellite SO_2 data over South Africa and to complete the gap in ground-based (GB) monitoring. The first two chapters of the thesis are focussed on Introduction and Instruments used. Later, the thesis was focused on the following three major result sections; namely,

- SO_2 seasonal variation and assessment of Ozone Monitoring Instrument (OMI) measurements at Sharpeville (27.86° E; 26.68° S) a South African ground-based station.
- Long-term temporal and spatial analysis of SO_2 over Gauteng and Mpumalanga monitoring sites of South Africa.
- Long-range transport of SO_2 over South Africa: A case study of the Calbuco volcanic eruption in April 2015.

This work has resulted into three journal publications and form part of the thesis in Chapters 3, 4 and 5. The results presented in chapter 3 which is published in *International Journal of Remote Sensing,* is focused on SO_2 seasonal variation and assessment of Ozone Monitoring Instrument (OMI) measurements at Sharpeville (27.86° E; 26.68° S) a South African ground-based station. Chapter 4 (under preparation) is focused on Long-term Temporal and Spatial analysis of SO_2 over Gauteng and Mpumalanga monitoring sites of South Africa, while Chapter 5, which is submitted to *Atmospheric Environment* is focused on Long-range transport of SO_2 over South Africa: A case study of the Calbuco volcanic eruption in April 2015. Finally, chapter 6 provides the overall summary of the thesis.

PREFACE

The work described by this thesis was carried out at the University of KwaZulu-Natal, School of Geography and Environmental sciences, Westville Campus, Durban, from February 2014 to November 2017, under the supervision of Dr. Michael Gebreslasie and Dr. Caradee Yael Wright.

This thesis is entirely, unless specifically contradicted in the text, the work of the author and has not been previously submitted, in whole or in part, to any other tertiary institution. Where use has been made of the work of others, it is duly acknowledged in the text.

Signed: S. K. Sangeetha Mrs. Sangeetha Venkataraman

Date: _____

As the candidate's supervisor I have/~~have not~~ approved this thesis/dissertation for submission.

Signed:_____ Dr. Michael Gebreslasie

Date: _____

As the candidate's co-supervisor I have~~/have not~~ approved this thesis/dissertation for submission.

Signed:_____ Dr. Caradee Yael Wright

Date: _____

DECLARATION 1 - PLAGIARISM

I **SANGEETHA VENKATARAMAN** declare that:

(i) The research reported in this thesis, except where otherwise indicated, is my original research.

(ii) This thesis has not been submitted for any degree or examination at any other university.

(iii) This thesis does not contain other persons' data, pictures, graphs or other information, unless specifically acknowledged as being sourced from other persons.

(iv) This thesis does not contain other persons' writing, unless specifically acknowledged as being sourced from other researchers. Where other written sources have been quoted, then:

a) their words have been re-written but the general information attributed to them has been referenced;

b) where their exact words have been used, their writing has been placed inside quotation marks, and referenced.

(v) Where I have reproduced a publication of which I am author, co-author or editor, I have indicated in detail which part of the publication was actually written by myself alone and have fully referenced such publications.

(vi) This thesis does not contain text, graphics or tables copied and pasted from the Internet, unless specifically acknowledged, and the source being detailed in the thesis and in the references sections.

Signed:

S. K. Sangeetha

DECLARATION 2 – PUBLICATIONS

DETAILS OF CONTRIBUTION TO PUBLICATIONS that form part and/or include research presented in this thesis (include publications in preparation, submitted, in press and published and give details of the contributions of each author to the experimental work and writing of each publication)

Publication 1

S.K. Sangeetha, V. Sivakumar, M. Josipovic, M. Gebreslasie and C.Y.Wright, SO_2 seasonal variation and assessment of Ozone Monitoring Instrument (OMI) measurements at Sharpeville (27.86° E; 26.68° S) a South African ground-based station

International Journal of Remote Sensing, 38:23, 6680-6696, 2017.

Publication 2

S. K. Sangeetha, M. Gebreslasie ….."Long-term Temporal and Spatial analysis of SO_2 over Gauteng and Mpumalanga monitoring sites of South Africa", to be submitted to International Journal of environment and pollution, 2018 (to be submitted).

Publication 3

S.K. Sangeetha, V. Sivakumar and M. Gebreslasie, Long-range transport of SO_2 over South Africa: A case study of the Calbuco volcanic eruption in April 2015, Revised and Submitted to Atmos. Environment (2018)

Other Publication (not included in this thesis)

A.M.Toihir, V.Sivakumar, N.Mbatha, **S.K. Sangeetha**, H.Bencherif, E.G.Brunke, and C.Labuschagne. "Studies on CO variation and trends over South Africa and the Indian Ocean using TES satellite data", South African Journal of Science 111, no. 9-10, 01-09, 2015.

Signed:

S. K. Sangeetha

ARTICLES IN PEER-REVIEWED NATIONAL/INTERNATIONAL CONFERENCE PROCEEDINGS

S.K. Sangeetha, V. Sivakumar M. Gebraslasie and C.Y.Wright , Seasonal vertical variation in SO_2 over South Africa as observed by the Ozone Monitoring Instrument (OMI), *Proc. of 33nd Annual conference of South African society for atmosphere science, Protea Hotel Ranch Resort, Polokwane, (South Africa), ISBN* 978-0-620-77401-7, *Pg 82-85, 21-22 September 2017.*

S. K. Sangeetha, V. Sivakumar, M. Josipovic, M. Gebreslasie and C. Wright, Comparative study of OMI BRD and PCA algorithm retrievals in relation to ground based measurements over a South African Site. *Proc. of 32nd Annual conference of South African society for atmosphere science, Lagoon Beach Hotel, Minerton, CapeTown (South Africa), ISBN 978-0-620-72974-1, Pg 119-122, 31 October-01 November 2016.*

Signed:

S. K. Sangeetha

ACKNOWLEDGEMENTS

Before, I begin the acknowledgement, my first and foremost salutations to **THE GOD**, who is the truthful driving force of all things, happened in a right way.

Even though, I was the main contributor of this work, there were many people behind me, whose manifold efforts made this journey to be a fruitful one. This project would have been impossible without the involvement of some people and organisations who provided indispensable guidance necessary for conducting this research. These people were directly or indirectly involved who offered me a continued support, knowledge and encouragement.

First, I would like to sincerely thank my supervisor Dr. Michael Gebreslasie for his guidance and valuable suggestions during the entire course of the work. His kindness and easygoing nature has assisted me in various aspects. In addition, he gave me a thorough appraisal on manipulating an article framework at every decisive moment of the study.

Secondly, Dr. Caradee Wright who gave me support and encouragement which were instrumental in pursuing a specific aim and overwhelming some of the difficult tasks. She always replied immediately and promptly even when she was away during a foreign visit.

Thirdly, my husband Prof. Siva for his vast knowledge, profound thoughts and fast response persuaded me to do the right assignments. He was more or less a third supervisor as he provided me an all-time support. He motivated me to acquire MATLAB skills and other programs that allowed for investigating the research work.

My genuine gratitude to Dr. Micky Jospivoic for accepting the co-authorship, which led to a successive paper.

Technical support by Dr. Raghu who guided me in developing the HYSPLIT analysis. His kind and generous nature made me to clarify the doubts through email.

My heartfelt gratefulness to Miss. Priyanka Singh for her assistance in applying me the ARGIS tool in this study.

Miss. Barbara accepted to proof read and improve the grammatical use of language, which has led to finish this documentation in time.

I would like to acknowledge South African National Space Agency (SANSA) for their financial support, for which I am greatly appreciative.

I extend my appreciation to all the participating members who could operate, maintain and data access for both ground and space-borne measurements employed here.

Finally, my whole hearted thanks to my beloved parents, sister and other immediate family members, who although were not officially involved, but donated me full positive support and motivation for the fulfillment of this work.

DEDICATIONS

First, I would like to dedicate this work to the ALMIGHTY GOD for fulfilling my wishes.

I would also dedicate this work to my husband, kids, parents, relatives and other true well-wishers who really encouraged me to complete this journey.

TABLE OF CONTENTS

List of Acronyms and Abbreviations

ADAS	Atmospheric data assimilation system
AERONET	Aerosol Robotic Network
AERMOD	American Meteorological Society/ Environmental Protection Agency Regulatory Model
AIRS	Atmospheric Infrared Sounder
AM	ante meridiem
AMF	Air mass factor
ARL	Air Resources Laboratory
BRD	Band Residual Difference
BRO	Bromine monoxide
cm	Centimeter
CO_2	carbon dioxide
CO	carbon monoxide
CALIPSO	Cloud-Aerosol Lidar and Infrared Pathfinder Satellite Observations
CCD	charge-coupled device
CH_4	Methane
CTM	chemical transport model
°	degree
°C	degree Celsius
DEA	Department of Environmental Affairs
DLR	Deutsches Zentrum für Luft- und Raumfahrt
DIAL	Differential Absorption Lidar technique
DU	dobson units
E	East

EOS	Earth observing system
Envisat	Environmental satellite
ERS	European remote-sensing satellite
ESKOM	Electricity Supply Commission
FGD	flue-gas desulfurization
GB	ground-based
GEOS	Goddard Earth Observing System
Gg	gigagrams
GMT	Greenwich Mean Time
GOME	Global Ozone Monitoring Experiment
GVP	Global volcanism program
H_2SO_4	sulphuric acid
H_2SO_3	sulphurous acid
HCHO	Formaldehyde
HNO_3	nitric oxide
hpa	hectopascal
HYSPLIT	Hybrid Single-Particle Lagrangian Integrated Trajectory
IASI	Infrared atmospheric sounding interferometer
IR	Infrared
kg	kilograms
km	kilometers
kt	kilotonnes
LASER	Light amplification by stimulated emission of radiation
LDL	Lower detectable limit
LED	light-emitting diode

LER	Lambertian effective surface reflectivity
LF	Linear fit
LIDAR	light detection and ranging
MATCH	multi-scale atmospheric transport and chemistry
MERRA	Modern-Era Retrospective analysis for Research and Applications
MetOP	Meteorological operational satellite
μm	Micrometer
μt	Microtons
Min	Minute
MIPAS	Michelson Interferometer for Passive Atmospheric Sounding
MISR	Multi-angle Imaging Spectro-Radiometer
MLS	Microwave limb sounder
Mt	Megatonnes
MTG	Meteosat third generation
MODIS	Moderate Resolution Imaging Spectroradiometer
N	North
NASA	National aeronautics and space administration
NATREF	National Petroleum Refiners of South Africa
NCAR	National Center for Atmospheric Research
NCEP	National Centers for Environmental Prediction
Nd:YAG	Neodymium-doped Yttrium Aluminum Garnet
NH_3	ammonia
NIR	Near infrared
nm	Nanometer
NO	nitric oxide

NO_2	nitrogen dioxide
NOAA	National Oceanic and Atmospheric Administration
O_3	Ozone
OH	Hydroxide
OK	Ordinary Kriging
OMI	Ozone Monitoring Instrument
OMPS	Ozone mapping and profiler suite
/	per
%	percentage
PBL	Planetary Boundary Layer
PCA	principal component analysis
pg	Page Number
p.	Paper/Article number
pm	Post meridiem
PMT	photomultiplier tube
ppb	parts per billion
ppbv	parts per billion volume
ppm	parts per million
pt	picotonne
RMS	Root mean square
sec	Second
S	South
SAA	South Atlantic radiation Anomaly
SCIAMACHY	Scanning Imaging Absorption Spectrometer for Atmospheric Cartography
SNPP	Suomi national polar-orbiting partnership

SO_2	Sulphur dioxide
SO_3	Sulphur trioxide
SO_x	sulphur oxides
STL	Upper tropospheric and Stratospheric Layer
SWIR	shortwave infrared
SZA	solar zenith angle
TEMPO	Tropospheric emissions: monitoring of pollution
TES	Tropospheric emission spectrometer
Tg	Teragram
TROPOMI	Tropospheric monitoring instrument
TOMS	Total Ozone Mapping Spectrometer
TRL	Lower Tropospheric Layer
TRM	Middle Tropospheric Layer
TSV	Total Spatial Variance
UK	United Kingdom
USA	United States of America
UTS	Universal Time Coordinated
UV	ultraviolet
VIS	visible
WHO	world health organization

List of figures

List of tables

Chapter 1

1. Introduction

Clean air is a basic requirement for living beings and the surroundings. On the other hand, air-pollution warns a significant threat to human health worldwide (Monks et al., 2009). Air pollution may be defined as the emission of gas or aerosol particles from anthropogenic activities at significant concentrations such that they result in direct or indirect damage to biotic organisms, ecosystems or structures (Monks et al., 2009). A number of natural physical processes such as volcanic eruptions, fires and weathering release various chemicals into the environment. However, anthropogenic activities may supersede these natural, background levels and result in environmental pollution (Kampa and Castanas, 2008). Air pollution is regarded as a border line-marker of sustainable development. This is because sources of air pollution produce climate-modifying compounds. As a direct result, air pollution concerns are reflected in the sustainable development goals. Exposure to air pollutants is largely beyond the control of individuals or general citizens and requires action from national, regional and international authorities. Many large cities worldwide suffer from serious air-quality problems and these have received increasing attention in the past decade. The world health organization (WHO) approximates that 2.4 million people die each year from air pollution related diseases (Monks et al., 2009).

The main source of atmospheric contamination is through the combustion of fossil fuels used for transportation and in the generation of energy. As a result, air pollutants enter the atmosphere mostly in the form of droplets or particles. Air pollutants differ according to their chemical composition, reactivity, emission levels, capacity to persist in the environment, ability to be transported long or short distances and their eventual impacts on human and/or animal health (World Health Organization, 2016). Sulphur dioxide (SO_2) is one of a group of highly reactive primary air pollutants. It is a noxious gas that can induce global climate forcing

depending on altitude. Furthermore, anthropogenic activities are primary emission sources in or above the boundary layer region (Krotkov et al., 2016).

1.1 Characteristics of SO_2

On the global scale, SO_2 is of major concern due to its harmful effects on the environment and human health and it is therefore considered one of the criteria pollutants. It is a colourless, invisible gas with a characteristic irritating smell and acidic taste. It is non-flammable, nonexplosive, readily soluble in water and about 2.5 times heavier than air. It dissolves in water vapour in clouds to form sulphurous acid (as indicated in equation (1.1)) and with hydrogen peroxide to form sulphuric acid (as indicated in equation (1.2)).

$$SO_2 + H_2O \rightarrow H_2SO_3 \qquad (1.1)$$

$$SO_2 + H_2O_2 \rightarrow H_2SO_4 \qquad (1.2)$$

1.2 Sources of SO_2

Sources of atmospheric SO_2 include both natural phenomena and anthropogenic activities. Volcanic eruptions, sulphate aerosols from sea spray, hot springs and the reaction of hydrogen sulphide (released from marshes) with oxygen in the air, all constitute natural emission sources of SO_2 (Robinson and Robbins, 1970). Primary anthropogenic emission sources of SO_2 include combustion of fossil fuels (such as coal and natural gas) by power plants and other industrial facilities for electricity generation, extraction of metal by smelting facilities, biomass burning and vehicular emissions from diesel engines in ships, cars and other forms of transport.

1.2.1 Natural sources of SO_2

The natural emission sources of SO_2 are unpredictable and unpreventable and often occur in uninhabited places. Of those listed, volcanic eruptions play a major part in releasing large quantities of SO_2 deep into the atmosphere. These plumes sometimes reach the stratosphere in the case of a major explosive eruption. Based on eruption data collected by Global Volcanism Program (GVP) 2005 - 2012, it was found that ~ 49% of volcanic plumes were injected above 4 km and ~ 4% above 10 km (Ge et al., 2016). Volcanic activity ranges from active unrest episodes including explosive eruptions to prolonged periods of passive emissions, which may

last a few months or years (Girona et al., 2014). Figure 1.1 illustrates major, global volcanic sources, most of which are located in the pacific region. Papua New Guinea is found in the southwest Pacific Ocean and has seventeen active volcanoes. It is considered as one of the world's top sources of volcanic SO_2. Primary volcanoes in this region are Bagana, Manam, Rabaul, Ulawun and Langila. During 2005 – 2008, these volcanoes contributed a total SO_2 burden over Papua New Guinea corresponding to ~ 1838×10^6 kg, as measured by Ozone Monitoring Instrument (OMI) (McCormick et al., 2012). A further significant volcanic source is the Anatahan volcano located in the Mariana Islands (northwest Pacific Ocean) which underwent a major eruption from January to September 2005. It was found that a total of 4110 - 4600 kt of SO_2 was released in this region during the decadal study period 2004-2014 (McCormick et al., 2015). Tungurahua, a stratovolcano, is one of the most active volcanoes in Eucador. According to OMI based measurements during October – November 2007, a mean daily SO_2 mass loading of ~ 450 tonnes was recorded (McCormick et al., 2014). Based on OMI measurements of SO_2 emissions, over 91 volcanoes contributed an average of 23 Mt/year during passive degassing between 2005 and 2015. Of these sources, some were newly identified such as Dukono and Ebulobo in Indonesia, Tofua and Tinakula in the Southwest Pacific and Erebus in Antarctica (Carn et al., 2017). Table 1.1 shows the top 20 global volcanic SO_2 sources according to the mean SO_2 flux/day estimated by OMI during 2005 – 2015.

Table 1.1: Ranking of global passive degassing volcanic sources for the period 2005 to 2015 as based on OMI estimated mean SO_2 flux/day (obtained from Carn et al., 2017)

Rank	**Volcano**	**Country**	**Mean SO_2 flux (tons/day)**
1	Ambrym	Vanuatu	7356
2	Kilauea	USA	5019
3	Bagana	Papua New Guinea	3779
4	Nyiragongo and Nyamuragira	Democratic Republic of Congo	3533
5	Aoba	Vanuatu	2870
6	Mount. Etna	Italy	2039
7	Tavurvur	Papua New Guinea	1729
8	Dukono	Indonesia	1726
9	Popocatepetl	Mexico	1658

10	Manam	Papua New Guinea	1484
11	Yasur	Vanuatu	1408
12	Anatahan	Northern Mariana Islands	1335
13	Soufriere Hills	Montserrat (UK)	1296
14	Nevado del Ruiz	Colombia	1074
15	Sakura-jima	Japan	1056
16	Miyake-jima	Japan	1018
17	Karymsky	Russia	911
18	Masaya	Nicaragua	867
19	Suwanose-jima	Japan	863
20	Bromo and Semeru	Indonesia	775

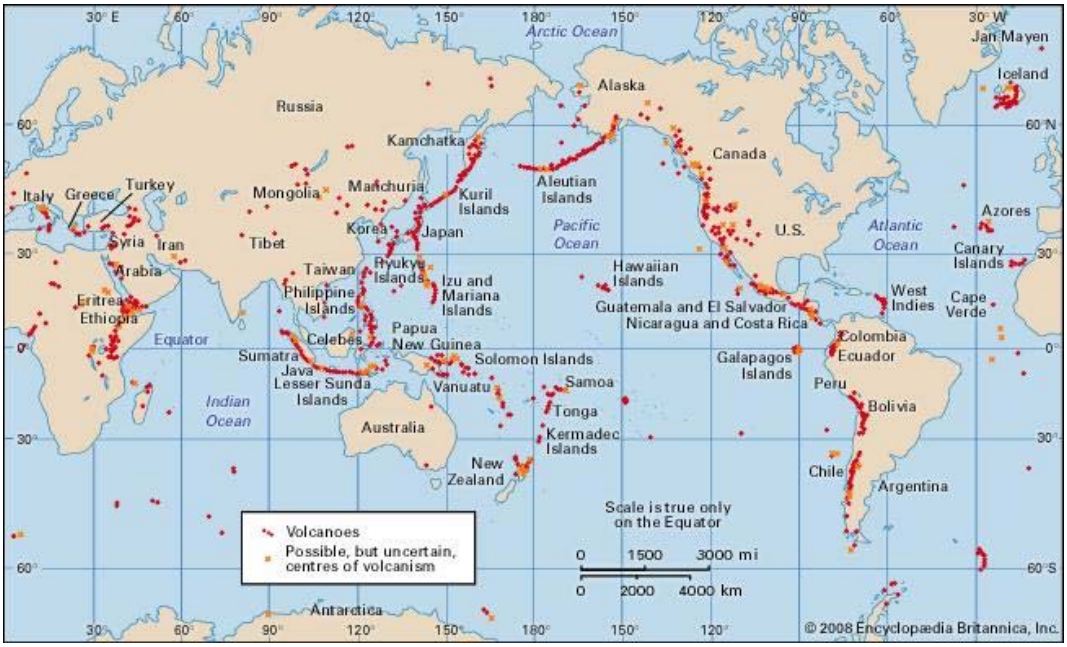

Figure 1.1: World map showing the location of major volcanic regions. (Source: https://www.britannica.com/science/volcano, Accessed on 20 October 2017)

Volcanic eruptions are more frequent in the northern hemisphere than in the southern hemisphere (Carn et al., 2016). Nyiragongo, Ambrym, Kilauea and Bagana are some of the persistently degassing volcanoes found in the northern and southern tropics (Ge et al., 2016). Global locations of primary active volcanoes are presented in Table 1. 2.

Table 1.2: Geolocations of global volcanic regions (Carn et al., 2016).

Latitude band	Locations
10˚ N - 20˚ N	Mexico, West Indies, Central America, Philippines, Marianas and Hawaii
50˚N - 60˚ N	Northern Kuriles, Kamchatka and Aleutian Islands
30˚ N - 40˚ N #	Sicily, Italy and Japan
0˚ S - 10˚ S	Ecuador, Galapagos islands, DR Congo, Indonesia and Papua New Guinea

minor volcanic activity

1.2.2 Anthropogenic sources of SO_2

Most anthropogenic sources of SO_2 are located in Asian countries such as China, India and the eastern USA and thus these sources contribute more than 60% of total SO_2 columns over all continental regions (Lee et al., 2011). Figure 1.2 shows the global anthropogenic fraction of SO_2 columns estimated from GEOS-Chem (global 3D chemical transport model [CTM] model from the Goddard Earth Observing System [GEOS]) in 2006 (Lee et al., 2011). According to OMI observations (2004 - 2015), a total of 415 anthropogenic sources were identified globally. The largest fraction was attributed to power plants (297 sources), oil and gas facilities (65 sources) and smelters (53 sources) (Fioletov et al., 2016). Ilo (Peru), Norilsk (Russia), Chuquicamata and Caletones (Chile) contain the most prominent smelters in the world. The annual mean emission of SO_2 from the Norilsk smelter was found to be 1.68 ± 0.3 Mt/year (Khokhar et al., 2008), while the annual SO_2 load measured by OMI (2004 - 2005) for the Peruvian copper smelters Ilo and La Oroya was 0.07 ± 0.03 and 1.2 ± 0.5 Mt respectively (Carn et al., 2007). Valero refinery, Aruba (Carribean Sea), Paraguana (Venezuela), Isla (Curacao) and refineries in the Middle East are some of the noteworthy oil refineries in the world (Fioletov et al., 2016). Countries including China, USA, Europe and India contribute the largest emissions due to power plants. The majority of the top power plants in USA were originally deployed with coal for power generation (Fioletov et al., 2011). However, since the beginning of this millennium, there was a switch from coal to natural gas in the USA and this resulted in a significant decrease in SO_2 emissions. It was calculated that the net decrease in SO_2 emission in the USA i.e., the emission in SO_2 per unit of electricity produced was ~ 56%

from 1995-2010 (Lu et al., 2012) and a reduction of 44% in 2012 (De Gouw et al., 2014). China, which is a developing nation, is more dependent on coal-based power plants and these contribute 50% of the total national SO_2 emissions. These power plants are primarily located in the Northern provinces Shandong, Henan and Hebei. Between 2000 and 2006, it was estimated that annual SO_2 emissions increased from 21.7 Mt to 33.2 Mt, this corresponded to an increase of 53%. However, from 2006, SO_2 emissions began to decrease due to the implementation of flue-gas desulfurization technology in power plant units, in addition to other control measures taken to reduce anthropogenic emissions in and around Beijing during the 2008 Olympic Games (Lu et al. 2010). This trend was further confirmed by OMI observations in that large reductions in SO_2 columns were observed between 2007 and 2008 in Inner Mongolia and northern China (Li et al., 2010). However, a decreasing trend over a large number of provinces in China was only detected after 2011. In a study employing OMI SO_2 data (2005-2015), SO_2 columns remained constant over the period 2010-2013. However, a steady decrease in levels was observed over the following years, in particular 2015 (Van der et al., 2017). Further evidence for this negative trend seen in Chinese megacities and power plant emissions was also provided by GOME-2 measurements (Koukouli et al., 2016). In the USA and China, strict regulatory measures are in place to reduce SO_2 emissions and these include the substitution of natural gas with coal and desulfurization procedures. However, in India (2005 - 2012), an approximately 60% increase in SO_2 concentrations in close proximity to coal fired power plants was observed. This is a direct result of lack of emission control regulations. Provinces including Uttar Pradesh, Gujarat, Orissa, Chhattisgarh, Maharashtra and Tamil Nadu recorded power plants emissions in excess of 500 Gg in 2012 and this accounted for ~ 60% of total SO_2 emissions in the same year (Lu et al., 2013).

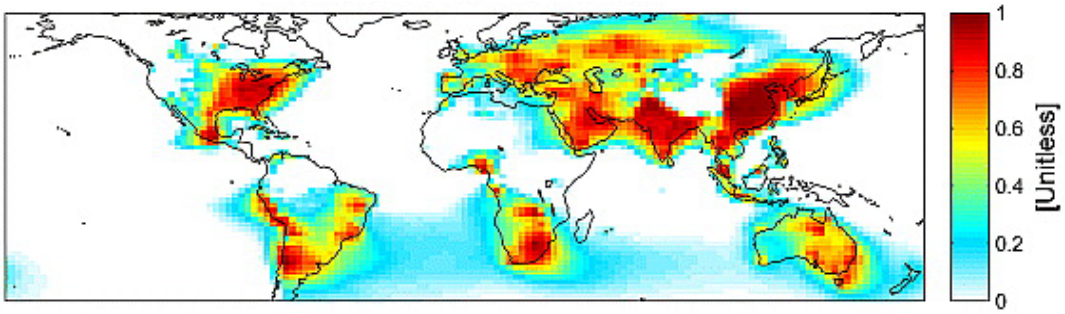

Figure 1.2: Global anthropogenic fraction of SO_2 columns in 2006 according to GEOS-Chem model simulations. (Obtained from Lee et al., 2011)

1.3 Sinks of SO_2

Oxidation by OH and deposition onto wet surfaces are the major sinks of SO_2. These reactions can occur in the gas or liquid phase or on a solid surface. The conversion rate of SO_2 depends upon many parameters including insolation of sunlight, humidity and the presence of oxidants. Reaction rates are faster during the day than at night and in summer compared to winter (Erisman and Baldocchi, 1994). Due to moisture in the atmosphere, SO_2 readily dissolves to form sulphuric acid. Equations (1.3) and (1.4) illustrate important gas phase reactions of SO_2. Equation (1.3) shows the reaction of SO_2 with diatomic oxygen to form Sulphur trioxide (SO_3) while equation (1.4) describes the reaction of SO_2 with the hydroxyl radical (OH) in the presence of sunlight to form sulphuric acid (Ramadan, 2004).

$$2SO_{2\,(g)} + O_{2\,(g)} \rightarrow SO_{3\,(g)} \qquad (1.3)$$

$$SO_{2\,(g)} + 2(OH)_{(g)} \rightarrow H_2SO_{4\,(g)} \qquad (1.4)$$

SO_3 may then react with moisture in the atmosphere to form sulphuric acid (Ramadan, 2004) as follows:

$$SO_{3\,(g)} + H_2O_{(L)} \rightarrow H_2SO_{4\,(L)} \qquad (1.5)$$

The above equations illustrate that sulphuric acid may be formed in both the liquid or gas phase. Acidic deposition may therefore occur through either dry or wet deposition processes.

1.3.1 Wet deposition

Wet deposition occurs when sulphuric acid mixes with precipitates such as rain, snow, fog and hail, which then fall to the surface. These precipitates are acidic and harmful to plants, animals, structures and the wider environment. This phenomenon is known as rainout or washout.

1.3.2 Dry deposition

Dry deposition occurs when SO_2 settles out of the atmosphere in the absence of moisture and is absorbed by plants, soil and water or deposited onto surfaces including buildings, trees and homes. Once dry deposition occurs, it may be further transported by wind. In deserts, dry deposition dominates over wet deposition (USEPA, Acid Rain). Figure 1.3 shows the sources and sinks of atmospheric SO_2.

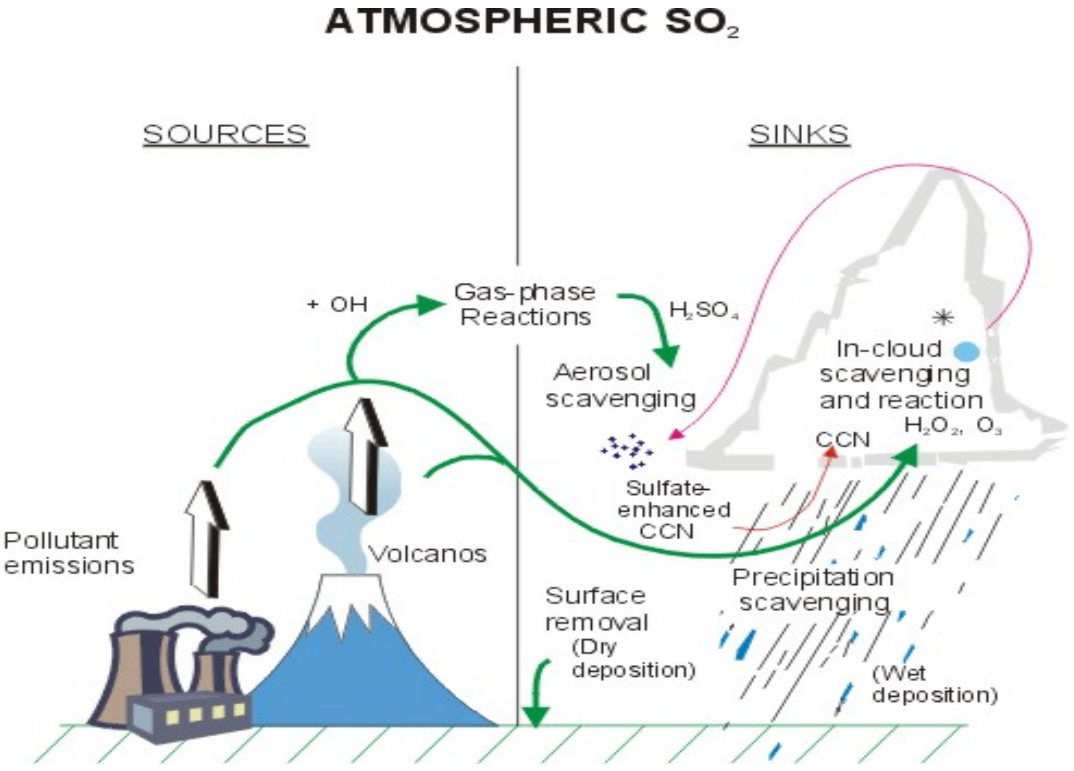

Figure 1.3: Sources and sinks of SO_2 illustrating the processes of dry and wet deposition. (Source: https://www.ems.psu.edu/~lno/Meteo437/AtmSO2.jpg. Accessed on 26 October 2017)

1.4 Effects of SO_2

The impact of SO_2 on the environment and human health is significant because of its reactive nature. These impacts may be direct or indirect, long or short term and range from reduction in visibility, climate change (on a global or regional scale) to problems involving the human upper and lower respiratory tract. The negative effects of SO_2 exposure can be broadly categorized into health impacts and environmental impacts.

1.4.1 Health impacts

The negative health impact of SO_x can be attributed to exposure to SO_2, sulphate aerosols and SO_2 adsorbed onto particulate matter which can be inhaled (Smith at al., 2011). The increase in SO_2 concentrations in ambient air has been associated with reduced lung function, increased incidence of respiratory diseases and premature mortality in cases of chronic exposure (Smith at al., 2011). The principle exposure route of SO_2 is through inhalation but may also occur though contact with the skin. The response of the human body to exposure is rapid and occurs within a few minutes. This is because SO_2 dissolves rapidly through the mucous lining of the lungs and nose. The response is short-lived and lung function returns to normal after some minutes to hours. However, this may vary from person to person (Air Quality Guidelines, Global Update 2005). Inhalation causes bronchiolar constriction, dyspnoea (Bernstein et al., 2004; Kampa et al., 2008), coughing, shortness of breath and pulmonary edema (CCOHS). Penetration into the air passages depends on the breathing volume. If nasal breathing is low to moderate, SO_2 reaches the upper respiratory tract and causes minor damage. However, if heavy breathing or oral inhalation occurs, SO_2 may reach deep into the bronchiolar portion of the lungs (Rall, 1974) resulting in airway resistance and wheezing. Chronic exposure leads to nose bleeds and tightness of the chest and may sometimes result in hospitalization for individuals suffering from asthma or respiratory diseases (Walters et al., 1994). Children, adults, athletes and asthmatic individuals are more susceptible to these adverse health effects (Air Quality Guidelines, Global Update 2005). Furthermore, SO_2 is also a strong irritant and causes nasal,

throat and eye irritation. Figure 1.4 illustrates the inflammatory response of the airways as a result of SO_2 exposure.

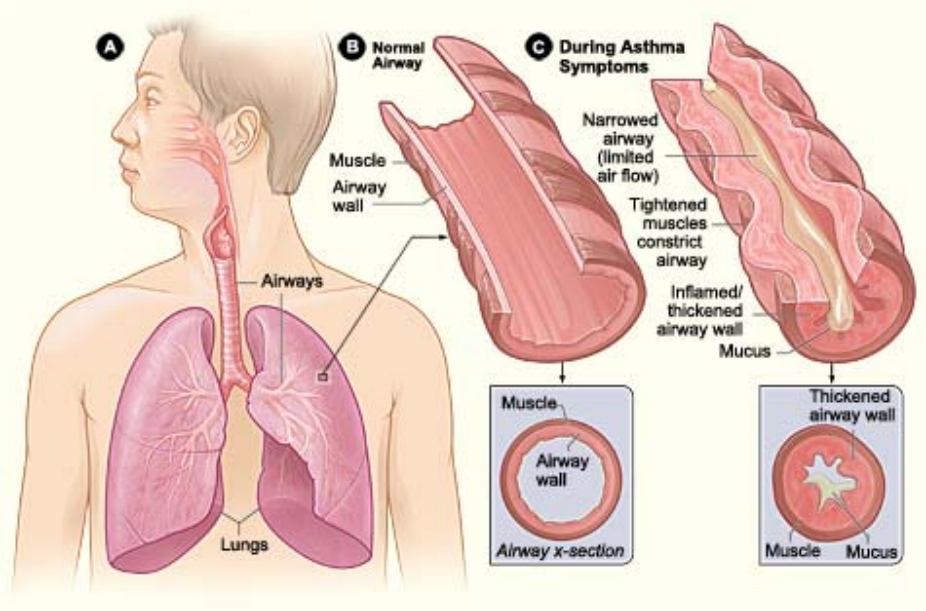

Figure 1.4: Inflammation of airways on exposure to ambient SO_2 (Source: https://www.nhlbi.nih.gov/health/health-topics/topics/asthma. Accessed on 25 October 2017)

1.4.2 Environmental impacts

SO_2 is a precursor of sulphur oxides (SO_X) and sulphate aerosols that have multiple negative impacts on the environment. Gaseous SO_X can reduce crop yields by damaging trees and plant foliage (see figure 1.5) as well as promoting deforestation. As previously mentioned, SO_2 reacts with water and the moisture in air to form sulphuric acid, a corrosive agent. This sulphuric acid can affect the environment directly or do so indirectly by dissolving in water droplets in clouds before falling to the surface in the form of acid rain. Acid rain has a number of significant harmful effects including the acidification of fresh water systems (such as lakes and rivers) and accompanying destruction of aquatic plants and animal life. It can also corrode buildings, paintwork monuments and damage crops.

Figure 1.5: SO_2 damage on blackberry leaf. (Source: http://www.missouribotanicalgarden.org/gardens-gardening/your-garden/help-for-the-home-gardener/advice-tips-resources/pests-and-problems/environmental/sulfur-dioxide.aspx, Accessed on 25 October 2017)

Sulphur dioxide emissions may also affect stone, ferrous and nonferrous metals while sulphuric acid is a well-known accelerant in the corrosion of iron, steel and zinc. Sulphur dioxide reacts with copper to produce the green patina of copper sulphate on the surface of the metal. Acids in the form of gases, aerosols or precipitation may chemically erode building materials such as marble, limestone and dolomite (Pollution prevention handbook, 1998). Chen et al. (2014) noted that SO_2 is one of the major constituents influencing the corrosion rates of steels. With China and other developing countries experiencing greater SO_2 levels due to the increase in industry, studies have shown that SO_2 has deleterious effects in terms of the corrosion of steels near coastal and industrial areas.

Another major adverse effect of SO_2 is the formation of sulphate aerosols. These aerosols may cool the climate directly by reflecting solar radiation back into space under clear sky conditions or indirectly by increasing the reflectivity (albedo) of clouds (Kiehl and Briegleb 1993). This cooling effect may offset global warming due to greenhouse gases and increases the complexity of climate forcing. Volcanic sulphate aerosols have a persistent effect as they are injected deep into the atmosphere, particularly in the tropics. As these aerosols are capable of migrating into the stratosphere in both hemispheres, they are capable of climate change on a global scale (Solomon et al., 2011). Sulphate aerosols also reduce visibility by means of haze formation during warm, humid and sunny days with corresponding negative consequences for

cars, trucks and aircrafts. In the case of aircraft this is particularly important during the loading of volcanic sulphate aerosols in the upper troposphere.

1.5 Emissions of SO_2

1.5.1 Global SO_2 emissions

Global emissions of SO_2 were almost equally shared between open sources such as domestic fuel burning, forest fires and industrial sources until the beginning of rapid industrialization. However, since this time, industrial SO_2 emissions have increased more than twice due to the use of coal as an energy source. The last few decades of the 20th century showed a mixed trend as the actual peak started in 1970s because of fast industrial growth in North America and Europe. However, these countries followed strict mitigation measures and as a result global SO_2 emissions started to decline until 2000. Since 2000, there has been a shift in peak SO_2 emissions towards developing nations in Asia, in particular China. In 2005, 40% of global emission was contributed by Asia and of this 23% was contributed by China (Smith et al., 2011). During 2000-2011, Asian countries increased their contribution to the global SO_2 load from 41% to 52%. China continues to be the single largest contributor to global SO_2 emissions, however, since 2011 a decline in SO_2 emissions has been noted due to flue-gas desulfurization installations. By comparison, contributions from India were comparatively smaller than that of China, however, it seems that India will become a leading contributor if no strict control measures are instituted (Klimont et al., 2013). Li et al. (2017) in their study on global anthropogenic emitters, it was calculated that emissions in India have been increased by 50% during 2005-2016 period and henceforth outstrips the Chinese SO_2 emissions. It has been proposed in a study by Van Vuuren et al. (2011) that there will be a declining trend in SO_2 emissions from 2020 and low SO_2 levels will be seen in 2100 and the emissions will be more centered in currently low-income regions.

1.5.2 SO_2 emissions in South Africa: Motivation for the current study

South Africa, similar to any other countries in the globe, SO_2 is categorized as a common air pollutant. The natural and anthropogenic release of this compound into the atmosphere has

been identified at the cause of severe health and environmental impacts ranging from crop reduction to various respiratory diseases.

South Africa is a developing country with many rural communities. These communities burn domestic fuel on a daily basis for cooking and heating purposes (Norman et al., 2007). Domestic fuel burning forms a minor role in the emission of SO_2 in the country as the release of SO_X is dependent on combustion and fuel characteristics (Norman et al., 2007). South Africa has a number of growing industries and has been identified as a major source of industrial air pollution. There has been a decline in SO_2 emissions in Europe and North America in response to stringent government regulations while emissions are rising in developing nations across the world (Josipovic, 2010).

South Africa has a number of large coalmines and power generation facilities. These are primarily located in Mpumalanga and Gauteng provinces and high ambient levels may be seen in satellite images of these areas. In a study conducted by Josipovic et al. (2010) the concentration of SO_2 was measured at 37 sites across northern and eastern areas of South Africa and low concentrations recorded upwind and in areas remote from the Mpumalanga industrial Highveld. Increased concentrations were recorded in the centre and immediately downwind from the Highveld source region. It was calculated that for 2000 – 2005, SO_2 emissions in South Africa increased by ~ 3.5%. This corresponded to 2.39 kt in 2000 and 2.47 kt in 2005 (Smith et al., 2011). From 2005 to 2010 levels increased a further ~ 9% from 2.522 kt to 2.750 kt (Klimont, et al., 2013). Industrial activity also results in SO_2 emissions in South-central Durban (Nriagu et al., 1999). This area is heavily industrialized and is one of the most polluted areas in southern Africa. Major industries include two refineries, petrochemical plants, pulp and paper mills, wastewater treatment works, lead, chromium and various other processing industries (Nriagu et al., 1999). Between 1989 and 1991, the average SO_2 concentration in this location was 57 $\mu t/m^3$ compared to 12 $\mu t/m^3$ at the municipal center. In terms of countrywide levels, Fioletov et al. (2016) found that the rate of SO_2 emissions over South Africa were moderately constant. In this study, it was estimated that the relative change in emission levels between 2005-2007 and 2012-2014 was only 0-25%. These results illustrate that little increase in SO_2 emissions occurred over the past decade when compared to countries such as China and India. However, it is a better policy to implement strict emission control

measures at this initial stage, before SO_2 concentrations rise to a level where the human and environmental impacts are significant.

1.6 References

Air Quality Guidelines, Global Update 2005, World Health Organization, Europe. Available online at : http://www.euro.who.int/data/assets/pdf_file/0005/ 78638/E90038.pdf (accessed on 25 October 2017).

Bernstein, J. A., Alexis, N., Barnes, C., Bernstein, I. L., Nel, A., Peden, D., Sanchez, D.D., Tarlo, S.M. and Williams, P.B., 2004. Health effects of air pollution. *Journal of Allergy and Clinical Immunology, 114*(5), pg. 1116-1123.

Carn, S.A., Krueger, A.J., Krotkov, N.A., Yang, K. and Levelt, P.F., 2007. Sulfur dioxide emissions from Peruvian copper smelters detected by the Ozone Monitoring Instrument. *Geophysical Research Letters*, *34*(9).

Carn, S.A., Clarisse, L. and Prata, A.J., 2016. Multi-decadal satellite measurements of global volcanic degassing. *Journal of Volcanology and Geothermal Research*, *311*, pg.99-134.

Carn, S.A., Fioletov, V.E., McLinden, C.A., Li, C. and Krotkov, N.A., 2017. A decade of global volcanic SO_2 emissions measured from space. *Scientific Reports,* doi: 10.1038/ srep44095.

De Gouw, J.A., Parrish, D.D., Frost, G.J. and Trainer, M., 2014. Reduced emissions of CO2, NOx, and SO2 from US power plants owing to switch from coal to natural gas with combined cycle technology. *Earth's Future*, *2*(2), pg.75-82.

Erisman, J.W. and Baldocchi, D., 1994. Modelling dry deposition of SO_2. *Tellus B*, *46*(3), pg.159-171.

Fioletov, V.E., McLinden, C.A., Krotkov, N., Li, C., Joiner, J., Theys, N., Carn, S. and Moran, M.D., 2016. A global catalogue of large SO 2 sources and emissions derived from the Ozone Monitoring Instrument. *Atmospheric Chemistry and Physics*, *16*(18), pg.11497.

Fioletov, V.E., McLinden, C.A., Krotkov, N., Moran, M.D. and Yang, K., 2011. Estimation of SO2 emissions using OMI retrievals. *Geophysical Research Letters*, *38*(21).

Fioletov, V.E., McLinden, C.A., Krotkov, N., Li, C., Joiner, J., Theys, N., Carn, S. and Moran, M.D., 2016. A global catalogue of large SO 2 sources and emissions derived from the Ozone Monitoring Instrument. *Atmospheric Chemistry and Physics*, *16*(18), pg.11497.

Ge, C., Wang, J., Carn, S., Yang, K., Ginoux, P. and Krotkov, N., 2016. Satellite-based global volcanic SO_2 emissions and sulfate direct radiative forcing during 2005–2012. *Journal of Geophysical Research: Atmospheres*, *121*(7), pg.3446-3464.

Girona, T., Costa, F., Newhall, C. and Taisne, B., 2014. On depressurization of volcanic magma reservoirs by passive degassing. *Journal of Geophysical Research: Solid Earth*, *119*(12), pg.8667-8687.

Josipovic, M., Annegarn, H. J., Kneen, M. A., Pienaar, J. J. and Piketh, S. J., 2010. Concentrations, distributions and critical level exceedance assessment of SO2, NO2 and O 3 in South Africa. *Environmental monitoring and assessment*, 171(1), pg.181-196.

Kampa, M. and Castanas, E., 2008. Human health effects of air pollution. *Environmental pollution*, *151*(2), pg.362-367.

Khokhar, M.F., Platt, U. and Wagner, T., 2008. Temporal trends of anthropogenic SO2 emitted by non-ferrous metal smelters in Peru and Russia estimated from satellite observations. *Atmospheric Chemistry and Physics Discussions*, *8*(5), pg.17393-17422.

Kiehl, J.T. and Briegleb, B.P., 1993. The relative roles of sulfate aerosols and greenhouse gases in climate forcing. *Science*, *260*(5106), pg.311-314.

Klimont, Z., Smith, S.J. and Cofala, J., 2013. The last decade of global anthropogenic sulfur dioxide: 2000–2011 emissions. *Environmental Research Letters*, *8*(1), pg.014003.

Koukouli, M.E., Balis, D.S., Van der A, R.J., Theys, N., Hedelt, P., Richter, A., Krotkov, N., Li, C. and Taylor, M., 2016. Anthropogenic sulphur dioxide load over China as observed from different satellite sensors. *Atmospheric Environment*, *145*, pg.45-59.

Krotkov, N. A., McLinden, C. A., Li, C., Lamsal, L. N., Celarier, E. A., Marchenko, S. V. and Boersma, K. F., 2016. Aura OMI observations of regional SO_2 and NO_2 pollution changes from 2005 to 2015. *Atmospheric Chemistry and Physics*, *16*(7), pg.4605-4629.

Lee, C., Martin, R.V., van Donkelaar, A., Lee, H., Dickerson, R.R., Hains, J.C., Krotkov, N., Richter, A., Vinnikov, K. and Schwab, J.J., 2011. SO_2 emissions and lifetimes: Estimates from inverse modeling using in situ and global, space-based (SCIAMACHY and OMI) observations. *Journal of Geophysical Research: Atmospheres*, *116*(D6).

Li, C., McLinden, C., Fioletov, V., Krotkov, N., Carn, S., Joiner, J., Streets, D., He, H., Ren, X., Li, Z. and Dickerson, R.R. 2017. India is overtaking China as the world's largest emitter of anthropogenic sulfur dioxide. *Scientific Reports*, doi: 10.1038/s41598-017-14639-8.

Lu, Xi., McElroy, M. B., Wu, G. and Nielsen, C.P., 2012. Accelerated reduction in SO2 emissions from the U.S. power sector triggered by changing prices of natural gas. *Environmental Science and Technology*, *46*(14), pg. 7882-7889.

Lu, Z., Streets, D.G., Zhang, Q., Wang, S., Carmichael, G.R., Cheng, Y.F., Wei, C., Chin, M., Diehl, T. and Tan, Q., 2010. Sulfur dioxide emissions in China and sulfur trends in East Asia since 2000. *Atmospheric chemistry and physics*, *10*(13), pg.6311-6331.

Lu, Z., Streets, D.G., de Foy, B. and Krotkov, N.A., 2013. Ozone Monitoring Instrument observations of interannual increases in SO2 emissions from Indian coal-fired power plants during 2005–2012. *Environmental science and technology*, *47*(24), pg.13993-14000.

McCormick, B.T., Edmonds, M., Mather, T.A. and Carn, S.A., 2012. First synoptic analysis of volcanic degassing in Papua New Guinea. *Geochemistry, Geophysics, Geosystems*, *13*(3).

McCormick, B.T., Herzog, M., Yang, J., Edmonds, M., Mather, T.A., Carn, S.A., Hidalgo, S. and Langmann, B., 2014. A comparison of satellite-and ground-based measurements of SO2 emissions from Tungurahua volcano, Ecuador. *Journal of Geophysical Research: Atmospheres*, *119*(7), pg.4264-4285.

McCormick, B., Popp, C., Andrews, B. and Cottrell, E., 2015. Ten years of satellite observations reveal highly variable sulphur dioxide emissions at Anatahan Volcano, Mariana Islands. *Journal of Geophysical Research: Atmospheres*, *120*(14), pg.7258-7282.

Monks, P. S., Granier, C., Fuzzi, S., Stohl, A., Williams, M. L., Akimoto, H., and Blake, N. 2009. Atmospheric composition change–global and regional air quality. *Atmospheric environment*, *43*(33), pg.5268-5350.

Nriagu, J., Robins, T., Gary, L., Liggans, G., Davila, R., Supuwood, K. and Naidoo, R. 1999. Prevalence of asthma and respiratory symptoms in south-central Durban, South Africa. *European journal of epidemiology*, *15*(8), pg.747-755.

Pollution prevention and Abatement handbook: Toward cleaner production 1998. World Bank group. Washington, DC. http://documents.worldbank.org/curated/en/259451468335037000/Pollution-prevention-and-abatement-handbook-1998-toward-cleaner-production (accessed on 07 November 2017).

Rall, D.P., 1974. Review of the health effects of sulfur oxides. *Environmental health perspectives*, *8*, pg.97.

Ramadan, A.E.K., 2004. Acid deposition phenomena. https://inis.iaea.org/search/search.aspx?orig_q=RN:40079323 (accessed on 07 November 2017).

Richter, A.,Wittrock,F., Ladstätter-Weißenmayer, A., Burrows, J.P. and Arlander, D.W., 2007. Institute of Environmental Physics/Remote Sensing, University of Bremen, http://www.iup.uni-bremen.de/doas/posters/dpg_2002_ richter.pdf (accessed on22 May 2017).

Robinson, E. and Robbins, R.C., 1970. Gaseous sulfur pollutants from urban and natural sources. *Journal of the Air Pollution Control Association*, *20*(4), pg.233-235.

Smith, S.J., Aardenne, J.V., Klimont, Z., Andres, R.J., Volke, A. and Delgado Arias, S., 2011. Anthropogenic sulfur dioxide emissions: 1850–2005. *Atmospheric Chemistry and Physics*, *11*(3), pg.1101-1116.

Solomon, S., Daniel, J.S., Neely, R.R., Vernier, J.P., Dutton, E.G. and Thomason, L.W., 2011. The persistently variable "background" stratospheric aerosol layer and global climate change. *Science*, *333*(6044), pg.866-870.

United States Environmental Protection Agency (USEPA), Acid Rain. Available online at: https://www.epa.gov/acidrain/what-acid-rain (accessed on 29 October 2017).

Van der A, Ronald J., Mijling, B., Ding, J., Koukouli, M.E., Liu, F., Li, Q., Mao, H. and Theys, N., 2017. Cleaning up the air: effectiveness of air quality policy for SO2 and NOx emissions in China. *Atmospheric Chemistry and Physics*, *17*(3), pg.1775-1789.

Van Vuuren, D.P., Edmonds, J., Kainuma, M., Riahi, K., Thomson, A., Hibbard, K., Hurtt, G.C., Kram, T., Krey, V., Lamarque, J.F. and Masui, T., 2011. The representative concentration pathways: an overview. *Climatic change*, *109*(1-2), pg.5.

Walters, S., Griffiths, R.K. and Ayres, J.G., 1994. Temporal association between hospital admissions for asthma in Birmingham and ambient levels of sulphur dioxide and smoke. *Thorax* 49(2), pg.133-140.

World Health Organization 2016. Ambient air pollution: a global assessment of exposure and burden of disease. In Ambient air pollution: a global assessment of exposure and burden of disease. http://www.who.int/iris/handle/10665/250141 (accessed on 07 November 2017).

Chapter 2

Instrumentation

Atmospheric monitoring of SO_2

Air pollution monitoring plays a vital role in disseminating information to policy makers, health officers and researchers as well as playing an important role in environmental management. Sulphur dioxide (SO_2) is an important gaseous pollutant that can have an extreme impact on the environment. It is also a precursor of sulphate aerosols, which can significantly affect air quality and climate (Li et al. 2013). The atmospheric lifetime of SO_2 is short and it exhibits considerable temporal variability. These factors, combined with the fact that it is easily transported from it point of origin, mean that there is a need for precise and accurate SO_2 measurements over multiple spatial and temporal scales (Li et al. 2013). In response to increasing anthropogenic SO_2 emissions, a global SO_2 sampling network has been developed. This consists of reliable measurements in order to investigate spatial and temporal variations in air quality on a local and global scale. Methods to monitor SO_2 in the atmosphere are broadly classified as remote sensing or *in-situ* measurements. Measurements using remote sensing technologies are not in direct contact with the target of interest and are hence located far from the subject of measurement. In this case, the instrument indirectly measures changes in radiation due to the presence of SO_2 molecules. Satellite-based instruments and light detection and ranging (LIDAR) systems are typical examples of remote sensing techniques. By comparison, *in situ* measurements take place in the same location as the subject of measurement. In the case of air quality monitoring, this may involve the direct sampling of air by ground-based (GB) instruments or aircraft. The aim of this chapter is to discuss various types of instrumentation used to monitor atmospheric SO_2, in particular those employed in the South African context. The application of a trajectory and reanalysis model used in this thesis will also be presented.

2.1 Remote sensing techniques

Remote sensing techniques may be classified as passive or active depending on the energy source. Passive techniques rely on natural or existing resources (such as radiation) in the atmosphere to measure SO_2 levels, as is the case in most satellite-based instrumentation. Active sensors such as LIDAR systems use a laser as an external energy source to study atmospheric structure.

2.1.1 Satellite-based instruments

Satellites have become a dominant feature in air pollutant studies. They have aided in discriminating surface emissions of atmospheric pollutants due to anthropogenic or natural sources as well as calculating annual global emission rates for target species. Furthermore, they have been used to retrieve data from unsafe locations where the installation of GB instruments would have created a security risk. They have also helped in the development of environmental mitigation measures by mapping the transmission of pollutants from source to target region. In some cases, this tracking can take several days to weeks if it involves the transport of pollutants on an interstate or intercontinental scale. Satellite observations may also be used to correlate plume chemistry and dispersion rate with climatological factors including wind speed, wind direction, turbulence and weather parameters as a result of localized monsoon activity. A general feature of these top-down measurements is that they have good spatial coverage and have the advantage that they can study the atmosphere at various altitude levels such as the boundary layer, lower and upper troposphere, stratosphere, mesosphere and ionosphere. Through the study of horizontal and vertical transport of target species, satellites act as an exceptional tool for the study of the atmosphere and its associated climatology. The orbit of spaceships can be a polar or nearly polar if they fly over or in close proximity to both poles. Satellites are geostationary if they orbit at a fixed altitude of 35,800 km above the equator. This allows them to assess temporal variation in pollutant concentrations at a specific location. Satellite sensors may be classified as nadir or limb viewing depending if they point directly downwards at the location of study or at a sideways angle. There are currently a number of instruments on board various satellites that are utilised for monitoring SO_2 sources. Monitoring of SO_2 levels via satellite was initiated with the launch of Total Ozone Mapping

Spectrometer (TOMS). This is therefore an important starting point when reviewing SO_2 satellite observations however, it should be noted that TOMS was initially designed to detect ozone (McLinden, 2014). In order to quantify SO_2, satellite-based instruments employ different spectral ranges including the ultraviolet (UV), infrared (IR) and visible (VIS) regions. One of the main advantages of IR sounders over backscattered UV sensors is their ability to operate at night (Clarisse et al., 2012) however, they can experience interference due to aerosols and water vapour in the atmosphere (Realmuto and Worden, 2000). UV based sensors have good SO_2 sensitivity due to strong SO_2 absorption features in the UV band which allows the detection of SO_2 even at low concentrations (Fioletov et al., 2016). Examples of instrumentation employing IR sensors for SO_2 detection are the Infrared atmospheric sounding interferometer (IASI), Atmospheric Infrared Sounder (AIRS) and Moderate Resolution Imaging Spectroradiometer (MODIS) which is an IR and VIS based instrument. The Global Ozone Monitoring Experiment-2 (GOME-2), Total Ozone Mapping Spectrometer (TOMS) and Ozone Monitoring Instrument (OMI) are both UV/VIS based instruments while the SCanning Imaging Absorption SpectroMeter for Atmospheric CHartographY (SCIAMACHY) operates in the UV to Shortwave Infrared (SWIR) spectral range.

2.1.1.1 OMI

Since 2004, the Ozone Monitoring Instrument (OMI) on board the NASA EOS Aura satellite platform has been used to observe aerosols and trace gases, including SO_2 (Zhang et al., 2017)]. OMI monitors four wavelength bands centered on the SO_2 absorption bands: 310.8 nm, 311.9 nm, 313.2 nm and 314.4 nm (Zhang et al., 2017). The commonly used OMI SO_2 PBL (planetary boundary layer) focuses on anthropogenic SO_2 that is mainly distributed within the PBL near the source regions. The advantage of OMI over other instruments includes daily global coverage, large dataset (data availability since 2004) and fine ground pixel resolution that is comparable to GB instruments. As OMI is used extensively in the work presented here, its design, principle of operation and data products are discussed in more detail in the following sections. Table 2.1 outlines details and specifications of various satellite-based instruments.

Table 2.1: Different types of satellite-based instruments that measures SO_2 and their specifications

Instrument	Onboard space craft	Operational time period	Measurement technique	Global coverage	Spatial resolution	Spectral resolution
TOMS *	Nimbus-7	1978-1993	UV/VIS	Daily	50 x 50 km^2	1 nm
GOME-2	MetOP-A & MetOP-B	2007-present	UV/VIS	Once in 3 days	40 × 40 km^2	0.25-0.5 nm
GOME *	ERS-2	1995-2011	UV/NIR	Daily	40 × 40 km^2	0.2-0.4 nm
IASI	MetOP-A & MetOP-B	2007-present	IR	Twice a day	4 × 12 km IFOV close to 48 × 48 km^2 cell	0.5 cm^{-1}
MODIS	NASA-Aqua & Terra	2000-present	VIS/IR	One or 2 days	250 m, 500 m & 1,000 m	0.405-14.385 μm
SCIAMACHY (nadir & limb) *	Envisat	2002-2012	UV/VIS/NIR /SWIR	Once in 3 days	Nadir horizontal 32 × 215 km; Limb vertical 3 × 132 km	0.2-1.5 nm

AIRS	EOS-Aqua	2002-present	IR	Twice a day	13.5 × 13.5 km	3.7-15.4 μm
TES (nadir & limb)	EOS-AURA	2004-present	IR	Once in every 3 days (limb)	0.5 × 5 km (nadir), 2.3 × 23 km (limb)	0.1 cm^{-1} (nadir); 0.025 cm^{-1} (limb)
OMI	EOS-AURA	2004-present	UV/VIS	Daily	13 × 24 km	0.5 nm
TROPOMI *	Sentinel-5 Precursor	Planned to launch on 21 September 2017	UV/VIS/NIR /SWIR	Daily	7 × 7 km	0.25-0.55 nm
OMPS (nadir & limb)	SNPP	2012-present	UV/VIS/NIR	Once in 4 days (limb)	Nadir profiler 250 km (nadir), 2.2 km vertical (limb)	1 nm (nadir), 0.75-25 nm (limb)
MLS	EOS-AURA	2004-present	Limb sounding	Daily	30 × 150 km	0.12-2.5 mm
TEMPO *	TEMPO	Planned to be launched in 2018	UV/VIS	3 times a day (North America)	8 × 4.5 km	0.6 nm
Senitel-4 *	MTG	Planned to be launched in 2019	UV/VIS/NIR	Continuous over Europe (hourly)	10 × 10 km	0.12 nm

* Indicates the instruments is no longer in use * Indicates future instruments

2.1.1.1a OMI: Principle of operation

NASA's Earth Observing System's (EOS) AURA satellite was launched on 15 July 2004 with OMI onboard. Data collection began in August 2004. OMI is an UV/VIS based spectrometer, which measures the amount of reflected solar radiation between 270 nm and 500 nm with a resolution between 0.42 nm and 0.63 nm. The incoming light is focused into a telescope and split into UV (270 nm - 365 nm) and VIS (365 nm - 500 nm) channels by a dichroic element. The UV channel is further divided into UV-1 (270 nm - 310 nm) and UV-2 (310 nm -365 nm) sub channels. The spatial sampling is therefore reduced by a factor of two in comparison to UV-2, this is done in order to increase the signal to noise ratio in the UV-1 region. Figure 2.1 is a schematic diagram illustrating the optical assembly of OMI.

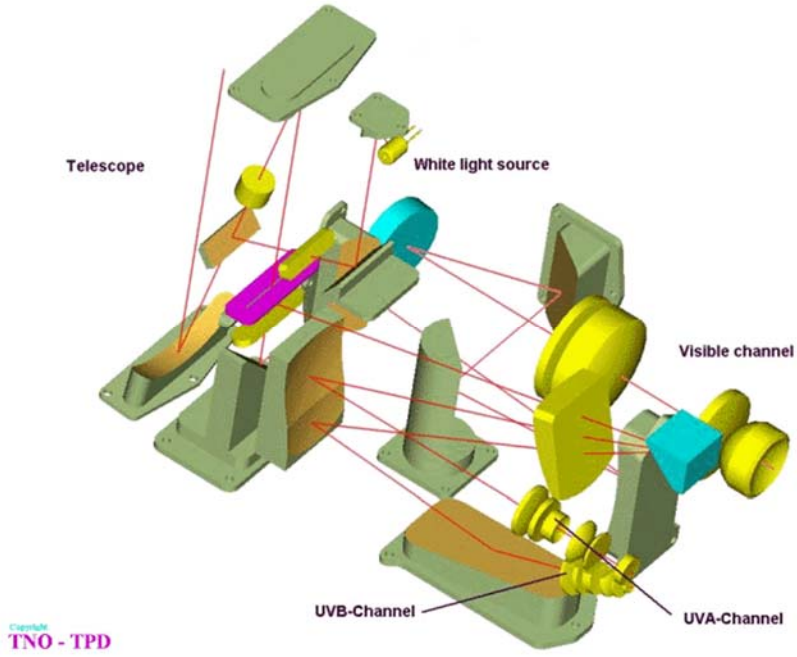

Figure 2.1: Optical asembly of OMI (obtained from https://aura.gsfc.nasa.gov/omi_gallery.html. Accessed on 31 August 2007*).*

The AURA spacecraft occupies a polar sun-synchronous orbit at an altitude of 705 km and inclination of 98.2º. It is therefore able to provide wide coverage from 82° N to 82° S with a local equator crossing time of 13:45 in an ascending node. OMI has two advantages over other satellite-based instruments. Firstly, the spatial sampling of OMI does not depend on the primitive scanning mirror technique, instead a 2-dimensional charge-coupled device (CCD) is

utilised to measure the spatial and spectral information concurrently. This gives OMI a very fine ground resolution of 13 km × 24 km with a daily global coverage. Secondly, the incoming light is depolarized with the help of polarization scramblers fitted in front of the instrument. This minimizes errors caused due to polarization of the instrument's other components (Caron et al., 2012). There are three types of operation modes in OMI namely global mode, spectral and spatial zoom-in modes. By default, OMI runs in the global mode (as this covers the entire spectral range) and a complete swath width on a daily basis. OMI has a ground pixel size of 13 km × 48 km for the UV-1 region and a 13 km × 24 km pixel size for the UV-2 and VIS channels at nadir position. Figure 2.2 illustrates the working principle of OMI together with its viewing angle and wide swath width of 2600 km.

The primary objectives of OMI are to provide daily measurements of trace gases including Ozone (O_3), Nitrogen dioxide (NO_2), Sulphur dioxide (SO_2), Bromine monoxide (BRO) and Formaldehyde (HCHO). Furthermore, data are also collected on some important aerosol characteristics such as aerosol optical depth, aerosol column burden, mass mixing ratio and aerosol composition (Levelt et al., 2006).

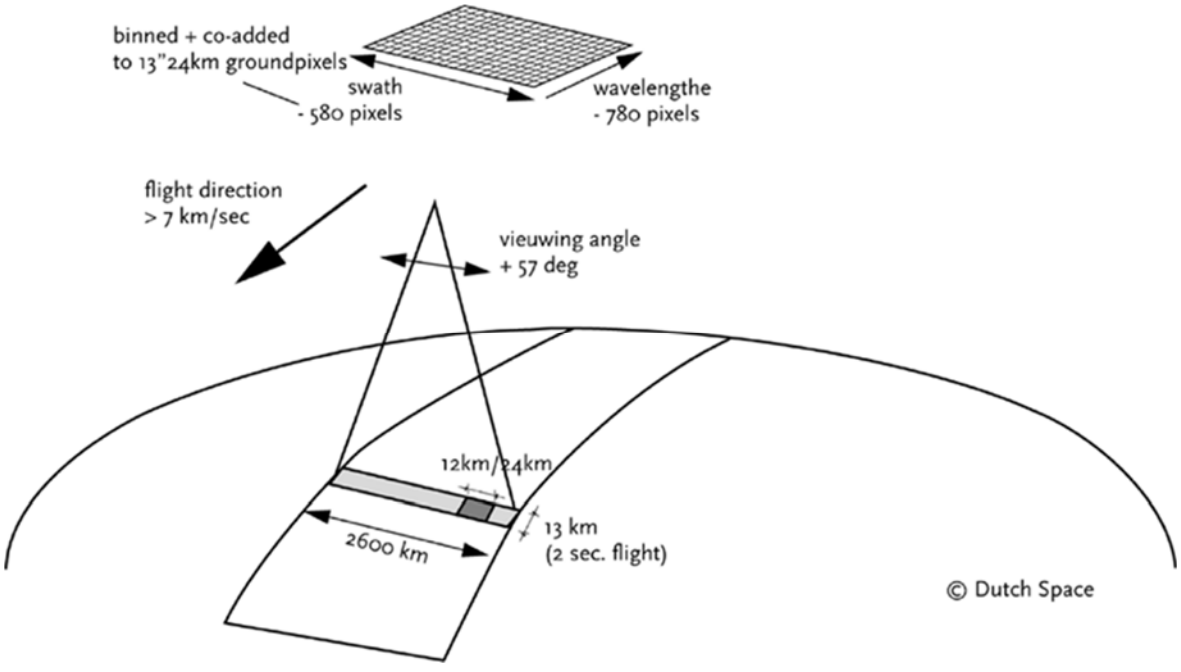

Figure 2.2: Schematic diagram illustrating OMI measurement technique (obtained from OMI data user's guide, 2012)

2.1.1.1b Levels of OMI data products

There are four levels of OMI data products namely, Level 0, Level 1B, Level 2 and Level 3. Level 0 are raw sensor counts. The executable data products start from Level 1B through Level 2, Level 2G and finally at Level 3. Level 1B are calibrated, geo-located, orbital products carrying earth view radiance and solar irradiance data. The Level 2 data contains atmospheric products relating to aerosols, trace gases and ozone along with additional information on terrain height, cloud fraction, ground pixel corner and data quality information. The Level 2 data are available in both default global mode and zoom-in mode. Level 2G data combines global information for the whole day via selection of appropriate Level 2 data fields. The Level 3 dataset contains globally gridded data products selected by choosing the best pixel data of each Level 2 product (OMI data user's guide, 2012).

There are two main OMI SO_2 data products: OMSO2e and OMSO2G. They have a spectral range between 310.8 nm - 314.4 nm and 345 nm - 370 nm. The OMSO2e is a daily globally gridded Level 3 data product chosen from the best pixel data of each Level 2 product. It has a latitude and longitude resolution of 0.25° x 0.25° for each grid (Krotkov et al., 2015a). The OMSO2G is a unique Level-2 product which is also globally gridded, but with a very fine resolution of 0.125°x 0.125° (Krotkov et al., 2012).

2.1.1.1c OMI SO_2 columnar products

The $OMSO_2$ product is available for four vertical distributions namely: Planetary Boundary Layer (PBL centred at 0.9 km), Lower Tropospheric Layer (TRL centred at 2.5 km), Middle Tropospheric Layer (TRM centred at 7.5 km) and Upper tropospheric and Stratospheric Layer (STL centred at 17 km) (OMSO2 README File, 2008). The first data product is specific to anthropogenic pollution including fossil fuel combustion and smelting. This is because SO_2 from these sources is mostly confined in the PBL. The remaining three products are recommended for studies of volcanic degassing. The TRM dataset is used for effusive eruptions and vents at altitudes in excess of 5 km height while the STL dataset is applicable to investigations of explosive volcanoes.

2.1.1.1d PCA algorithm

PBL SO_2 columns are based upon the operational principal component analysis (PCA) algorithm which replaced the previous Band Residual Difference (BRD) algorithm in October 2014. It applies the PCA technique to OMI radiance data, where a set of PCs that carry measurement and physical details regarding SO_2 interferences are extracted. They are ordered according to the spectral variance and used with pre-estimated SO_2 Jacobians to compute the SO_2 columns. This therefore removes the need for an AMF conversion factor in order to transform slant column density into vertical column density (Li et al., 2013). BRD produced large noise and systemic biases. However, the use of PCA has improved accuracy by a factor of two when compared to BRD (OMSO2 README File, 2008). This could be due to strong SO_2 absorption in the spectral range 310.5 nm - 340 nm with strongest absorption centered at 310.8 nm (Theys et al., 2015). The PCA algorithm also has a lower detectability limit of approximately 2 times better than BRD (Krotkov et al., 2015b). Theys et al. (2015) compared OMI-PCA SO_2 measurements and measurements using the Differential Optical Absorption Spectroscopy (DOAS) algorithm and found that DOAS overestimated PCA by the range from 0.2 DU to 0.6 DU in eastern USA and China, this is because of a lack of background correction factor in the PCA analysis.

Errors and data quality assessment of PCA algorithm

The noise and bias in retrievals depend upon the latitude and surface albedo. These factors both increase with increasing solar zenith angle (SZA) and South Atlantic radiation Anomaly (SAA). Differences were found to be ~0.5 DU for tropical regions between 30˚S and 30˚N and ~0.7 DU to 0.9 DU for high latitude regions. Over highly reflective surfaces like deserts, these retrievals have a negative bias of -0.5 DU. Overestimation in SO_2 retrievals occurs in snowy, cloudy and icy locations. In some instances, there are errors due to the Jacobian look up table and they increase with deviations of the actual observations from the pre-assumed SO_2 in the Jacobian calculation. Lastly, retrievals errors may also depend upon by the number of Principal Components included in the fitting (OMSO2 README File, 2008).

2.1.1.1e Linear Fit (LF) algorithm

The LF algorithm uses TOMS total ozone algorithm (OMTO3) as a linearization step to derive an initial estimate of total ozone by assuming zero SO_2 and OMTO3 surface reflectivity that is independent of wavelength (this is called the Lambertian effective surface reflectivity (LER)). The residual at the 10 other wavelengths are calculated as the difference between the measured and computed N-values. The residuals might also contain errors from other interferences and this is reduced by applying a sliding median empirical correction of SO_2-free and cloud-free locations. The LF algorithm simultaneously adjusts total SO_2 and O_3 to minimize the different subsets of residuals that are produced. The subsets are determined when the shortest wavelength bands are dropped one at a time until 322 nm wavelength is reached and the largest SO_2 value of all is estimated as the final SO_2 amount (OMSO2 README File, 2008;Yang et al., 2007).

Errors and data quality assessment of LF algorithm

A sliding median empirical residual correction factor is applied to the LF algorithm and therefore no data filtering and quality flags are needed. The LF algorithm is highly dependent upon the SO_2 loading. The LF algorithm works optimally when SO_2 levels are below 50 DU, however, when the SO_2 loading exceeds 100 DU, it actually underestimates the actual SO_2 amount. Cloud-related fill values occur in TRL data when the radiative cloud and terrain pressure is below ~500 hpa. However, for TRM this occurs when the cloud top height exceeds 8 km. TRL has a 1-sigma noise level of ~0.7 DU in the tropics and for TRM (under background conditions) it is ~0.3 DU at low and mid-latitudes. STL has a low background noise level of 0.2 DU. The averaging kernel is weakly dependent at height levels above the troposphere and therefore errors produced are smaller in STL (OMSO2 README File, 2008).

OMI level 2G SO_2 data PBL product was used in chapters 3, 4 and 5 for the assessment of ground based SO_2 measurements in South Africa. In chapter 3, a comparison is presented between OMI SO_2 data and GB instrumentation over Sharpeville, Gauteng province. In addition, daily mean, inter-annual and seasonal variation in OMI SO_2 data for 2004 to 2014 are calculated for this location. The final part of the chapter 3 deals with the comparison of

PCA and BRD algorithms used in OMI SO_2 data. In chapter 4, an investigation of the seasonal variation of SO_2 over South Africa at four different altitude levels was completed using OMI SO_2 products for the period 2004 to 2013. In chapter 5, OMI data are used to assess elevated SO_2 levels over South Africa at various altitudes during the post-eruption period of the Calbuco volcano in April 2015.

2.1.2 LIDAR

Because of the importance of SO_2 emission from stationary sources, in particular those resulting from combustion of coal or fuel oil, real-time remote measurement of SO_2 concentrations with LIDAR systems have gained popularity. LIDAR is widely used in laser remote sensing for the detection of pollutants in the atmosphere. It is the optical equivalent of radar, except that a laser is used rather than a microwave source. LIDAR employs electromagnetic radiation at optical frequencies in order to obtain data on a number of parameters important in meteorological and atmospheric studies. The radiation used by LIDAR systems is 10 000 to 100 000 times shorter than that used in conventional radar technologies. The LIDAR principle of operation involves a laser beam of a specified wavelength being directed from the instrumentation towards the target. The beam is reflected off atmospheric constituents and the resulting backscattered photons are collected and processed to yield information relating to the target and/or the path to the target. LIDAR systems offer real-time monitoring of many parameters including aerosols, temperature, amount of water vapour present in the atmosphere, optical depth of particulate matter, boundary-layer growth and cloud layering. In terms of SO_2 monitoring studies, the Differential Absorption Lidar technique (DIAL) and Raman LIDAR are the most commonly used technologies.

2.1.2.1 Differential Absorption LIDAR

The Differential Absorption Lidar (DIAL) system employs the selective light absorption properties of a specific pollutant in the atmosphere. The wavelength of the incident laser is therefore chosen so that it lies within an absorption band of the specific pollutant to be studied (Gimmestad, 2005). The emitted laser light pulses are of two different wavelengths, one for

resonance and the other as a reference. A portion of the light at both wavelengths is scattered by gas molecules or aerosols and returns back to the LIDAR system (Gimmestad, 2005). A detector records the intensity of backscattered light and by comparing the signal intensities at the two wavelengths, a concentration profile along the trajectory of the laser pulses can be determined. DIAL can be used directly to measure concentrations of chemical species in the atmosphere including SO_2, O_3, CH_4, NH_3, CO, CO_2) or indirectly to measure atmospheric temperature and pressure (Gimmestad, 2005). In the last few years, the DIAL technique has been used in investigations of atmospheric SO_2 as it allows for the measurement of SO_2 concentrations in plumes and in ambient air at a distance (Zhou et al., 2014). Many studies have favoured the Nd:YAG laser (532-nm output) for SO_2 monitoring in conjunction with a rhodamine dye laser as reference. Other lasers used in DIAL systems are CO_2 and excimer (with or without Optical Parametric Oscillator (OPO)) lasers.

2.1.2.2 Raman LIDAR

Raman LIDAR is based on Raman scattering of molecules. The excitation due to a variety of molecular rotational and vibrational transitions leads to several bands of Raman scattered radiation, the frequency shifts of which are characteristic of the interacting molecule (Wandinger, 2005). Raman LIDAR techniques are a very direct means of remote sensing pollutant concentrations as they require low spectral energy of the emitted laser and frequency stabilization of the receiver (Wandinger, 2005). However, the small signal-to-noise ratio of these measurements require Raman LIDAR systems operated at night when it is clear atmosphere without cloud and no rain. Raman measurements do not require specific laser wavelengths as is the case for the DIAL technique. This is because the wavelength dependency of the Raman scattering cross section is proportional to wavelength of the laser light and hence shorter emission wavelengths are preferred (Wandinger, 2005). The Raman LIDAR technique developed in early studies measured the rotational or vibrational rotational component of Raman scattering from the atmosphere using a telescope as a receiver. More commonly, this system is operated using Ruby, Nd:YAG or Excimer lasers.

2.2 *Insitu* based techniques

2.2.1 Ground Based Instruments

Anthropogenic sources release atmospheric pollutants at the surface. Here they rapidly react with other species present to form secondary pollutants. In order to understand the physicochemical characteristics of air pollution, it is necessary to continuously monitor the levels of individual target species. GB instruments provide uninterrupted measurements at a specific location (Chu et al., 2003) and can be either stationary or mobile (in the case of a portable device).

South Africa has a variety of *in situ* air monitoring stations across the country covering locations from the Western Cape to Mpumalanga. These stations are a joint effort between the South African government and various stakeholders. The South African Air Quality Information System (SAAQIS) provides a common platform for the management of air quality information in the country. Using data gathered from air quality stations around the country, SAAQIS makes data available to stakeholders, including the public, and provides a mechanism to ensure uniformity in the way air quality data is managed i.e. captured, stored, validated, analysed and reported over South Africa. There are varieties of data products available from this database as it is generated from various sources therefore allowing for unbiased results. In this section, further details are presented relating to ground based instrumentation employed in South Africa.

2.2.1.1 Portable sensors

The modern trend in assessing roadside SO_2 concentrations and that in street canyons is through the use of portable sensors. These systems deliver real time pollutant measurements and this informations may provide guidelines for policies to limit vehicular emissions and associated health risks. Statistical analysis was applied to evaluate the efficacy of the AQMesh wireless SO_2 monitor against monitoring stations in London and Vancouver and found that SO_2 sensors were strong and did not require extra periods of stabilising (Wang, 2017). A further device is the light-emitting diode (LED) based SO_2 sensor, which operates in the deep UV spectral range. It is equipped with a silica waveguide and consumes less space and is more

efficient than optic fibers in that it can detect SO_2 down to levels of 1 ppm (Elmlinger et al., 2017). Miniaturized sensors connected or fixed to smartphones provide an innovative trend in assessing pollutant levels (Theunis et al., 2017), an example of which is the UV camera fitted in modified Raspberry Pi cameras (Wilkes et al., 2017). However, these portable devices still face some drawbacks such as high maintenance cost because of short battery life and high data management costs. Further technological issues include sensitivity and stability of gas sensors (where advanced correction factors are required). This is because outdoor conditions are more prone to variations in temperature and relative humidity than laboratory conditions (Kumar et al., 2015).

2.2.1.2 Passive sampling

Passive sampling systems are primitive sampling methods. Passive sampling is also known as diffusive sampling as gases are either chemically absorbed or physically adsorbed through a diffusive medium onto a surface. Unlike active sampling, these systems do not depend on electricity to pump air into the sampling device, instead the sampling rate is controlled by processes such as molecular diffusion through ambient air or permeation through a filter (Salem et al., 2009).

These systems are inexpensive, compact, portable, cost effective and do not require skilled professionals to operate them. As a result, they are ideally suited for easy, long-term assessment of outdoor and indoor air quality. Inside passive filters, there is an absorbent, which is often coated with a chemical capable of reacting with the specific containments to be quantified and thus the pollutant of interest is trapped. The absorbents used for SO_2 sampling are sodium carbonate, sodium hydroxide and triethanolamine and are employed in ion chromatography or colorimetry methods (Krupa and Legge, 2000 and references therein). The rates at which gases in ambient air diffuse into the sampler are often dependent on the diffusion coefficients of the gases being studied. The average atmospheric concentration of pollutants is calculated based on diffusion rate, sampling period and specific meteorological conditions.

A variety of different passive samplers are available and many play a vital role in ambient air pollution studies. Some samplers are species specific and may therefore provide additional

pollutant coverage at existing measurement sites. Passive samplers are also relatively simple to use and can be handled with computer-based programs, thereby ensuring sound datasets. Commonly used passive samplers are the Ogawa badge (De Santis et al., 1997) and IVL passive sampler. IVL passive samplers (Swedish Environmental Research Institute, Sweden) which employ ion chromatography analysis, were deployed in Al-Ain city, United Arab Emirates, to study SO_2 concentrations. Furthermore, these samplers are durable and can withstand rain, wind, humidity and temperature variations (Salem et al., 2009). These samplers were also used to measure SO_2 variations in Asia, South America, Europe and Africa, of which Elandsfontein and Cape point (South Africa) were among the 50 stations selected (Carmichael et al., 2003). These passive samplers were useful in conducting long term measurements such as in a study by Martins et al. (2007). In this work, ten years of SO_2 measurements in Southern Africa were undertaken. Locations of investigation included Louis Trichardt, Cape point, Amersfoort (South Africa) and Okaukuejo (Namibia). Later, similar research followed and extended the number of locations to include central and west Africa (Adon et al., 2010). Figure 2.3 shows an IVL sampler and its component parts.

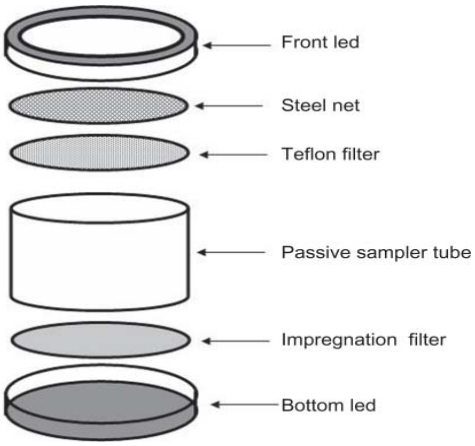

Figure 2.3: Design of IVL sampler and its constituent parts (obtained from Salem et al., 2009).

2.2.1.3 Active sampling

Active sampling systems are those that have a pumping mechanism to actively suck a fixed volume of air through the sampling apparatus. This process requires electricity to forcibly pull air into the device, as opposed to passive sampling, which does not require any mechanical process to facilitate sampling. Many government-operated networks employ this technique in order to monitor air quality on a routine basis. These stationary networks provide a full description of time series data (at 10 min or hourly resolution) and are frequently used to provide countrywide coverage in terms of major cities and industrial areas. Data collection from these monitoring networks is often completed using different types of SO_2 analysers from different manufacturers. The Chinese National Environmental Monitoring Center uses SO_2 analysers (Model 43i (Thermo Fisher) and EC9850 (Ecotech)) in 31 cities in China for the purpose of monitoring criteria pollutants (Zhao et al., 2016). During August-September 2008, an EC9850 series SO_2 analyser was installed in a mobile laboratory and setup to monitor SO_2 emission and transport over Beijing and surrounding areas (Wang et al., 2009, 2011). Typically, SO_2 analysers quantify SO_2 in ambient air by means of a fluorescence based technique. The principle of operation of these fluorescence analysers is discussed in detail in the following section.

2.2.1.3a Pulsed fluorescence SO_2 analysers: Principle of operation

This technique is based on the principle that SO_2 molecules become excited through the absorption of UV radiation at a specific wavelength. The molecules then decay to a lower energy state with the emission of UV radiation at a second wavelength. This process is known as fluorescence. The intensity of fluorescence emitted is proportional to the amount of SO_2 present in the sample (Analytical Methods). Equation (2.1) illustrates this fluorescence mechanism, where $SO_2{}^*$ indicates excited SO_2 molecules and *hv(1)* and *hv(2)* represent photons of initial and emitted wavelengths.

$$SO_2 + hv(1) \rightarrow SO_2{}^* \rightarrow SO_2 + hv(2) \qquad (2.1)$$

The fluorescence analyser consists of a hydrocarbon scrubber, fluorescence chamber, UV radiation source, photodetector, data display and internal memory. Before entering the

fluorescence chamber, the air sample flows through a hydrocarbon kicker, which removes hydrocarbons in the sample. Pulsating UV radiation in the reaction chamber excites SO_2 molecules present in the sample and results in fluorescence, which is then quantified by a photomultiplier tube (PMT). A device called an optical filter selectively allows only those wavelengths emitted by the SO_2 molecules to pass through the PMT. The pulsating UV light source is recorded by a photodetector fitted at the back of the fluorescence chamber. The air sample passes through a flow sensor, capillary tube and the shell side of the hydrocarbon kicker and exhausted outside. The analyser displays the SO_2 concentration as an end product. Figure 2.4 shows a schematic design of the SO_2 fluorescence analyser.

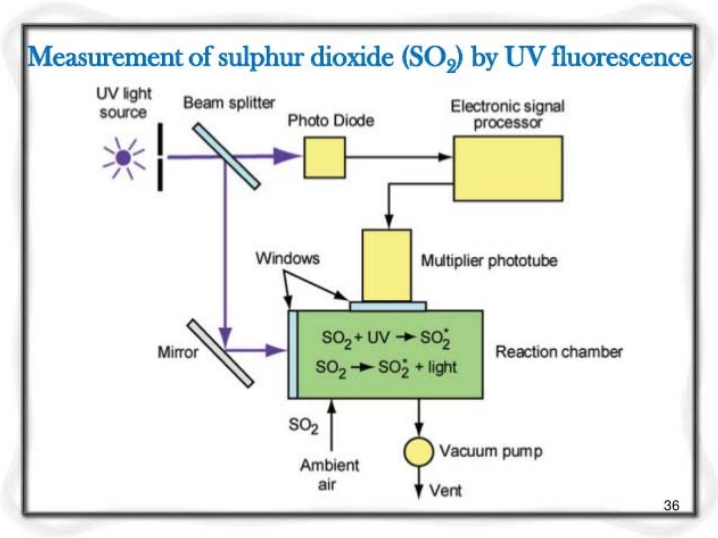

Figure 2.4: Schematic design of SO_2 fluorescence analyser (obtained from https://www.slideshare.net/bibhabasumohanty/air-quality-sampling-and-monitoring-m5, Accessed on 08 November 2017).

Pulsed fluorescence SO_2 analysers come in a wide variety of models from different manufacturers. Figures 2.5 and 2.6 show the Thermo Scientific 43i and OPSIS AR-500 analysers.

Figure 2.5: Thermo Scientific Model 43i SO_2 analyser (obtained from https://www.thermofisher.com/order/catalog/product/43I?SID=srch-srp-43I. Accessed on 07 September 2017)

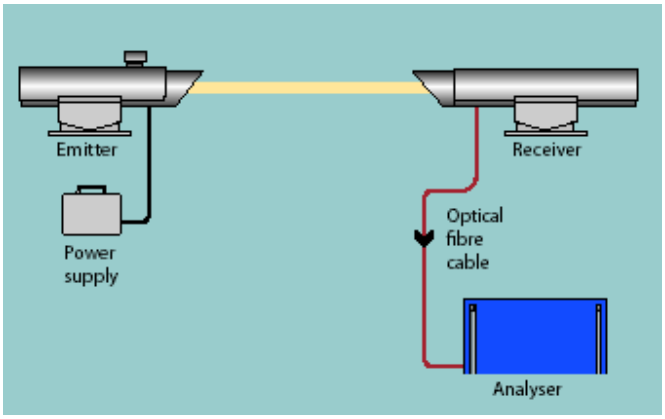

Figure 2.6: Schematic diagram of OPSIS AR-500 (obtained from http://nevcoengineers.com/solutions/Continuous_Air_Quality_Monitoring/System_300 (Opsis),Accessed on 04 November 2017).

Pulsed fluorescence SO_2 analysers are commonly used in South African air quality monitoring networks and data obtained from such instrumentation are used in chapters 3, 4 and 5 of the present study. In this thesis (chapter 3), data collected from GB instrumentation are used in a comparative study together with OMI measurements in order to assess the performance of BRD and PCA algorithms. In chapter 4, GB data are used to study SO_2 temporal and spatial variations over Gauteng and Mpumalanga. While in chapter 5, GB instruments are used to study the rise in SO_2 levels over South Africa due to transport of SO_2 plumes resulting from

the Calbuco volcanic eruption in April 2015. Table 2.2 gives details of instrumentation and the stations in which they are used.

2.2.2 Aircraft measurements

Samples from airborne platforms can represent both spatial and vertical distributions of pollutants however, this may depend on the prevailing weather conditions during the sampling period. Aircraft-borne measurements were used to validate OMI SO_2 retrievals over northeastern China (Krotkov et al., 2008). Furthermore, vertical SO_2 profiles collected through airborne sampling were recorded in the Pearl River Delta in China (Wang et al., 2008), northeastern, northwestern and central eastern regions of China (Xue et al., 2010) and northeastern Pacific Ocean (Andreae et al., 1988). In Southern Africa, SO_2 measurements have been carried out over major areas by means of aircraft campaigns. During August and September 2000, vertical SO_2 profiles were recorded over 5 major Southern African regions including north-eastern South Africa, northern Botswana, coastal Mozambique, southern Zambia and western Namibia. This study was part of the Southern African Regional Science Initiative 2000 (SAFARI 2000) project and used an aircraft (Convair-580) that belonged to the University of Washington. In total, 64 vertical profiles (ranging from ground level to an altitude of 5 km) were recorded with 25 of them recorded over locations in South Africa (Sinha et al., 2003). Burger et al., (2016), utilised flight-based measurements in order to focus on the spatial distribution of trace gases over primary areas including the Highveld, Richards Bay, Cape Town, Durban and Port Elizabeth. Two Aero-commander A690 aircraft were used in this campaign with a total of 208.9 hours of data collection. In an earlier study, the same aircraft was used to concentrate on the Highveld (Secunda, Witbank and Rustenburg) and Vaal Triangle regions (Ncipha, 2011).

Table 2.2: Different types of GB instruments employed in South Africa with their operational characteristics.

Features	Thermo 43C	Thermo 43i	Horiba APSA 370	EC 9850	Monitor Europe ML 9850	Serinus 50	OPSIS AR 500	Teledyne M100A and 100E
Stations/ network employed	Orange farm, Jabavu (Johannesburg network), Booysens, Mamelodi, Olievenhoutbosch (Tshwane network)	All stations in Vaal Triangle network, some stations in Mpumalanga ESKOM network	Diepsloot, Ivory park, some stations in Mpumalanga ESKOM network	Pretoria west and Ekandustria (Tshwane network)	North West provincial government network system	Highveld network	Alexandra (Johannesburg network)	Bodibeng and Rosslyn (Tshwane network), Some stations in Mpumalanga ESKOM; Mogale city and Randfontein
Ranges	0-0.05 to 10 ppm (custom ranges)	0-0.05 to 100 ppm (custom ranges)	0-0.05/0.1/ 0.2/0.5 ppm	0-50 ppbv to 0-20 ppm (auto-ranges)	0-20ppm (auto-ranges)	0-20 ppm (auto-ranging)		50-20,000 ppbv in 1 ppbv increments
Zero noise	1.0 ppbv RMS (10 sec averaging time)	1.0 ppbv RMS (10 sec averaging time)		0.2 ppbv with Kalman filter active	0.25 ppbv with Kalman filter active	<0.15 ppbv		0.2 ppbv RMS
Lower Detectable	2.0 ppbv (10 sec averaging time)	< 0.5 ppbv	0.5 ppbv (3 sigma)	0.4 ppbv with	<0.5 ppbv	0.3 ppbv with	0.9 and 1.4 ppbv for NO	0.4 ppbv RMS

limit (LDL)				Kalman filter active		Kalman filter		
Zero Drift	Less than 1 ppbv	Less than 1 ppbv	< LDL/day at lowest range	<0.4 ppbv (24 hours)	<0.1 ppbv per ˚C	<0.5 ppbv (24 hours)		<0.5 ppbv (24 hours)
Response time	80 secs (10 secs averaging time)	<20 secs (60 sec or less averaging time)	Within 120 secs at lowest range	<120 secs	<120 secs	60 secs to 95%		20 secs
Precision	1% or 1 ppbv	1% or 1 ppbv		0.4 ppbv or 0.5 %	0.5 ppbv or 1% of concentration	0.5 ppbv or 0.15%	0.46% for NO	0.5%
Linearity (full scale)	±1%	±1%	±1%	<1%	±1%	±1%	slope 1.02, r^2 0.99 for NO	1%

2.3 *HYSPLIT* Model

The Hybrid Single-Particle Lagrangian Integrated Trajectory (HYSPLIT) model is an important tool for the analysis of simple air transportation to complex dispersion and deposition of air masses from source, along a trajectory, to a target location (Rolph et al., 2017). HYSPLIT was developed in 1997 by the National Oceanic and Atmospheric Administration's (NOAA) Air Resources Laboratory (ARL) and was the first web based dispersion model. It was initially used in forward trajectory and cluster analysis. However, since 1997 the model has progressed and can now run on a personal computer under the windows operating system. In this format, executables are installed into selected directories and the results computed on a desktop basis. Trajectories are estimated using a combination of a Lagrangian approach and Eulerian methodology. The Lagrangian approach uses a moving frame of reference for advection and diffusion calculations in order to determine the trajectory of air parcels as they move from their initial location. The Eulerian methodology uses a fixed three-dimensional grid as a frame of reference to compute pollutant air concentrations.

In this study, HYSPLIT forward trajectory analysis is used in chapter 5 to trace the path of air masses originating from the Calbuco volcanic eruption on 22nd April (Chile) to South Africa. The results of these calculations are discussed fully in chapter 5.

2.4 MERRA

Modern-Era Retrospective analysis for Research and Applications (MERRA) is a NASA reanalysis product using Goddard Earth Observing System Data Assimilation System Version 5 (GEOS-5) (https://gmao.gsfc.nasa.gov/reanalysis/MERRA-2/). The Global Modeling and Assimilation Office (GMAO) has used its GEOS-5 atmospheric data assimilation system (ADAS) to synthesize the various observations based on long historical satellite data so that it is as consistent as possible over time. In this study, MERRA data is used with a 0.5° latitude × 0.625° longitude × 72 layers model configuration (Rienecker et al., 2011). The MERRA reanalysis provides 8 different timings over a 24 hour period, that is every three hours beginning from 01:30 a.m and running to 22:30 p.m. Further details on MERRA can be found in Rienecker et al. (2008, 2011). In this work, MERRA-2 is used to estimate the pressure at planetary boundary layer and surface pressure over Sharpeville and for the time corresponding to 10:30 GMT, as it is closer to the OMI overpass over

South Africa. Thus, the surface SO_2 level is calculated based on surface and PBL pressure level from MERRA and using the OMI satellite SO_2 PBL value (see.. Chapter 3).

2.5 References

Adon, M., Lacaux, C. G., Yoboue, V., Delon, C., Lacaux, J.P., Casteral, P., Gardrat, E., Pienaar, J., Al Ourabi, H., Laouali, D., Diop, B., Sigha-Nkamdjou, L., Akpo, A., Tathy, J.P., Lavenu, F. and Mougin, E., 2010. Long term measurements of sulfur dioxide, nitrogen dioxide, ammonia, nitric acid and ozone in Africa using passive samplers. *Atmospheric Chemistry and Physics*, *10*(15), pg. 7467-7487.

Analytical Methods. https://www.atsdr.cdc.gov/toxprofiles/tp116-c6.pdf (accessed on 6 September 2017].

Andreae, M.O., Berresheim, H., Andreae, T.W., Kritz, M.A., Bates, T.S. and Merrill, J.T., 1988. Vertical distribution of dimethylsulfide, sulfur dioxide, aerosol ions, and radon over the northeast Pacific Ocean. *Journal of Atmospheric Chemistry*, *6*(1-2), pg. 149-173.

Azid, A., Juahir, H., Toriman, M.E., Endut, A., Rahman, M.N.A., Kamarudin, M.K.A., Latif, M.T., Saudi, A.H.S.M., Hasnam, C.N.C. and Yunus, K., 2015a. Selection of the most significant variables of air pollutants using sensitivity analysis. *Journal of Testing and Evaluation*, *44*(1), pg. 376-384.

Azid, A., Juahir, H., Toriman, M.E., Endut, A., Kamarudin, M.K.A., Rahman, M.N.A., Hasnam, C.N.C., Saudi, A.H.S.M. and Yunus, K., et al., 2015b. Source apportionment of air pollution: A case study in Malaysia. *Jurnal Teknologi*, *72*(1), pg. 83-88.

Burger, R.P., 2016. *The Distribution of Aerosol and Trace Gases in the Lower Troposphere over South Africa* (Doctoral dissertation), University of Witwatersrand, Johannesburg.

Carmichael, G.R., Ferm, M., Thongboonchoo, N., Woo, J.H., Chan, L.Y., Murano, K., Viet, P.H., Mossberg, C., Bala, R., Boonjawat, J. and Upatum, P., 2003. Measurements of sulfur dioxide, ozone and ammonia concentrations in Asia, Africa, and South America using passive samplers. *Atmospheric Environment*, *37*(9), pg.1293-1308.

Caron, et al., 2012. Polarization scramblers in Earth observing spectrometers: lessons learned from Sentinel-4 and 5 phases A/B1. In *Proceedings of the International Conference on Space Optics (ICSO), Ajaccio, Corse, France*.

Chu, D.A., Kaufman, Y.J., Zibordi, G., Chem, J.D., Mao, J., Li, C. and Holben, B.N., 2003. Global monitoring of air pollution over land from the Earth Observing System-Terra Moderate Resolution Imaging Spectroradiometer (MODIS). *Journal of Geophysical Research: Atmospheres*, 108(D21). doi: 0.1029/2002JD003179.

Clarisse, L., Hurtmans, D., Clerbaux, C., Hadji-Lazaro, J., Ngadi, Y. and Coheur, P.F. 2012. Retrieval of sulphur dioxide from the infrared atmospheric sounding interferometer (IASI). *Atmospheric Measurement Techniques*, *5*(3), pg. 581-594.

De Santis, F., Allegrini, I., Fazio, M. C., Pasella, D., and Piredda, R. 1997. Development of a passive sampling technique for the determination of nitrogen dioxide and sulphur dioxide in ambient air. *Analytica Chimica Acta*, *346*(1), pg.127-134.

Elmlinger, P., Schreivogel, M., Weida, S. and Kneissl, M., 2017. A Miniaturized UV-LED Based Optical Gas Sensor Utilizing Silica Waveguides for the Measurement of Nitrogen Dioxide and Sulphur Dioxide. In *Multidisciplinary Digital Publishing Institute Proceedings, 1*(4), pg. 556).

Environmental Technology Verification Report, OPSIS INC. AR-500, ULTRAVIOLET OPEN-PATH MONITOR. https://archive.epa.gov/nrmrl /archive-etv/web/pdf/01_vr_opsis.pdf (accessed on 16 August 2017).

Fioletov, V.E., McLinden, C.A., Krotkov, N., Li, C., Joiner, J., Theys, N., Cam, S.A. and Moran, M.D., 2016. A global catalogue of large SO2 sources and emissions derived from the Ozone Monitoring Instrument. *Atmospheric Chemistry and Physics*, *16*(18), pg. 11497-11519.

Fluorescence SO_2 Analyzer, Ecotech EC9850 Sulfur Dioxide Analyzer. http://www.keisokuki.com/EC9850a.pdf (accessed on 17 August 2007).

Gimmestad, G., 2005. Differential-absorption lidar for ozone and industrial emissions. *Lidar*, pg.187-212.

Horiba Process and Environmental, Air Pollution Monitor, AP-370 Series. http://www.horiba.com/fileadmin/uploads/Process-Environmental/ Documents/HRE2858E-AP_Series.pdf (accessed on 20 October 2014).

Instruction Manual, Model 100A Sulfur Dioxide Analyser. http://www.teledyne-api.com/manuals/02164h_100a.pdf (accessed on 16 August 2017].

Kattner, L., Mathieu-Üffing, B., Burrows, J.P., Richter, A., Schmolke, S., Seyler, A. and Wittrock, F., 2015. Monitoring compliance with sulfur content regulations of shipping fuel by in situ measurements of ship emissions. *Atmospheric Chemistry and Physics*, *15*(17), pg.10087-10092.

Kourtidis, K.A., Ziomas, L., Zerefos, C., Kosmidis, E., Symeonidis, P., 2002. Benzene, toluene, ozone, NO2 and SO2 measurements in an urban street canyon in Thessaloniki, Greece. *Atmospheric Environment*, *36*(34), pg. 5355-5364.

Krotkov, et al., 2008. Validation of SO_2 retrievals from the Ozone Monitoring Instrument over NE China. *Journal of Geophysical Research: Atmospheres*, *113*(D16).

Krotkov, N.A. and C. Li. 2012. OMSO2 Version 003: OMI/Aura Sulphur Dioxide (SO2) Total Column 1-orbit L2 Swath 13x24 km. Greenbelt, MD, USA: Goddard Space Flight Center Distributed Active Archive Center (GSFC DAAC). doi:10.5067/Aura/OMI/DATA2022. (Accessed on 28 February 2016) .

Krotkov, et al., 2015a. Shortname: OMSO2e Longname: OMI/Aura Sulfur Dioxide (SO2) Total Column Daily L3 Best Pixel Global 0.25 deg Lat/Lon Grid PFS Version: 1.1. 7.

Krotkov, et al., 2015b. Aura OMI observations of regional SO2 and NO2 pollution changes from 2005 to 2014. *Atmospheric Chemistry and Physics Discussions*, *15*(19), pg. 26555-26607.

Krueger, A. J., Walter, L. S., Bhartia, P. K., Schnetzler, C. C., Krotkov, N. A., Sprod, I. T., and Bluth, G. J. S., 1995. Volcanic sulfur dioxide measurements from the total ozone mapping spectrometer instruments. *Journal of Geophysical Research: Atmospheres*, *100*(D7), pg.14057-14076.

Krupa, S.V. and Legge, A.H., 2000. Passive sampling of ambient, gaseous air pollutants: an assessment from an ecological perspective. *Environmental Pollution*, *107*(1), pg.31-45.

Kumar, P., Morawska, L., Martani,, C., Biskos, G., Neophytou, M., Sabatino, S. D., Bell., M., Norford, L. and Britter, Rex., 2015. The rise of low-cost sensing for managing air pollution in cities. *Environment international*, *75*, pg.199-205.

Laakso, et al., 2010. South African EUCAARI–measurements: a site with high atmospheric variability. *Atmospheric Chemistry and Physics Discussions, 15,* pg. 30691-30729.

Laakso, et al., 2012. South African EUCAARI measurements: seasonal variation of trace gases and aerosol optical properties. *Atmospheric Chemistry and Physics*, *12*(4), pg. 1847-1864.

Levelt, et al., 2006. Science objectives of the ozone monitoring instrument. *IEEE Transactions on Geoscience and Remote Sensing*, *44*(5), pg. 1199-1208.

Li, C., Joiner, J., Krotkov, N. A. and Bhartia, P. K., 2013. A fast and sensitive new satellite SO_2 retrieval algorithm based on principal component analysis: Application to the ozone monitoring instrument. *Geophysical Research Letters, 40*(23), pg. 6314-6318. doi:10.1002/2013GL058134.

Martins, J.J., Dhammapala, R.S., Lachmann, G., Galy-Lacaus, C. and Pienarr, J.J., 2007. Long-term measurements of sulphur dioxide, nitrogen dioxide, ammonia, nitric acid

and ozone in southern Africa using passive samplers. *South African journal of science*, *103*(7-8), pg.336-342.

ML 9850 Sulphur Dioxide Analyser. http://www.ecomonitoring.pl/Imisja/ME/Analizator%20m.s.SO2/9850.pdf (accessed on 16 August 2017).

Model 43C SO_2 Analyzer. http://www.thermo.com.cn/Resources/200802/productPDF_12267.pdf (accessed on 18 August 2017).

Ncipha, X.G., 2011. *Comparison of air pollution hotspots in the Highveld using airborne data* , University of Witwatersrand, Master degree thesis.

OMI (Ozone Monitoring Instrument) Data User's Guide, OMI-DUG-5.0, January 5, 2012, Produced by OMI Team. https://docserver.gesdisc.eosdis.nasa.gov/repository/Mission/OMI/3.3_ScienceDataProductDocumentation/3.3.2_ProductRequirements_Designs/README.OMI_DUG.pdf (accessed on 02 August 2014).

OMSO2 README File v1.2.0 Released Feb 26, 2008 Updated: September 26, 2014. https://so2.gsfc.nasa.gov/Documentation/OMSO2Readme_V120_20140926.pdf. (accessed on 02 September 2015).

Operational Manual, Model 100E, UV Fluorescence SO_2 Analyser. http://www.teledyne-api.com/manuals/04515F_100E.pdf (accessed on 17 August 2017).

Realmuto, V.J. and Worden, H.M., 2000. Impact of atmospheric water vapor on the thermal infrared remote sensing of volcanic sulfur dioxide emissions: A case study from the Pu'u 'O'vent of Kilauea Volcano, Hawaii. *Journal of Geophysical Research: Solid Earth*, *105*(B9), pg. 21497-21507.

Salem, A.A., Soliman, A.A. and El-Haty, I.A., 2009. Determination of nitrogen dioxide, sulfur dioxide, ozone, and ammonia in ambient air using the passive sampling method associated with ion chromatographic and potentiometric analyses. *Air Quality, Atmosphere and Health*, *2*(3), pg. 133-145.

Serinus 50 Sulphur Dioxide Analyser, User Manual, Version 2.2. http://www.ecotech.com/wp-content/uploads/2015/01/M010029-Serinus-50-SO2-User-Manual-2.2.pdf (accessed on 16 August 2017).

Sinha, P., Hobbs, P.V., Yokelson, R. J., Blake, D.R., Gao, S. and Kirchstetter, T.W., 2003. Distributions of trace gases and aerosols during the dry biomass burning season in southern Africa. *Journal of Geophysical Research: Atmospheres*, *108*(D17).

Thermo Scientific Model 43i, Sulfur Dioxide Analyzer. https://assets.thermofisher.com/TFS-Assets/LSG/Specification-Sheets/EPM-43i-Datasheet.pdf (accessed on 18 August 2017).

Theunis J., Stevens, M. and Botteldooren, D., 2017. Sensing the Environment. In: Loreto V. et al. (eds) Participatory Sensing, Opinions and Collective Awareness. Understanding Complex Systems. Springer, Cham. doi: https://doi.org/10.1007/978-3-319-25658-0_2 (accessed on 28 August 2017). .

Theys, N., De Smedt, I., van Gent, J., Danckaert, T., Wang, T., Hendrick, F., Stavrakou, T., Bauduin, S., Clarisse, L., Li, C., Krotkov, N., Yu, H., Brenot, H. and Van Roozendael, M., 2015. Sulfur dioxide vertical column DOAS retrievals from the Ozone Monitoring Instrument: Global observations and comparison to ground-based and satellite data. *Journal of Geophysical Research: Atmospheres*, *120*(6), pg. 2470-2491.

Vetres, I., Ionel, I., Cazacu, M.M. and Balin, I., 2012. Necessity of complementary vertically-resolved LIDAR observations for ground air pollution analysis in western Romania. *Journal of environmental protection and ecology*, *13*(2), pg. 409-419.

Wandinger, U. (2005). Raman lidar. in Lidar – Range resolved optical remote sensing of the atmosphere, Ed. Weitkamp, C., *Springer series in optical sciences, New York,* , pg.241-271.

Wang, W., Ren, L. H., Zhang, Y. H., Chen, J. H., Liu, H. J., Bao, L. F., Fan, S. J. and Tang, D. G., 2008. Aircraft measurements of gaseous pollutants and particulate matter over Pearl River Delta in China. *Atmospheric Environment*, *42*(25), pg. 6187-6202.

Wang, M., Zhu, T., Zheng, J., Zhang, R. Y., Zhang, S. Q., Xie, X. X., Han, Y. Q., and Li, Y., 2009. Use of a mobile laboratory to evaluate changes in on-road air pollutants during the Beijing 2008 Summer Olympics. *Atmospheric Chemistry and Physics*, *9*(21), pg. 8247-8263.

Wang, M., Zhu, T., Zhang, J. P., Zhang, Q. H., Lin, W. W., Li, Y., and Wang, Z. F., 2011. Using a mobile laboratory to characterize the distribution and transport of sulfur dioxide in and around Beijing. *Atmospheric Chemistry and Physics*, *11*(22), pg. 11631-11645.

Wang, A.Y., 2017. A spatial and temporal analysis of neighbourhood air quality in downtown Vancouver, Master of Science dissertation, University of British Columbia.

Wilkes, T.C., Pering, T.D., McGonigle, A.J.S., Tamburello, G. and Willmott, J.R., 2017. A Low-Cost Smartphone Sensor-Based UV Camera for Volcanic SO_2 Emission Measurements. *Remote Sensing*, *9*(1), pg. 27.

Xue, L., Ding, A., Gao, J., Wang, T., Wang, W., Wang, X., Lei, H., Jin, D. and Qi, Y., 2010. Aircraft measurements of the vertical distribution of sulfur dioxide and aerosol scattering coefficient in China. *Atmospheric Environment*, *44*(2), pg. 278-282.

Yang, K., Krotkov, N. A., Krueger, A. J., Carn, S. A., Bhartia, P. K. and Levelt, P. F., 2007. Retrieval of large volcanic SO2 columns from the Aura Ozone Monitoring Instrument: Comparison and limitations. *Journal of Geophysical Research: Atmospheres*, 112(D24). doi: 10.1029/2007JD008825.

Yinchao Zhang, A.E.R., 2005, DIAL Measurements of SO2, NO2, and O3 in Beijing. In *2nd Symposium on Lidar Atmospheric Applications*.

Zhang, Y., Li, C., Krotkov, N. A., Joiner, J., Fioletov, V. and McLinden, C., 2017. Continuation of long-term global SO2 pollution monitoring from OMI to OMPS. Atmospheric Measurement Techniques, *10*(4).

Zhao, S., Yu, Y., Yin, D., He, J., N. Liu., Qu, J. and Xizo, J., 2016. Annual and diurnal variations of gaseous and particulate pollutants in 31 provincial capital cities based on in situ air quality monitoring data from China National Environmental Monitoring Center. *Environment International*, *86*, pg. 92-106.

Zhao, G.Y., Wu, X.X., Lian, M. and Svanberg, S., 2014, August. Lidar monitoring of atmospheric atomic mercury and sulfur dioxide in Guangzhou, China. In *Proc. PIERS*, pg. 2711-2714.

Chapter 3

SO_2 seasonal variation and assessment of Ozone Monitoring Instrument (OMI) measurements at Sharpeville (27.86° E; 26.68° S) a South African ground-based station

This chapter is based upon

S.K. Sangeetha, V. Sivakumar, M. Josipovic, M. Gebreslasie and C.Y.Wright, SO_2 seasonal variation and assessment of Ozone Monitoring Instrument (OMI) measurements at Sharpeville (27.86° E; 26.68° S) a South African ground-based station *International Journal of Remote Sensing, 38:23,* pg. *6680-6696,* 2017.

S. K. Sangeetha, V. Sivakumar, M. Josipovic, M. Gebreslasie and C. Y. Wright, Comparative study of OMI BRD and PCA algorithm retrievals in relation to ground based measurements over a South African Site. *Proc. of 32nd Annual conference of South African society for atmosphere science, Lagoon Beach Hotel, Mlnerton, CapeTown (South Africa), ISBN 978-0-620-72974-1, pg 119-122, 31 October-01 November 2016.*

Abstract

In this study, seasonal, inter-annual variations of sulphur dioxide (SO_2) were analysed for Sharpeville, South Africa (27.86° E; 26.68° S) for the period 2007-2013. Sharpeville is a residential site located within a highly industrialised region. Inter-annual variations were investigated by analysis of data collated by a Ground-based (GB) instrument as well as the SO_2 retrievals recorded by the Ozone Monitoring Instrument (OMI), a satellite-based sensor. The Planetary Boundary Layer (PBL) SO_2 vertical column data recorded by OMI were converted to surface SO_2 volume mixing ratios using the pressure difference between surface and PBL. Accordingly, the OMI derived SO_2 measurements overestimated GB values and showed a relatively good correlation with GB data in the austral winter compared to the other seasons where only low correlation of ~30 % obtained. The results showed that OMI-BRD retrievals underestimated them throughout the entire period. The daily, monthly regression analysis and seasonal correlation studies have also indicated that PCA technique performed better than BRD algorithm. Besides this, the overall comparisons i.e. their daily, seasonal and yearly correlation studies found that OMI derived measurements was in better agreement with GB regardless of its moderate relative percentage of difference with GB. The seasonal variations of SO_2 demonstrated that GB and OMI derived measurements followed a general pattern of increasing trend from autumn until late winter and decreased from the onset of spring, however the latter showed unique high SO_2 levels in summer. Together with this, the inter-annual variations of both computations displayed a small decrement in SO_2 values during the period 2011-2013. This however proved to be a stable variation when compared to other countries.

3.1. Introduction

Several satellite-based instruments are currently in operation to meet the increasing demand for air pollution monitoring. They have the advantage of providing wide spatial coverage of continuous data and location of hot spot regions compared to Ground-based (GB) measurements. They are utilised in a variety of applications such as monitoring of unpredictable emissions from volcanoes, ships and biogenic sources; trans-boundary emissions; intercontinental transport of dust aerosols and other pollutants (Streets et al., 2013). Satellite instruments also serve as a major tool in investigating the seasonal and inter-annual trends of a pollutant over long time periods on a local, regional, zonal and even

global scale. However, satellite-borne instruments have some basic disadvantages related to uncertainties in the retrieval algorithms and the instruments themselves, which can lead to random and systematic errors (Duncan et al., 2014). Their temporal resolution is reduced because of their limited overpass timings and as a result, they may not be able to record outlying values or anomalies. These data gaps can be filled up only by anticipated geostationary satellites such as the forthcoming Tropospheric Emissions: Monitoring of Pollution (TEMPO) which is planned to be launched in 2018. TEMPO will remain in a geostationary orbit over North America to continuously measure pollutant levels on an hourly basis (Chance 2013). At present, it is only possible to relate satellite data with data from GB instruments and the output of air quality models in order to determine a well-defined profile of atmospheric pollutants. Many approaches are therefore possible to study the atmospheric lower strata, namely the lower tropospheric and planetary boundary layers, with the aid of satellite measurements.

In a study conducted on global volcanic SO_2 emissions from 2005 to 2012, it was shown that Ozone Monitoring Instrument (OMI) detected about 50 volcanic eruptions (Ge et al., 2016). The largest OMI based volcanic SO_2 sources during this time period were from eight continuously degassing volcanoes in the tropics (Ge et al., 2016). In another study based on volcanic SO_2 from the 2014 to 2015 eruption at the Holuhraun lava in Iceland, it was demonstrated that OMI could trace down the high SO_2 plumes similar to those detected by air quality monitoring stations and thereby disproved the notion that the retrieval of OMI in high latitudinal regions is demanding (Schmidt et al., 2015). OMI observations of SO_2 emissions from two Peruvian copper smelters and active volcanoes in Ecuador and Southern Colombia between September 2004 and June 2005 confirmed that OMI could detect both natural and anthropogenic SO_2 sources (Carn et al., 2007).

Global maps of OMI mean total SO_2 columns between 2004 and 2009, showed high emission anthropogenic point sources over Asia such as the Persian Gulf region and India. In addition to this, OMI detected weak SO_2 signals from shipping routes near the Red sea and Gibraltar (Theys et al., 2015). It has been shown that the choice of appropriate Air Mass Factor (AMF) in the OMI retrievals plays a vital role in reducing the bias (Bauduin et al., 2016). The relative change in the percentage of SO_2 emissions based on OMI measurements found that there was 70% -80% and 40%-50% decline in SO_2 emissions during the period 2005-2014 over USA and European sources respectively, while an 80% increase was observed over India. However, large emitting source regions in Middle East,

Mexico, Russia, and South Africa showed fixed up trends (Fioletov et al., 2016). Finally, it has been estimated that nearly 6%-12% of total global anthropogenic SO_2 emissions has been accounted for by the Persian Gulf regions (McLinden et al., 2016).The annual mean SO_2 column simulations with GEOS-Chem (global 3-D chemical transport model (CTM) from the Goddard Earth Observing System (GEOS)) chemical transport model for 2006 shows that anthropogenic SO_2 emissions contribute to nearly 1×10^{16} molecules cm^{-2} in the industrialised regions of Highveld, South Africa and the whole fraction of SO_2 column is from these anthropogenic emissions (Lee et al., 2011). In this study, our objective is to compare the OMI SO_2 measurements at a South African site against GB measurements. Based on our knowledge, the study would be one of a few of its kind that explores the applicability of SO_2 satellite measurements in Africa/Southern Hemisphere and likely the first comprehensive comparative study on the assessment of long-term GB and OMI SO_2 measurements made in South Africa. Prior to this study there were a few comparative studies using in-situ measurements and research aircrafts, which have been carried out on a short timescale (Sinha et al., 2003).

The major scope of this investigation is the comparative study between the GB and OMI satellite SO_2 data, where the latter is converted into comparable units by following the application of Josipovic et al., (2013) who has adopted from Ziemke et al. (2006). Based on this comparison, it can be inferred if the adopted method correlates better with the GB results and whether the OMI satellite SO_2 measurements can be used as proxy concentrations in areas of GB station shortfall places. A further aim of this chapter is to study SO_2 seasonal variation over Sharpeville (South Africa) using, data sets from OMI derived measurements and GB data. It should be noted that since OMI data is available for 2004 to 2013 and GB data available for 2007 to 2013, the comparative study was performed for the period 2007 to 2013. However, SO_2 seasonal variations were studied individually according to their respective available measurement time periods.

3.2. Location, Data and Methodology

3.2.1. Location of Ground-based station

The SA GB SO_2 measurement station selected is Sharpeville. Sharpeville station was chosen as it is the station with the highest number of paired (both OMI overpass and GB) data sets available. The monitoring station is located in Sharpeville, Sedibeng Municipality,

in the Gauteng province of South Africa at 26.68° S 27.86° E (see. Figure 3.1(*a*)). Sharpeville is situated in the Vaal Triangle Airshed Priority Area managed by the Department of Environmental Affairs. The major sources of pollution in this area are residential fuel burning and the industrialised urban areas of Vereeniging, Sasolburg and Vanderbijlpark. Lethabo coal-fired power station is also located near Sharpeville. Figure 3.1(*b*) shows an enlarged view of Sharpeville and its nearby industrial sites.

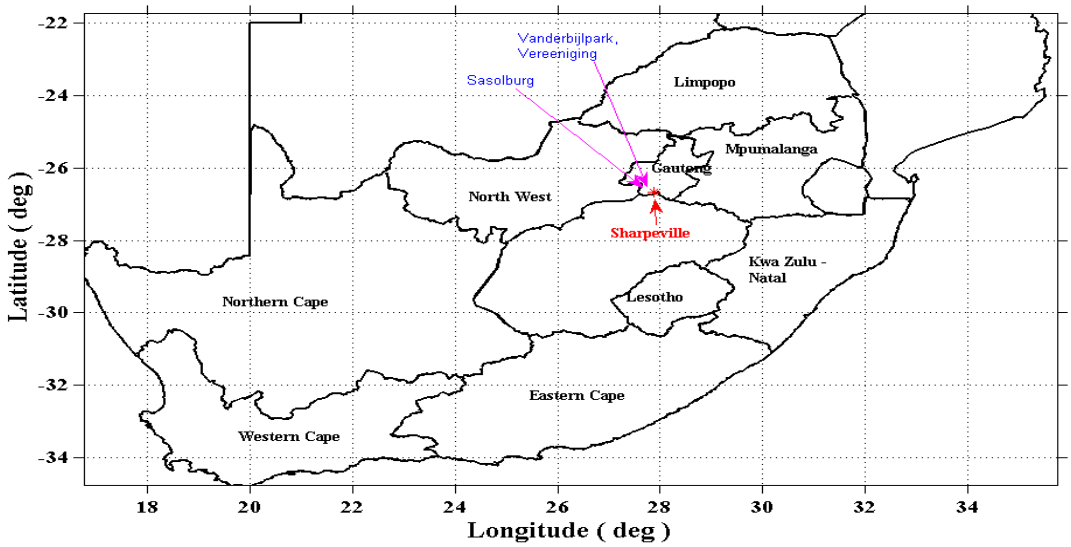

Figure 3.1(a): Geographical map of South Africa depicting the Geo-location of the Sharpeville ground station and nearby towns with large industries.

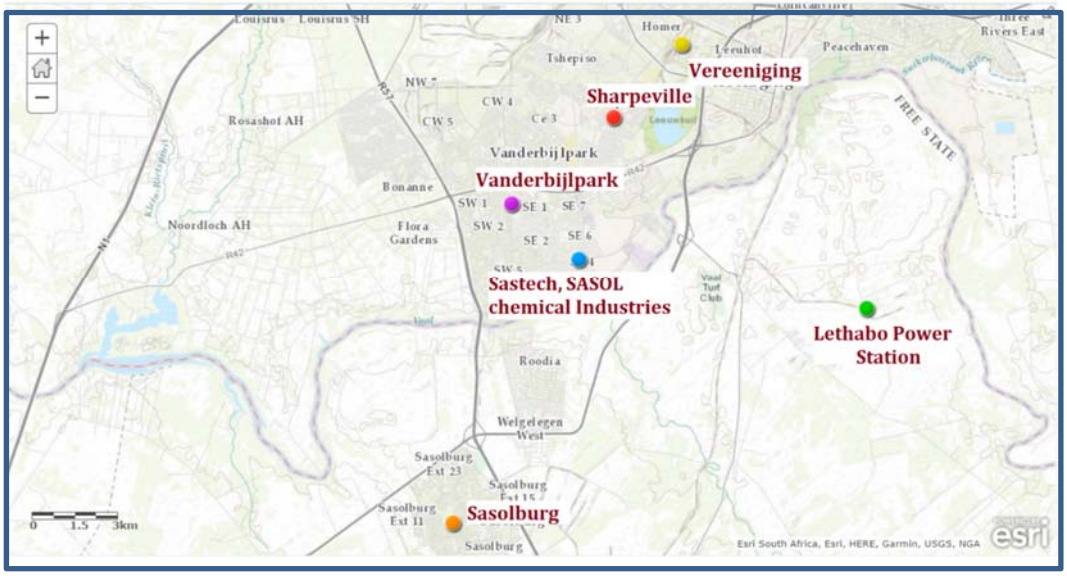

Figure 3.1(b): Map of Sharpeville and its neighbourhood industries and Lethabo power station (created through web-ArcGIS)

3.2.2 Ground-based instrumentation

The instrument used at the GB station is the Thermo Electron 43i SO_2 analyser. It is a pulsed fluorescence SO_2 analyser and employs the principle of fluorescence by adopting the absorption in the ultraviolet light region, i.e. UV light is allowed to pass through the fluorescent chamber, where SO_2 molecules absorb in this range thereby emitting decay radiation, which is sensed by a photomultiplier tube. The amount of energy emitted is measured in terms of electric voltage by the electronic signal processors and is directly proportional to the SO_2 concentration. The instrument was maintained under South African National Accreditation System and routinely calibrated on a bi-monthly basis. The precision of the instrument is around 1 ppbv with zero drift value less than 1 ppbv and a response time of approximately 60 seconds with a detection limit of about 2 ppbv.

3.2.3. Ground-based data

Measurements of SO_2 at Sharpeville were performed by the South African Weather Service (SAWS) and archived in the South African Air Quality Information System (SAAQIS). In this investigation, GB SO_2 data starting from 23 March 2007 to 31 January 2014 was used and this high resolution data was averaged hourly for each day to give a total of 24 data points per day. The following data gaps should be noted: 16 February 2009 to 7 March 2009; 21 February 2010 to 21 June 2010; 22 January 2011 to 20 May 2011; 5 September 2012 to 11 September 2012; and 21 May 2013 to 27 May 2013. In order to improve the quality of data and accuracy of results, data validation was carried out. In this process, 70% data completeness was followed, namely data points having a zero or negative value were discarded as well as missing data points. The data gaps and anomalies were filtered out in order to obtain uniformity in the data sets programmatically. The daily means were calculated from the hourly averaged data for each day from March 2007 to January 2014. The calculated daily means were assumed to be within the standard deviation of hourly recorded data. The reason for calculating daily averages was to increase the uniformity in the data set as some hourly data were missing. Thereafter, individual monthly means were obtained by calculating the monthly mean for each year of the time period in order to evaluate inter-seasonal variations. The overall monthly means were calculated to investigate overall seasonal variation. This was accomplished by sorting the data with respect to monthly measurements discounting the years of measurement (for example, all January values were combined for all the years from 2008 to 2014 and the resultant mean

was calculated for the corresponding month) and their corresponding mean and standard deviation were obtained. The measurements which had high positive and negative anomalies were removed (those over/below the mean $\pm 2\sigma$ (standard deviation)).

3.2.4. Satellite–based instrument (OMI) and retrieval of SO_2 data

The satellite-based instrument used in this study is the OMI. When compared to other satellites the unique features of OMI are the high spatial resolution of about 13 km × 24 km and its daily global coverage. The Global Ozone Monitoring Experiment (GOME) has a spatial resolution of 320 km × 40 km (Boersma et al., 2006) whereas the SCanning Imaging Absorption spectroMeter for Atmospheric CHartographY (SCIAMACHY) has 60 km × 30 km and it takes about 6 days for complete global coverage (Blond et al., 2007). Thus, the daily measurements of OMI help in forecasting the air quality, near real-time monitoring, transport of pollutants and sudden increase in pollution levels that are associated with public health issues. The fine spatial resolution of OMI allows regional scale mapping of highly polluted areas. In OMI, reflected solar radiation is measured in the ultraviolet (UV) and visible regions with a spectral range between 270 nm and 500 nm. The UV channel has two sub-channels with UV-1 (270-310 nm) and UV-2 (310-365 nm) and a spectral resolution of 0.5 nm. This permits the measurement of concentrations of several trace gases in the atmosphere. The spectral band used for SO_2 measurements is from 310.5 nm to 340 nm (UV-2 band). A newly improved retrieval algorithm based on Principal Component Analysis (PCA) to radiance data, has been used in this study. Based on this technique, the SO_2 retrieval quality using the PCA algorithm is greatly improved when compared to its predecessor the Band Residual Difference (BRD) algorithm, in particular, the negative bias seen under cloudy conditions has been eliminated with the use of PCA (OMSO2 README File 2008). Further information on this algorithm is fully explained in the referred OMI SO_2 data product document (OMSO2 README File 2008). The errors and biases have been largely decreased with the use of the PCA algorithm (nearly 2 orders of magnitude) when compared to the BRD algorithm. This demonstrates the applicability of this technique (Li et al., 2013), it can also be applied to determine a wider range of point source emissions. An estimated uncertainty limit of approximately 0.5 DU is expected by OMI SO_2 measurements over the latitudinal regions between 30°S and 30°N (OMSO2README File 2008). In addition, the errors due to row anomaly where blockage

in the field of view and light scattering affects track positions (Fioletov et al., 2011) has been undertaken and corresponding values are disregarded (GES DISC, News).

In this investigation, the daily 'OMSO2 product' from 2004 to 2013 is used. The level 2 OMI SO_2 product with version 003 was accessed from the National Aeronautics and Space Administration (NASA) Goddard Earth Sciences (GES) Data and Information Services Center (DISC) (http://disc.sci.gsfc.nasa.gov/Aura/data-holdings/OMI/omso2_v003.shtml). The radiation calibrations of this data product are improved compared to the previous version (Krotkov and Li, 2012). The OMSO2 product has four distinct categories of the vertical distribution of SO_2 namely planetary boundary layer (PBL); lower tropospheric; middle tropospheric; upper tropospheric and stratospheric SO_2 (OMSO2 README File 2008). In order to perform further analysis, the OMI PBL SO_2 data for the Sharpeville region (26.68° S and 27.86° E) were extracted from the global OMI SO_2 data. The OMI satellite measurements over Sharpeville were selected with a discrepancy in sampling grid of 0.125° × 0.125° (i.e. 27.86° ± 0.125° E and 26.68° ± 0.125° S). As instructed in the OMI data manual, data was discarded if the Radiative Cloud Fraction (RCF) was more than 0.2 and the Solar Zenith Angle (SZA) greater than 50° (OMI Data User's Guide 2012). It is noted that there is a data gap in June for every year of this investigation as there was no satellite overpass during this month for the location under study.

In order to perform a reasonable comparison of the OMI SO_2 data expressed as vertical column density (VCD) with its corresponding GB measurement which was recorded in volume mixing ratios (VMR), the OMI SO_2 PBL VCD were extracted down to surface level values assuming well mixed layers. In this method, the VCD in the PBL layer were converted into VMR into parts per million volume (ppmv) by using the pressure difference between the surface and top of the PBL layer (Josipovic 2009; Josipovic et al. 2013 as adjusted from Ziemke et al., 2001; 2006). The equation for this conversion follows the above basic assumption but at two different pressure levels, i.e.

$$\Delta\Omega \approx 0.79 \int_{P_S}^{P_{BL}} x \, dP_{atm}$$

$$X_{VMR} = (1.27 \, VCD_{PBL}) / (P_S - P_{BL}) \qquad (3.1)$$

Where:

$\Delta\Omega$ stands for vertical column density (DU) and X_{VMR} is volume mixing ratio of trace gas, VCD_{PBL} is the Daily OMI PBL columnar SO_2 in DU, and P_S and P_{BL} denote the hourly

atmospheric pressure in hPa at the surface layer and top of the boundary layer respectively corresponding to the satellite overpass timings. Daily OMI PBL columnar SO_2 measurements stand here for the entire atmosphere. In this investigation hourly surface pressure, PBL pressure data using Modern ERA-Retrospective Analysis for Research and Applications (MERRA) (Reichle, 2012) was obtained for the same OMI satellite overpass timings, i.e. local noontime for the same period (2004 to 2013).

The anomalies in data and data gaps were discarded by calculating the overall mean (regardless of the day, month and year) and the corresponding standard deviation (σ) i.e. daily mean values have been checked with the above obtained overall mean and $\pm 2\sigma$. Since our primary objective was to extract climatological results and thus to avoid extreme high and low values, the data have been discarded if the values were lower or higher than the overall mean and $\pm 2\sigma$ level. Such a criterion has been followed in earlier research for a sub-tropical station at Reunion Island when extracting ozone climatology from GB measurements (Sivakumar et al., 2007; Toihir et al., 2015). Similar to GB data, daily mean variations were also estimated by calculating the mean of the daily columnar values for the corresponding station latitude and longitude zones and then extracting down to surface ppbv values by the application of equation (3.1).

3.3. Results

3.3.1. *Comparative study between Ground-based and OMI derived measurements*

3.3.1.1. Daily mean comparisons:

The scatter plot between GB hourly mean values around the OMI overpass timings (i.e. mean values of hourly GB data before, after and during overpass) and OMI derived SO_2 measurements is shown in Figure 3.2. It is evident from the figure that OMI derived measurements showed a low linear relationship with GB data with a regression coefficient of about 0.3.

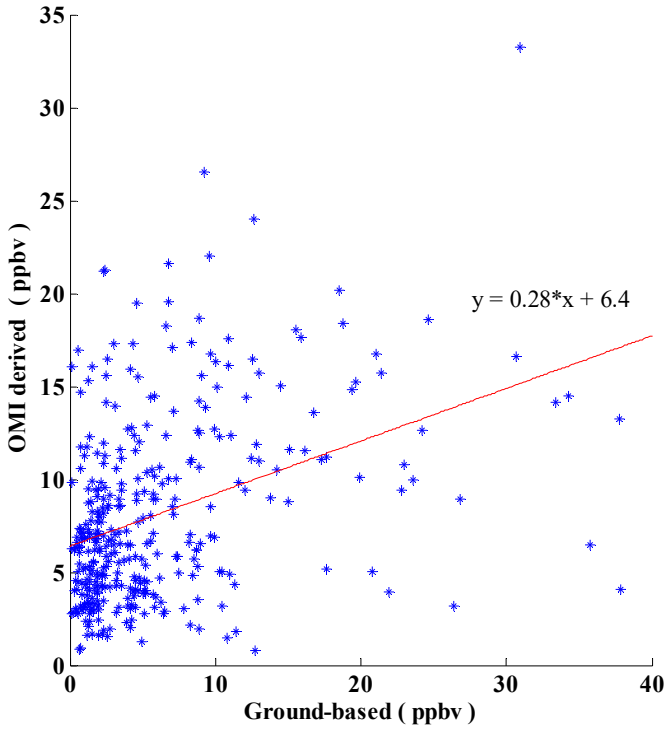

Figure 3.2: Scatter plots between Ground-based hourly mean values around the OMI overpass time and OMI derived SO_2 measurements. The regression line slope (red line) represents the correlation coefficient of ~ 30 %.

We also calculated the difference between GB data and OMI derived measurements (figure not shown). The mean difference between them was found to be -1.08 ppbv, which indicated that the satellite data overestimated values recorded at the surface. The observed difference might also be influenced by the input parameters (i.e. pressure values) used in these calculations and the assumptions employed while obtaining OMI PBL SO_2 including the height elevation. It should be noted here that Sharpeville has elevation (mean sea level) altitude of about 1.5 km.

3.3.1.2. Inter-annual mean comparisons

***3.3.1.2.1. Inter-annual variations*:** According to the inter-annual variations, the highest SO_2 values of GB and OMI derived measurements were only in winter periods of all the selected years. This further proved that pollutants accumulate at surface levels during the winter period. GB underestimated OMI derived measurements in most of the cases, which is illustrated in Figure 3.3. This result was similar to the study conducted on SO_2 emissions from major power plants in Turkey (Firatli and Kaynak-Tezel, 2015). They have found that

the difference between OMI (level 2 and based on PCA algorithm) and GB measured SO_2 were high nearer to the location of electric generation power plants. The average SO_2 mean differences from 2007 to 2013, between OMI and GB was found to be around 2.24 ppbv, however the difference was found to be within the standard deviations (see Figure 3.3, vertical lines). These results were similar to those obtained by Lee et al., (2011). According to their estimation, OMI SO_2 columns and the bottom-up GEOS-chem model varied by a factor of 2 in the Highveld region during their study period of 2006, this was approximately equivalent to the present study. The scatter plot of OMI derived measurements (figure not given) is similar to that of daily mean scatter plot with a regression slope of about 0.42.

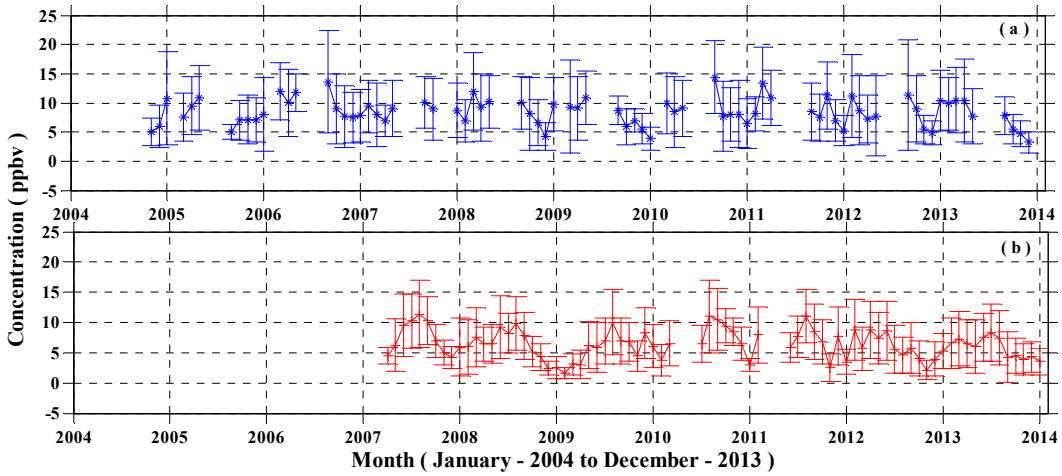

Figure 3.3: Year to year SO_2 variations by OMI derived (a) and Ground-based (b). Vertical lines represent ± 1 standard deviation.

3.3. 1.2.2.Yearly correlation*:* The yearly correlation analysis between GB and OMI derived measurements was done based on their monthly mean SO_2 values (see Table 3.1). Based on the results, years 2007, 2008, 2010 and 2013 showed high correlation *r* values of about 0.7, which was a good correlative result, whereas other years had a poor *r* value. However, it is noteworthy that the *r* value between their annual averages was 0.80.

Table 3.1. Correlation Coefficient (r) between Ground-based and OMI derived SO_2 measurements based on their monthly SO_2 averages for different year

Year	2007	2008	2009	2010	2011	2012	2013
	0.89	0.65	-0.42	0.65	-0.20	0.46	0.87

3.3.1.3. Seasonal comparisons

3.3.1.3.1. Seasonal Variations: The seasonally based comparisons indicated that GB and OMI derived measurements exhibited a fair seasonal variation. During summer, OMI derived calculations gave higher values and indicated a well marked difference with GB measurements as demonstrated in Figure 3.4. Both the SO_2 datasets (i.e. derived from GB and OMI) showed a general increasing trend between autumn (during April) and winter (during July), with a few exceptional cases, such as in March and August, where OMI derived measurements and GB data decreased, respectively. GB measurements thus showed a winter peak similar to that of the Vaal Triangle spatial SO_2 average concentration (Ncipha 2011). During spring, OMI data decreased steadily through the entire spring period. GB measurements also showed a rapid decreasing trend in October corresponding to a decrease of about 2 ppbv, this was followed in November by a slight increase. The deviations from the mean values ($\pm 1\sigma$) found to be almost similar for both OMI and GB. This observation was similar to the seasonal trends estimated by Laakso et al., (2012), in Elandsfontein (about 180 km from Sharpeville) between 2009 and 2011, where high SO_2 levels occurred in winter and early spring. Monthly mean values in winter were more than 20 ppbv as the site was impacted by a substantial number of industries and power stations. The SO_2 mean values in this study were at minimum levels during October–December (summer) when rainfall was a maximum (Janowiak 1988; Davis 2011; Laakso et al., 2012). Further, it has been noted from a study conducted on atmospheric transport by South African Fire-Atmosphere Research Initiative (SAFARI) in 1992, that during the spring season the main subsidence induced stable layer in the middle troposphere at a height of about 3.5 km above the surface was persistent throughout almost the entire period, whereas the lowest inversion layer at a height of about 1.5 km above the surface was frequently broken down by the passage of westerly wave disturbances. The wind speed was also maintained at high levels. These factors might lead to less accumulation of surface SO_2 and frequent long range transport, thereby lowering GB and OMI derived measurements of SO_2

values (Garstang et al., 1996). The average seasonal mean difference of surface SO_2 during the entire period between GB and OMI derived measurements was -2.32, whereas the relative percentage of difference was approximately -34.5%.

Therefore, the results suggest that OMI derived measurements overestimated GB SO_2 measurements throughout the entire period. It has been observed that OMI derived data was not compatible with GB especially in late spring and autumn where they both sometimes followed opposite trends.

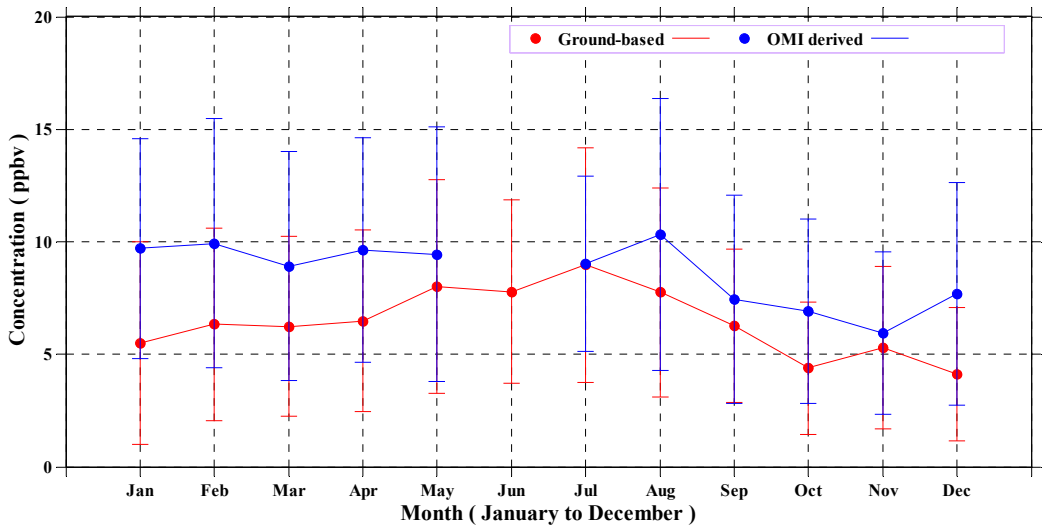

Figure 3.4: Overall seasonal SO_2 variations of Ground-based and OMI derived SO_2 measurements with data gap in June in OMI data. Vertical lines represent $\pm$1 standard deviation.

3.3.1.3.2. Seasonal correlation coefficient: The correlation coefficients (*r*) between GB and OMI derived measurements was calculated using the monthly mean SO_2 values of GB and OMI data for each season (Table 3.2). The results of correlation assessments are as follows:

Winter and summer had an average *r* value of nearly 0.6 and 0.38 respectively, whereas the transitional periods namely spring had a lower *r* value of 0.21 and autumn had lower negative *r* value. It is notable that *r* values based on daily means for all the seasons were

about 0.4 and had a reasonable correlative result as shown in Figures 3.5(*a*) and (*b*), (*c*) and (*d*), in particular for spring and winter.

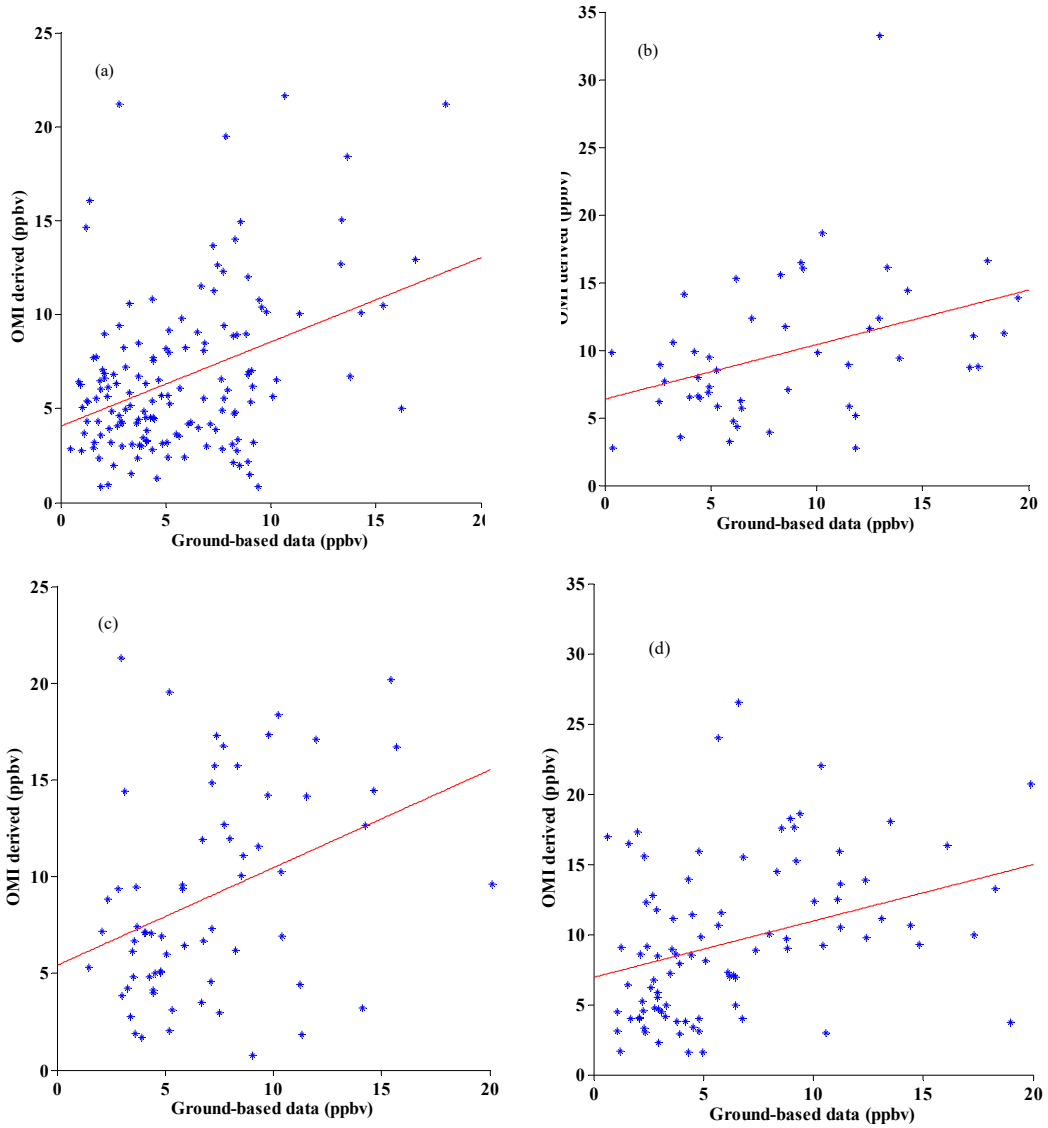

Figure 3.5: Scatter plots based on daily mean of Ground-based and OMI derived SO_2 measurements in spring (a); winter (b); autumn (c) and summer (d).

Table 3.2. Correlation Coefficient (r) between Ground-based and OMI derived SO_2 measurements based on their monthly SO_2 averages for various seasons

Season	Autumn	Winter	Spring	Summer
	-0.10	0.6	0.21	0.38

Thus, the seasonal correlative studies showed that winter had the better correlative result between the two types of measurements. This is an interesting result as the surface based

measurements of SO_2 cannot be a representative of the PBL in winter, as factors such as stable inversion layer, low surface albedo and high pressure could have negative effects. It could also due to different in two measurements techniques and employed instruments.

3.3.2 Comparative study of OMI BRD and PCA algorithm retrievals in relation to ground based measurements

Here, a comparative study of two OMI planetary boundary layer (PBL) sulphur dioxide (SO_2) products with Band Residual Difference (BRD) and Principal Component Analysis (PCA) techniques have been studied by estimating their monthly and seasonal variations in relation to their corresponding ground-based (GB) instrument variations during the time period from 2007 to 2013. The results showed that PCA retrievals followed similar trend and overestimated GB SO_2 values, whereas BRD retrievals underestimated them throughout the entire period. The SO_2 overall monthly variations measured by the GB instrument showed maximum values during winter. The daily, monthly regression analysis and seasonal correlation studies have also indicated that PCA technique performed better than BRD algorithm.

There are two types of OMI Planetary Boundary Layer (PBL) SO_2 data products. The former product was produced using BRD algorithm and after October 2014, a newly developed product was available which relies on PCA algorithm (OMSO2 README File, 2008). The BRD algorithm uses differential residuals at the following 3 wavelength pairs: 310.8 nm – 311.9 nm, 311.9 nm – 313.2 nm, 313.2 nm – 314.4 nm. Each pair residual is converted into SO_2 slant column density (SCD). The resulting SCD's of three pairs are averaged and converted into total SO_2 vertical column density (VCD) with the help of air mass factor (AMF) of 0.36 (Krotkov et al., 2006). The BRD algorithm depends on the instrument specific correction factor for radiance data set in order to decrease the noise and systemic biases on SO_2 retrieval (Li *et al.*, 2013). The newly developed PCA algorithm, instead of depending on the above said correction factors, directly applies PCA technique (a statistical procedure of inputting large set of correlated variables into small set of uncorrelated variables) to OMI level 1b radiance and irradiance data in the full spectra from 310.5- 340 nm, with the strongest SO_2 absorption band at 310.8 nm (Li et al., 2013). The retrieval noise is almost reduced by a factor of 2 when compared to BRD algorithm (see..OMSO2 README File, 2008).

Here, we have interpreted the performance of the earlier BRD algorithm OMSO2 PBL product and the newly launched PCA algorithm OMSO2 PBL product and check their agreement with GB data. This was done by performing a comparative study between the two OMI data products in relation to the ground-based (GB) data for a time period between 2007 and 2013.

3.3.2.1. Inter-annual Variations

Annual averages based on monthly means of GB data, PCA and BRD algorithms for each year were calculated and are given in Figure 3.6. It is to be noted that OMI data from 2004 was considered for trend analysis. It was found that GB values showed a steady decreasing trend between 2010 and 2012, where 15% reduction was found. The same trend was followed by both PCA and BRD algorithms, however BRD algorithm showed only a moderate annual variation while PCA showed a well defined annual variation where year 2006 had the highest SO2 value of 10 ppbv, followed by 2010 of 9 ppbv, but after 2010 showed a decreasing trend of 16% similar to GB data. However, BRD algorithm showed the highest value of only 5.4 ppbv in 2004, but between 2010 and 2012 a 12% decreasing trend was shown. Thus, all the three measurements resembled each other by showing a decline in SO2 after 2010.

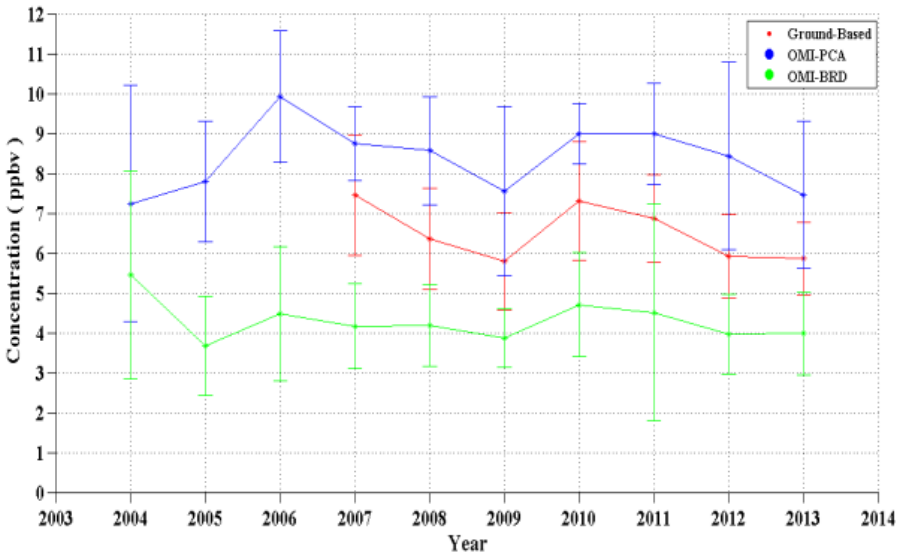

Figure 3.6: Inter-annual average values of GB data, OMI PCA and BRD algorithm retrievals. The vertical line represents ± 1 standard deviation.

3.3.2.2 Seasonal Variations

Seasonal variations of GB values, PCA and BRD algorithm retrievals for the time period were estimated by calculating the overall monthly mean values and is displayed in Figure 3.7. It is noted that there is no satellite overpass data for the month of June. The GB data showed a well marked seasonal difference where it started to increase from March (entire period) and reached a peak value of 9 ppbv in July (entire period), but later on showed a decreasing trend until it reached a minimum value of 3.5 ppbv during December. The comparative study of the three methods showed that PCA algorithm overestimated, whereas BRD algorithm underestimated GB values. The underestimation of BRD algorithm might be due to the errors caused by non-linear relationship between the band residual differences of three wavelength pairs selected in the BRD algorithm and high ozone residuals during high SO_2 events, which limit the retrieval capacity of BRD algorithm (Yang et al., 2007 and 2009). It showed lower ranges between 3 ppbv and 5 ppbv throughout the entire season, GB data ranged between 4 and 9 ppbv and PCA algorithm showed slightly higher ranges between 6 ppbv and 10 ppbv. Hence, the overall mean for the entire period for PCA algorithm was almost twice as that of BRD algorithm (8.6 ppbv for PCA and 4.1 ppbv for BRD) and the GB data had medium range levels of 6.4 ppbv. PCA algorithm showed better seasonal variation similar to GB data, with higher values until winter, but later on started to decline in spring where lower levels were maintained during this season. Contrary to this, BRD algorithm did not exhibit clear seasonal changes and measurements remained below 5 ppbv all throughout the entire period. The absolute overall relative percentage differences for PCA and BRD algorithms with GB data was almost the same at 35%, but in summer the relative percentage of differences between GB data and PCA algorithm was higher when it reached almost -80% . Besides this, PCA algorithm had higher standard deviations of almost double than that of BRD algorithm.

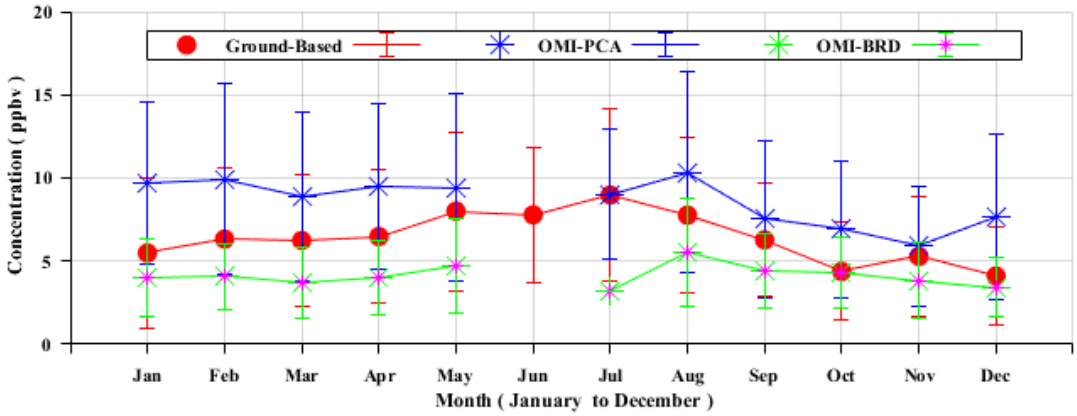

Figure 3.7: Overall seasonal variations of GB values, OMI PCA and BRD algorithm retrievals. The vertical line represents ± 1 standard deviation.

3.3.2.3 Relationship between GB values and OMI PCA and BRD algorithm retrievals

The correlation studies were conducted between GB values and PCA algorithm, and GB data and BRD algorithm for each season based on their daily mean values. Table 3.3 lists the correlation coefficient value (R) of PCA and BRD algorithms with GB values for each season. The table shows that PCA algorithm showed a better correlation result with GB values in comparison to BRD algorithm. However, only a moderate relationship was seen in PCA algorithm for all the seasons. The reason is also due to the daily mean values of GB data and a single overpass data from satellite data considered for this study. The background atmospheric conditions (such as pressure, humidity, wind speed, temperature), PBL dynamics (including turbulence, buoyancy, height) varies and various other parameters play an important role. The scatter plots of daily mean values between GB data and PCA algorithm, and GB data and BRD algorithm in Figures 3.8(a) and (b) also showed that PCA algorithm agreed with GB data better than BRD algorithm, where the slope of the regression line was 0.47 which was in contradiction with BRD algorithm where the slope was only 0.067. The monthly mean scatter plots (figure not shown) also supported this finding where the PCA algorithm had a slope of 0.42 and BRD algorithm had only 0.11. However, coefficient values of 0.7 and 0.67 for PCA and BRD algorithms, respectively, between annual averages were found.

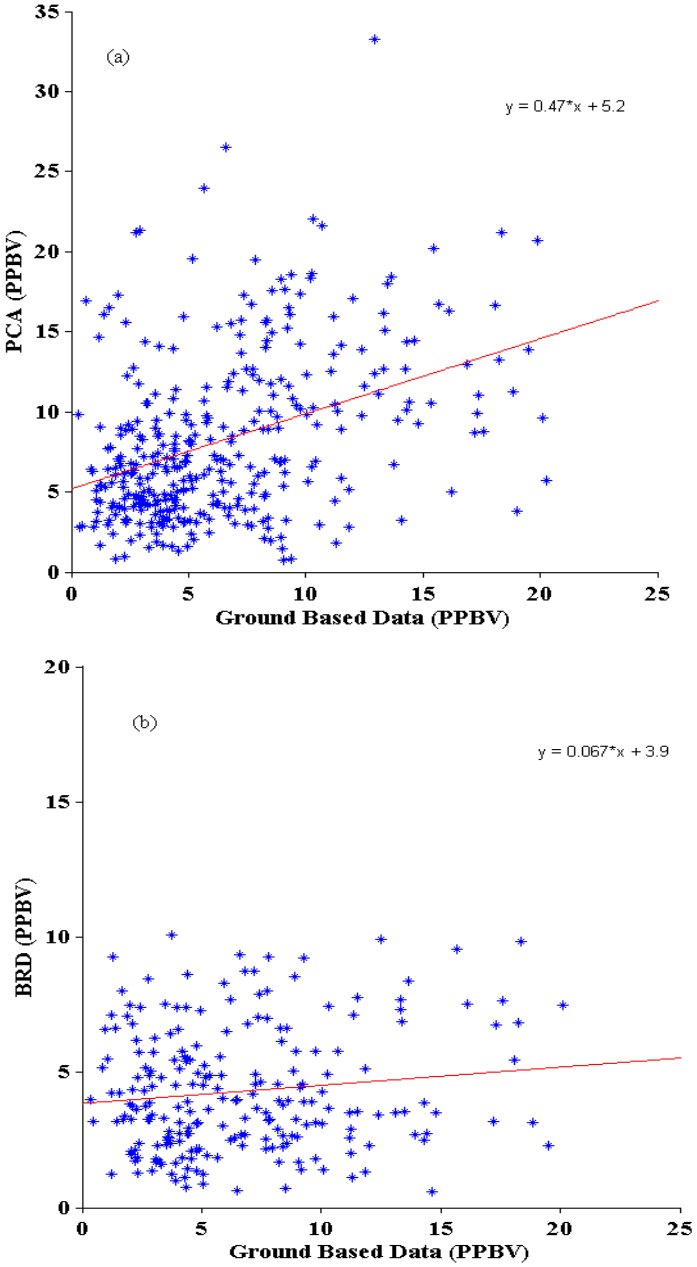

Figure 3.8: Scatter plots (Daily Mean): GB values & PCA (a); GB & BRD (b) algorithm retrievals.

Table 3.3: Correlation Coefficient between GB values & PCA algorithm retrievals and GB values & BRD algorithm retrievals over different seasons

Season	**Summer**	**Autumn**	**Winter**	**Spring**
PCA	0.34	0.37	0.38	0.39
BRD	0.25	0.22	-0.04	0.07

A comparative study showed that PCA algorithm overestimated GB data whereas BRD, which always had lower ranges thus underestimated GB data. A strong inter-annual variation was seen in both GB data and PCA algorithm than BRD algorithm. Nonetheless, the three measurements proved that SO_2 levels reduced eventually after 2010. Similarly, clear seasonal changes were shown by both GB data and PCA algorithm whereas BRD algorithm showed fair variations. Besides this, the daily, monthly mean values further indicated that PCA values were correlated better with GB data than BRD values.

The overall results thus proved that the newly developed PCA algorithm retrievals were in better agreement with GB values than BRD algorithm retrievals and could identify increase in SO_2 values both on seasonal and yearly time scales. Thus, the newly developed OMI PCA algorithm could be used as a surrogate for remote areas with no ground based stations, in examining SO_2 variations in such areas on long time basis qualitatively.

3.3.3. SO_2 variations from satellite-borne measurements

3.3.3.1. OMI Daily Mean: The daily mean values for OMI derived SO_2 measurements are plotted in the Figure 3.9. The obtained results are as follows:

Nearly 75% of the SO_2 values remained below 20 ppbv. The ranges were between 5 and 20 ppbv. The occurrence of values exceeding 20 ppbv was both in late summer and in winter periods, unlike GB where high values occurred only in winter and rarely in summer. This was similar to the results obtained over the global SO_2 level in 2006 by Lee et al. (2011). In their study, the same level 2 PBL SO_2 data product was used, but the retrieval algorithm was BRD. According to their results, a weak seasonal variation was exhibited, however high SO_2 columns were seen in the central region of South Africa, both in summer and in winter. The highest SO_2 value measured by OMI in this study was noted in July 2012 with a corresponding value of 33 ppbv.

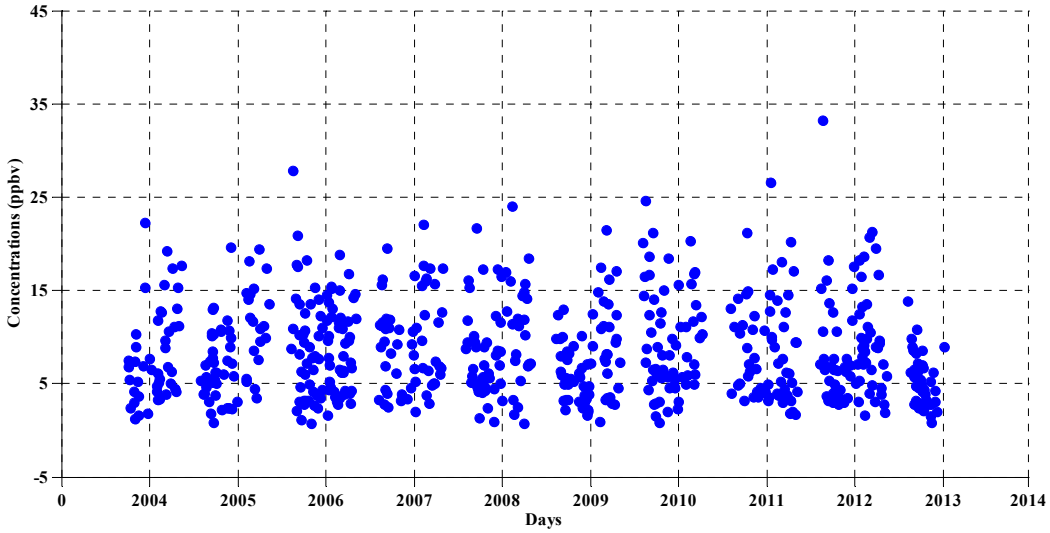

Figure 3.9: Daily mean SO_2 variations based on OMI derived measurements.

3.3.3.2.OMI annual variations: The annual (year to year) variations of OMI derived SO_2 measurements is shown in Figure 3.10. The figure is overlaid with GB SO_2 measurements for comparative purposes. It is noted from the figure that a decreasing trend in the last three years corresponding to approximately 15% reduction in SO_2 average was observed by GB between 2011 and 2013. In addition to this, OMI derived measurements had two sharp rises in SO_2 value one in 2006 and other in 2010, but after this there was a gradual decrease in SO_2 level similar to GB and reached minimum level in 2013. A 17% decrement was seen during 2011-2013. However, this decreasing trend was relatively small when compared to other countries like U.S.A and Europe, where more than 40% emission reduction was made over the period 2005 to 2010 (Klimont et al., 2013), but still resembled that of the Middle East where about 20% decreasing trend was estimated by OMI for the period 2010 to 2013 (Krotkov et al., 2015). The overall average SO_2 values from 2004 to 2013 for OMI derived measurements was 8.5 ppbv, thus it had approximately ~ 1.5 DU. This was slightly higher than that estimated by Theys et al. (2015). They applied the Differential Optical Absorption Spectroscopy (DOAS) algorithm to OMI SO_2 data. In their study on the global distribution of SO_2 columns, they found that the overall average of the SO_2 columnar amount from 2004 to 2009 in the Highveld region was approximately 1 DU. This might be due to the removal of more biases by principal components and strong SO_2 spectra in PCA technique.

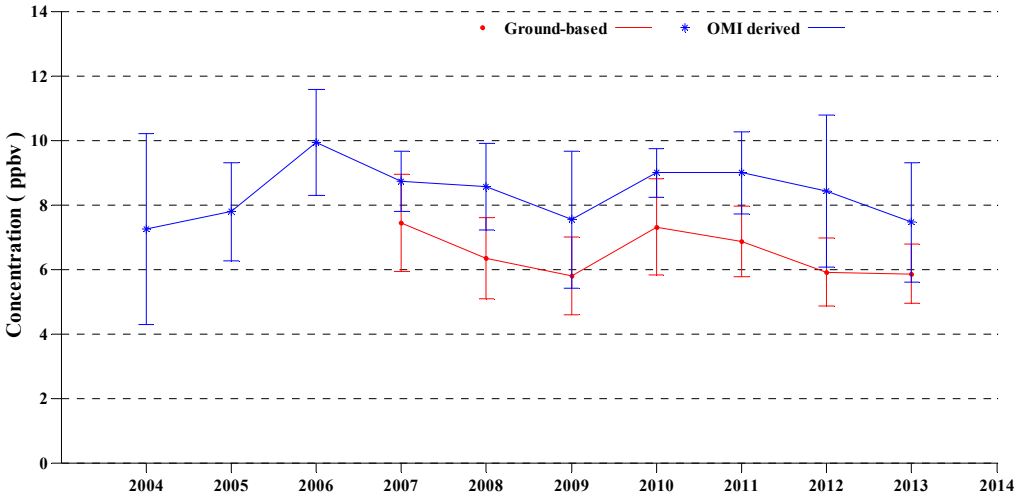

Figure 3.10: Inter-annual variations of Ground-based and OMI derived measurements of SO_2. Vertical lines represent ± 1 standard deviation.

3.3.3.3. OMI seasonal variations*:* The intra-seasonal variations of OMI derived SO_2 measurements with vertical lines representing ± 1 standard deviation is displayed in Figure 3.11 for four different seasons (see Figures 3.11*a-d*). The obtained main results are as follows:

The SO_2 values ranged between 4.4 ppbv and 15 ppbv. In contrast to GB data, only 60% of the values were within 10 ppbv. The outliers occurred during summer and winter periods. The year 2010 had the highest SO_2 mean value of about 14.4 ppbv in winter. The standard deviation ranged from approximately 2 ppbv to 9 ppbv. The fact that the deviation was found to be higher in winter which could be due to fewer measurements as there were no measurements recorded during June and July. The overall mean standard deviation during the entire time period was approximately 4 ppbv.

Thus, it is evident that the SO_2 values were high when compared to GB data. Furthermore, the number of outliers above 10 ppbv was greater with around 13. This was in contradiction with GB SO_2 outliers, which were 6 in total. However, the OMI derived SO_2 measurements had a mean standard deviation of about 4 ppbv (equivalent to about 0.8 DU) which was insignificant with the expected root mean square of approximately 0.5 DU by PCA algorithm over the regions between 30°S and 30°N (See..OMSO2 README File, 2008).

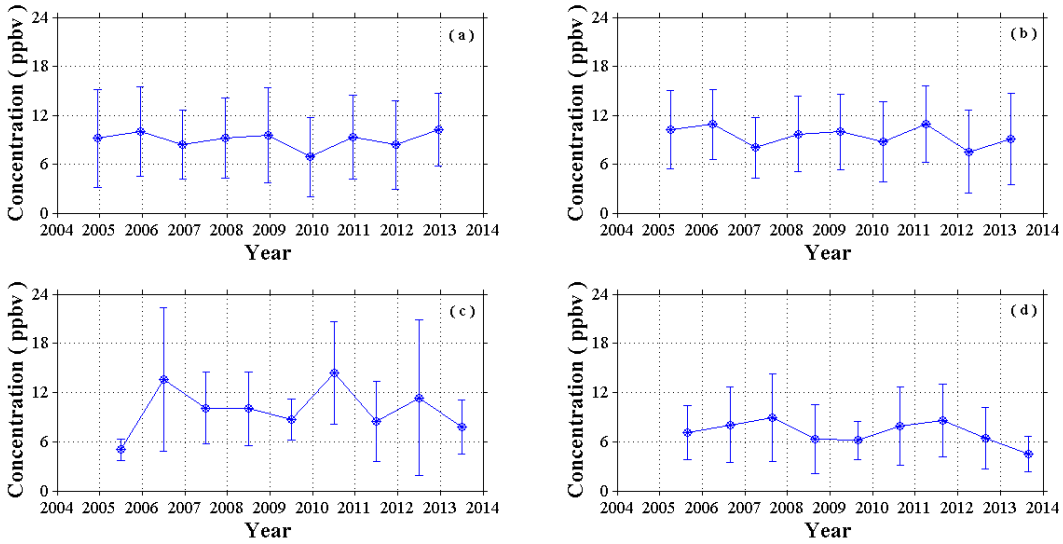

Figure 3.11: Intra-seasonal variations of OMI derived measurements depicting monthly SO_2 averages in four main seasons where Top left (a) summer (Dec-Feb); Top Right (b) autumn (Mar-May); Bottom Left (c) winter (Jun-Aug); Bottom Right (d) spring (Sep-Nov), based on the data from Dec 2004-Dec 2013. Summer mean values calculated for the December (corresponding year), January to February of the following years. Vertical lines represent $\pm$1 standard deviations.

The overall seasonal variations of OMI derived SO_2 measurements showed that the SO_2 mean values did not exceed 10 ppbv for all the seasons except in winter (August) where it reached 13.5 ppbv. The values were about 9$\pm$3.5 ppbv throughout the entire period, excluding the spring and early summer, where they were lower than below 8 ppbv. The lowest value of 4.5 ppbv was recorded in spring 2013.

3.4. Discussion and conclusion

The outcome of this study illustrates two important findings. Firstly, it was found that both the estimations from GB data and OMI surface-based measurements showed higher SO_2 values in winter and secondly, in summer only OMI surface-based measurements showed higher SO_2 values. Several meteorological factors play a vital role with respect to this observation. The wind speed estimation in this investigation, found that wind speed was low in winter and also noted high pressure exists during this period, which is characterised by calm conditions. The prevalence of low wind speed controls the horizontal transport of pollutants (Annegarn and Scorgie, 1997) and thus the surface SO_2 rise from January until

July. After the post winter period until early summer, the wind speed increased. This could lead to long range transport and dispersion of pollutants thereby lowering SO_2 amounts in these periods. Apart from this, periodic recirculation of air from the Highveld region occurs mostly in the lower troposphere (800-700 hPa) (Freiman and Piketh, 2003). When this re-circulated air mixes with the pre-existing ground level SO_2 rich air, this could lead to high surface level episodes in winter. A contrasting phenomenon occurs in summer when the recirculation of air from the Highveld was more frequent in the upper troposphere (600-500 hPa) than the surface level (Freiman and Piketh, 2003). In addition, the 500 hPa stable layer was more frequent and persistent, whereas the lowest 700 hPa was eroded frequently by easterly waves in summer (Freiman and Tyson, 2000). Apart from this, in summer the convergence of air masses occur by two main principal mechanisms namely Congo air boundary and Intertropical Convergence Zone (ITCZ). These two convergence systems in summer bring thunderstorms and frequent uplift of air (Kruger et al., 2010). These climatological conditions prevailing in winter and summer support our findings for higher SO_2 values in winter by both the measurements whereas in summer by OMI only. Furthermore, Li et al. (2013) have indicated that the newly developed PCA algorithm is able to capture SO_2 variations even on daily time scales. Thus the daily mean comparisons in this study also proved that the OMI surface-based method Upper Range Limit (URL) were equivalent and they even exceeded that of the GB amount in some cases and therefore could measure increase in SO_2 values similar to GB data (especially in winter) on a daily basis.

In a study conducted on the relationship between the SO_2 concentration and the meteorological conditions prevailing in the North China Plain during winter periods of 2006 - 2015, they found that the top 10% percentile of high SO_2 days detected by OMI were highly influenced by increase in geopotential metre (gpm) height over 850 hpa, high surface pressure and relative humidity, warm temperature, slow wind speed. According to them, high gpm was the major causative source for the observed higher SO_2 levels, as it led to more stagnant conditions and thus hindered the dispersal of air. In addition, they noticed increased SO_2 concentration when the precipitation was slightly drier. They also observed a good agreement between OMI measurements and chemistry transport model SO_2 emissions during winter while a non-linear relationship existed when SO_2 emissions were

compared with the ground based SO_2 measurements. It was suggested that the background meteorological parameters play a major role for such discrepancies (Calkins et al., 2016).

It should be noted that since the monitoring station was located near to some major industrial sources, an analysis on seasonal variation of wind direction should be estimated and hence the meridional and zonal wind velocity for the time period from 2004 to 2013 were obtained from MERRA data over the site location (figures are not shown). It has been identified from both meridional and zonal wind velocity that during January to March, the wind direction was north easterly, whereas from April to December, it was north westerly. These results were similar to those obtained by a study conducted on Air quality impact assessment at Vanderbijlpark works during January 2005 to December 2007 where the annual average wind rose were predominantly from north westerly and easterly direction, but in contrast, in winter both north westerly and south westerly winds prevailed (Watson and Thompson, 2014). In another study on population exposure to pollutants in the VAAL Triangle, the seasonal average wind rose in Vereeniging during 1994-1997 showed that northerly to north-north westerly winds predominated in winter, whereas in summer, easterly winds were dominant (Liebenberg,1999). Thus, this study also found that the majority of wind flow was from northerly to north westerly direction in almost all seasons. These events might have carried additional SO_2 amounts from its neighbouring industrial sites like Vereeniging CBD and Arcelo- Mittal Vanderbijlpark works rather than aiding dilution.

The overall results of this study showed that OMI derived method followed a similar trend equivalent to its counterpart i.e. the GB data, although they differ in magnitudes, where several meteorological parameters, physical and chemical complexity in the PBL layer acts as a barrier for OMI's retrieval. Thus, it can be concluded that OMI data in lieu of GB quantitative SO_2 measurement may be used in conjunction with air pollution models in order to clearly monitor the seasonal or monthly SO_2 trends qualitatively in places where there is no GB monitoring station. However, this study must be extended to many more ground site measurements for higher confidence and is demonstrated in the following chapter.

3.5 References

Annegarn, H. J. and Scorgie. Y., 1997. An Air Quality Management Strategy for the Vaal Triangle Part II. *Clean Air Journal 9*, pg.11-20.

Bauduin, S., Clarisse, L., Hadji-Lazaro, J., Theys, N., Clerbaux, C. and Coheur. P.F., 2016. Retrieval of near-surface sulfur dioxide (SO_2) concentrations at a global scale using IASI satellite observations. *Atmospheric Measurement Techniques, 9*(2), pg.721-740.

Blond, N., Boersma, K.F., Eskes, H.J., van der, A.R.J., Van Roozendael, M., De Smedt, I., Bergametti, G. and Vautard. R., 2007. Intercomparison of SCIAMACHY nitrogen dioxide observations, in situ measurements and air quality modeling results over Western Europe. *Journal of Geophysical Research: Atmospheres, 112*(D10). doi:10.1029/2006JD007277.

Boersma, K. F., Eskes, H.J., Veefkind, J. P., Brinksma, E. J., Van Der R. J., Sneep, A. M., Van Der Oord, G. H. J., et al. 2006. Near-real time retrieval of tropospheric NO_2 from OMI. *Atmospheric Chemistry and Physics Discussions, 6*(6): pg.12301-12345.

Calkins, C., J. Wang, C.Ge., Anderson, M. and Yang. K., 2016. Effects of meteorological conditions on sulfur dioxide air pollution in the North China Plain during winters of 2006-2015. *Atmospheric Environment, 147*: pg.296-309.

Carn, S. A., Krueger, A.J., Krotkov, N.A., Yang, K. and Levelt, P.F., 2007. Sulfur dioxide emissions from Peruvian copper smelters detected by the Ozone Monitoring Instrument. *Geophysical Research Letters, 34*(9). doi: 10.1029/2006GL029020.

Chance, K. 2013. NASA ups the TEMPO on monitoring air pollution. *Earth Observer 25*(2): pg.10.

Davis, C. L. 2011. Climate Risk and Vulnerability: A Handbook for Southern Africa*Council for Scientific and Industrial Research, Pretoria, South Africa*: ISBN 978-0-620-50627-4: pg.1-92.

Duncan, B.N., Prados, A.I., Lamsal, L.N., Liu, Y., Streets, D.G., Gupta, P., Hilsenrath, E., et al., 2014. Satellite data of atmospheric pollution for U.S. air quality applications: Examples of applications, summary of data end-user resources, answers to FAQs, and common mistakes to avoid. *Atmospheric Environment, 94*: pg.647-662.

Fioletov, V. E., McLinden, C.A., Krotkov, N.A., Li, C., Joiner, J., Theys, N., Carn, S. and Moran, M.D., 2016. A global catalogue of large SO2 sources and emissions derived from Ozone Monitoring Instrument. *Atmospheric Chemistry and Physics Discussions, 16*: pg.11497–11519. http://dx. doi. org/10.5194/acp-2016-417.

Fioletov, V. E., McLinden, C.A., Krotkov, N., Moran, M.D. and K. Yang, K., 2011. Estimation of SO_2 emissions using OMI retrievals. *Geophysical Research Letters, 38*(21). doi:10.1029/2011GL049402.

Firatli, E. and Kaynak-Tezel. B., 2015. Evaluation Of SO_2 Emissions From Large Scale Power Plants Using OMI SO_2 Retrievals For Turkey. *Wessex Institute of Technology (WIT) Transactions on The Built Environment, 168*: pg.677-688.

Freiman, M. T. and Piketh, S. J., 2003.Air transport into and out of the industrial Highveld region of South Africa. *Journal of Applied Meteorology, 42*(7): pg.994-1002.

Freiman, M. T. and Tyson, P. D., 2000. The thermodynamic structure of the atmosphere over South Africa: Implications for water vapour transport. *Water SA-Pretoria- 26*(2): pg.153-158.

Garstang, M., Tyson, P.D., Swap, R., Edwards, M., Kållberg, P. and Lindesay, J.A., 1996. Horizontal and vertical transport of air over southern Africa. *Journal of Geophysical Research: Atmospheres, 101*(D19): pg.23721-23736.

Ge, C., Wang, J., Carn, S., Yang, K., Ginoux, P. and Krotkov. N., 2016. Satellite-based global volcanic SO_2 emissions and sulfate direct radiative forcing during 2005–2012. *Journal of Geophysical Research: Atmospheres, 121*(7): pg.3446-3464.

GES DISC News (Goddard Earth Sciences Data and Information Services Center). New algorithm improves observation of sulfur dioxide in the atmosphere by OMI. Accessed 25 February 2015. https://disc.sci.gsfc.nasa.gov/data-holdings/gesNews/omi_so2_new_algorithm. https://en.wikipedia.org/wiki/Data_consistency (Accessed on 05 June 2017).

Janowiak, J. E. 1988. An investigation of interannual rainfall variability in Africa. *Journal of Climate, 1*(3): pg.240-255.

Josipovic, Miroslav. 2009. Acid deposition emanating from the South African Highveld-a critical levels and critical loads assessment. Ph.D thesis, Faculty of Science, University of Johannesburg, Johannesburg, South Africa.

Josipovic, M., Burger, R. P., Annegarn, H. J., Pienaar, J. J., Piketh, S. J. and Kneen, M. A., 2013. Atmospheric boundary layer reduction enabled comparison of remotely sensed and surface measured trace gas concentrations over South Africa *29th Annual conference of South African Society for Atmospheric Sciences (SASAS) 2013*, Salt Rock Hotel, Kwa-Zulu Natal, 26/09/2013 - 27/09/2013. ISBN 978-0-620-56626-1: 91-94.

Klimont, Z., Smith, S. J. and Cofala, J.,. 2013. The last decade of global anthropogenic sulfur dioxide: 2000–2011 emissions. *Environmental Research Letters, 8*(1): 014003. doi: http://dx.doi.org/10.1088/1748-9326/8/1/014003.

Krotkov, N.A. and Li, C. 2012. OMSO2 Version 003: OMI/Aura Sulphur Dioxide (SO2) Total Column 1-orbit L2 Swath 13x24 km. Greenbelt, MD, USA: Goddard Space Flight Center Distributed Active Archive Center (GSFC DAAC). doi:10.5067/Aura/OMI/DATA2022 (accessed on 28 February 2016).

Krotkov, N. A., McLinden, C. A., Li, C., Lamsal, L. N., Celarier, E. A., Marchenko, S.V.,. Swartz, W.H., et al., 2015. Aura OMI observations of regional SO_2 and NO_2 pollution changes from 2005 to 2014. *Atmospheric Chemistry and Physics Discussions, 15*: pg.26555-26607.

Kruger, A. C., Goliger, A. M., Retief, J. V. and Sekele, S., 2010. Strong wind climatic zones in South Africa. *Wind and Structures, 13*(1): p.37.

Laakso, L., Vakkari, V., Virkkula, A., Laakso, H., Backman, J., Kulmala, M., Beukes, J. P., et al. 2012.South African EUCAARI measurements: seasonal variation of trace gases and aerosol optical properties. *Atmospheric Chemistry and Physics, 12*(4): pg.1847-1864.

Lee, C., Martin, R. V., van Donkelaar, A., Lee, H., Dickerson, R. R., Hains, J. C., Krotkov, N., Richter, A., Vinnikov, K. and Schwab, J.J., 2011. SO_2 emissions and lifetimes: Estimates from inverse modeling using in situ and global, space-based (SCIAMACHY and OMI) observations. *Journal of Geophysical Research-Atmospheres, 116*(D6). doi:10.1029/2010JD014758.

Li, C., Joiner, J., Krotkov, N. A. and Bhartia, P. K., 2013. A fast and sensitive new satellite SO_2 retrieval algorithm based on principal component analysis: Application to the ozone monitoring instrument. *Geophysical Research Letters, 40*(23): 6314-6318. doi:10.1002/2013GL058134.

Liebenberg, Hanlie., 1999. Air pollution population exposure evaluation in the Vaal triangle using GIS. Masters of Science diss., Faculty of Science, Rand Afrikaans University, South Africa.

McLinden, C.A., Fioletov, V., Shephard, M.W., Krotkov, N., Li, C., Martin, R.V., Moran, M.D. and Joiner, J., 2016. Space-based detection of missing sulfur dioxide sources of global air pollution. *Nature Geoscience, 9*: 496–500. doi:10.1038/ngeo2724.

Ncipha, Xolile Gerald, 2011. Comparison of air pollution hotspots in the Highveld using airborne data. Masters of Science, thesis, University of the Witwatersrand, Johannesburg.

OMI (Ozone Monitoring Instrument) Data User's Guide, OMI-DUG-5.0, January 5, 2012, Produced by OMI Team. https://docserver.gesdisc.eosdis.nasa.gov/repository/Mission/OMI/3.3_ScienceDataProductDocumentation/3.3.2_ProductRequirements_Designs/README.OMI_DUG.pdf (accessed on 19 August 2014).

OMSO2 README File v1.2.0 Released Feb 26, 2008 Updated: September 26, 2014. https://so2.gsfc.nasa.gov/Documentation/OMSO2Readme_V120_20140926.pdf. (accessed on 02 September 2015).

Reichle, R. H., 2012. The MERRA-Land Data Product GMAO Office Note No. 3 (Version 1.2): 38.. http://gmao.gsfc.nasa.gov/pubs/office_notes. (accessed on 9 July 2016).

Schmidt, A., Leadbetter, S., Theys, N., Carboni, E., Witham, C. S., Stevenson, J.A.,Birch, C.E., et al. 2015. Satellite detection, long-range transport, and air quality impacts of volcanic sulfur dioxide from the 2014–2015 flood lava eruption at Bárðarbunga (Iceland). *Journal of Geophysical Research: Atmospheres, 120*(18): pg.9739-9757.

Sinha, P., Hobbs, P.V., Yokelson, R. J., Blake, D. R., Gao, S. and Kirchstetter, T. W., 2003. Distributions of trace gases and aerosols during the dry biomass burning season in southern Africa. *Journal of Geophysical Research: Atmospheres, 108*(D17). doi: 10.1029/2003JD003691.

Sivakumar, V., Portafaix, T., Bencherif, H., Godin-Beekamnn, S. and Baldy, S., 2007. Stratospheric ozone climatology and variability over a southern subtropical site: Reunion Island (21°S; 55 °E). *Annales Geophysicae, 25*(11): pg.2321-2334.

Streets, D.G., Canty, T., Carmichael, G.R., de Foy, B., Dickerson, R.R., Duncan, B.N., Edwards, D.P., et al. 2013. Emissions estimation from satellite retrievals: A review of current capability. *Atmospheric Environment, 77*: pg.1011-1042.

Theys, N., De Smedt, I., Gent, J., Danckaert, T., Wang, T., Hendrick, F., Stavrakou, T., et al. 2015. Sulfur dioxide vertical column DOAS retrievals from the Ozone Monitoring Instrument: Global observations and comparison to ground-based and satellite data. *Journal of Geophysical Research: Atmospheres, 120*(6): pg.2470-2491.

Toihir, A.M., Bencherif, H., Sivakumar, V., El Amraoui, L., Portafaix, T. and N. Mbatha, N., 2015. Comparison of total column ozone obtained by the IASI-MetOp satellite with ground-based and OMI satellite observations in the southern tropics and subtropics. *Annales Geophysicae, 33*(9): pg.1135-1146.

Watson, R. M. and Thompson, S., 2014. Air Quality Impact Assessment for the upgrade of the Vacuum Arc Degasser Unit at ArcelorMittal South Africa Vanderbijlpark Works., Environment. Summary Report, ArcelorMittal South Africa Ltd. (http://southafrica.arcelormittal.com/Portals/0/Vanderbijlpark-Works-Environmental-Summary-Report-2014-Web.pdf - (accessed on 05 June 2017).

Yang, K., Krotkov, N.A., Krueger, A.J., Carn, S.A., Bhartia, P.K. and Levelt, P.F., 2007. Retrieval of large volcanic SO2 columns from the Aura Ozone Monitoring Instrument: Comparison and limitations, *Journal of geophysical research, 112(D24)*:DOI: 10.1029/2007JD008825.

Yang, K., Krotkov, N.A., Krueger, A.J., Carn, S.A., Bhartia, P.K. and Levelt, P.F., 2009. Improving retrieval of volcanic sulphur dioxide from backscattered UV satellite observations. *Geophysical research letters, 36(3)*: DOI: 10.1029/2008GL036036.

Ziemke, J.R., Chandra, S. and Bhartia, P.K., 2001. Cloud slicing: A new technique to derive upper tropospheric ozone from satellite measurements. *Journal of geophysical research, 106*(D9): pg9853-9867.

Ziemke, J.R., Chandra, S., Duncan, B.N., Froidevaux, L., Bhartia, P.K., Levelt, P.F. and Waters, J.W., 2006. Tropospheric ozone determined from Aura OMI and MLS: Evaluation of measurements and comparison with the Global Modeling Initiative's Chemical Transport Model. *Journal of Geophysical Research: Atmospheres, 111*(D19). doi: 10.1029/2006JD007089.

Chapter 4

Long-term Temporal and Spatial analysis of SO_2 over Gauteng and Mpumalanga monitoring sites of South Africa

This chapter is based upon

S. K. Sangeetha, M. Gebreslasie …..Long-term Temporal and Spatial analysis of SO_2 over Gauteng and Mpumalanga monitoring sites of South Africa, to be submitted to International Journal of environment and pollution, 2017 (to be submitted).

S.K. Sangeetha, V. Sivakumar, M. Gebraslasie and C.Y.Wright, Seasonal vertical variation in SO_2 over South Africa as observed by the Ozone Monitoring Instrument (OMI), *Proc. of 33nd Annual conference of South African society for atmosphere science, Protea Hotel Ranch Resort, Polokwane, (South Africa), ISBN* 978-0-620-77401-7, *Pg 82-85, 21 - 22 September 2017.*

Abstract

This chapter is focused on the temporal and spatial variability of sulphur dioxide (SO_2) from 2004 to 2013 over 36 ground-based (GB) stations located in Gauteng and Mpumalanga provinces of South Africa. The assessment was based on the *in situ* SO_2 data, where the GB stations were sorted into different groups and in addition, kriging based analysis were deployed to study their seasonal spatial variability. It was observed that Pretoria west, Witbank and Rand water had high SO_2 levels and standard deviations. Although, winter played a major role in having peak SO_2 values in most of the stations, a unique feature was observed in spring. It was noted that both diurnal and inter-seasonal variations in spring displayed lower SO_2 for Witbank and Pretoria west stations compared to other station in the region. The SO_2 values of these two stations were always maintained at high levels in all other seasons. Rand water had the highest standard deviation of 11.2 ppbv in October. A prominent seasonal variation was seen in all the groups, excluding Mpumalanga power stations (MP) group. This was particularly seen in the Vaal Triangle group. MP group ranked topmost level with elevated SO_2 values proceeded by the Highveld group in all the temporal time scales. The kriging based method, further proved that the highest SO_2 levels were centred around major industrial regions of Mpumalanga, regardless of all the seasons. The vertical variations of SO_2 using OMI measurements illustrated that winter was characterized by high and mostly dispersed than summer. In spring, relatively small amounts of SO_2 were seen in TRL, TRM and STL over the southern parts of the country. PBL and STL showed negligible SO_2 concentrations in all seasons over the regions except those falling inside the industrial Highveld.

4.1 Introduction

Air pollutants, particularly sulphur dioxide (SO_2) has become an important concern as it impacts on human health in many ways, like chronic obstructive pulmonary diseases (COPD) (Ghozikali, Mosaferi, Safari, and Jaafari, 2015), early asthmatic attacks in children (Clark et al., 2015) and also on the environment such as acid deposition and sulphate aerosol formation. In the past few decades, the developing countries in Asia, particularly China and India, increased the global SO_2 emissions by ~ 60% because of their rapid industrial growth (Smith et al., 2011). African countries provide ~ 5% of the total global SO_2 emissions and this will increase to about 30% by 2030 (Liousse, Assamoi, Criqui, Granier, and Rosset, 2014). South Africa as a developing nation rich in coal mines, with

progressive industrial growth still facing challenges regarding air pollution. The major percentage (~ 93%) of electricity generations is based on coal based power plants in the country (Menyah and Wolde-Rufael, 2010), due to the plentiful coal reserves in the country and releases nearly 1.5 million tons of SO_2 annually (Lloyd, 2002). Nearly ~ 95% of electricity generation is owned by ESKOM and the remaining percentage is maintained by the municipalities and private sectors (Pretorius, Piketh, Burger, and Neomagus, 2015; Spalding-Fecher and Matibe, 2003). The health outcomes from these municipalities owned power station emissions, however might be more vulnerable than that of ESKOM, as they are old and have low stack heights (Splading Fecher and Matibe, 2003). Thus in order to gain insight of SO_2 over a specific region it is worth to analyse its trend both on temporal and spatial basis. A continuous monitoring and reporting of air quality data is essential for effective air quality management practices to ensure that the pollutants are maintained within the standards (Macpherson et al., 2017). Spatial distribution of air pollutants and determining their seasonal trends using Geographic Information System (GIS) has become a helping tool in this era. A precise regional mapping of air quality is important for a constructive environmental mitigation and monitoring plan (Hamm, Finley, Schaap, and Stein, 2015). The temporal and spatial assessments of pollutants have been made in many countries over the past years. Zou et al. (2011) pursued AERMOD dispersion modelling and applied Ordinary Kriging (OK) method for the period from 1996 to-2002, to study the spatial and temporal trend of SO_2 in Dallas, USA. In addition, they mapped the variations of annual SO_2 concentrations according to specific sources and found that the traffic emission sources were the main contributor for significant variations in annual SO_2 concentrations. Wang et al. (2014) reported a study on spatial and temporal variations of six criteria pollutants including SO_2 in 31 cities in China utilising the hourly downloaded data from March 2013 to February 2014 and found that high SO_2 levels in the northern region during winter were due to coal consumption for domestic heating. In South Africa, Lourens et al. (2011), used passive sampling method to conduct the spatial and temporal distributions of gaseous pollutants for a year from August 2007-July 2008, over eight representative sampling sites for the Highveld region and perceived the contribution of industrial sources or the sites located downwind from these sources for high SO_2 concentrations. A decadal study on monthly mean SO_2 concentrations from 1995- to 2005 time period at four remote sites in southern Africa also confirmed that the highest SO_2 levels are concentrated in the industrial hot spot region of Mpumalanga (Martins et al., 2007). Venter et al. (2012), assessed a two year time period (2008-2010) of study on the

air quality in the Bushveld Igneous Complex of South Africa, where they selected Marikana, Northwest province as the representative site and explored the tall stack industrial sources for SO_2 emissions. Although a comprehensive exposition on SO_2 can be drawn from these studies, none of them deal with a complete spatial representation of SO_2, as conventional passive sampling and either a single representative or a remote site was used.

The main aim of the current study is to investigate the temporal and spatial variations of SO_2 derived from Ground-based (GB) data over 36 monitoring stations in South Africa. Since these GB measurements provide vital information even on small temporal resolutions, the first part analyses the temporal variation of the selected stations starting from the smaller resolutions (diurnal variations) through the daily, monthly variations and finally ending with the annual basis. Second part focusses on the spatial aspect, utilising the GIS based approach.

4.1. Data and methodology

4.2.1. *Ground-based data*

South African government has a wide variety of air quality monitoring stations, which are under the control of several network systems across the nation. The air quality data are collected, maintained, analysed and controlled by the South African Weather Service (SAWS) through the South African Air Quality Information System (SAAQIS). The raw data for this study was provided by the respective networks that are under the SAAQIS system. The SO_2 data were collected across 36 monitoring stations of different network providers from a time period of 2004 to 2013. Of these, 21 were from Gauteng, 14 from Mpumalanga and 1 (Zamdela) from the Free State province. Figure 4.1 shows the Geo Location of monitoring stations with some major power stations. These stations cover major coal industries, power stations, 2 air shed priority areas namely Vaal Triangle and Highveld priority areas and traffic related emissions in the metro cities of Pretoria and Johannesburg, which are of primary concern in relation to major pollutants. Eleven stations monitor the urban pollution, six in industrial areas and the rest falls in semirural or rural and mixed up categories.

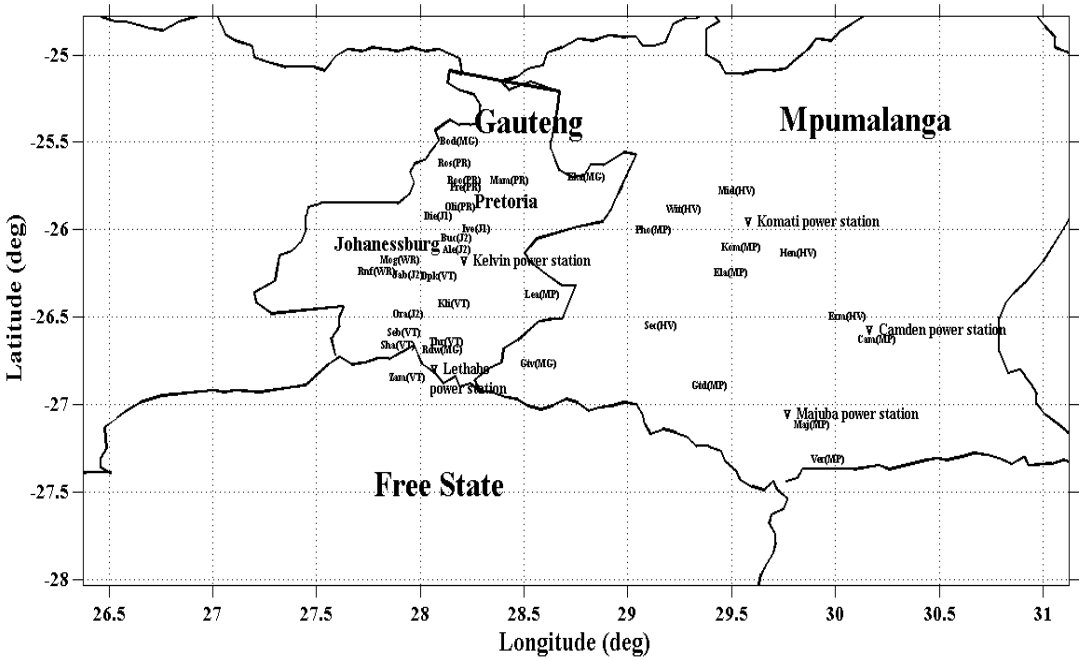

Figure 4.1: Geo-location of 36 monitoring stations with some power stations located near by some stations. The station names are abbreviated as in Table 4.1 and the group names given in brackets.

4.2.2. *Methodology*

It has been noted that there was no consistency in the time period of the stations and therefore, they were grouped according to the time period of SO_2 data available and also on the type of network. For example, it has been found that some of the Johannesburg stations had two different time periods although the network provider is the same for both (City of Johannesburg), so they were grouped into two categories Johannesburg 1 and 2. On the other hand, the miscellaneous group contains stations from the Tshwane Air Quality and ESKOM networks. Such grouping of data was done by Qu et al. (2010), in their study on spatial and temporal analysis of PM_{10} concentrations in 86 cities of China, where they have grouped the cities according to the time period of Air Pollution Index data and the geographical location of the cities. Table 4.1 shows the details of each group with their station names and time period. The abbreviations for each group and their station are given in brackets.

4.2.3. *Spatial Interpolation*

In this study, ordinary kriging (OK) method was used to interpolate the spatial distribution of SO_2 concentration between the monitoring stations, based on the ground-based data for each season. Kriging is a geo-statistical approach that is widely used in different fields such as remote sensing, environmental science and mining (Bayraktar, and Turalioglu, 2005). It depends on spatial autocorrelation that not only predicts the spatial measurement of values at certain points, but also measures the accuracy of the predictions. Numerous studies have been based on spatial dispersion of atmospheric pollutants using the kriging based approach. Xia et al. (2016) used OK for seasonal spatio-temporal variations of major pollutants during 2013 in Shenzhen city, China using GB data from 19 monitoring sites. Similarly, Feng et al. (2014) used the OK method and population distribution data to analyse the spatial distribution of domestic heating and found that the SO_2 were highly concentrated in the suburbs of Beijing during winter.

Table 4.1: Details of each grouping of stations with their time period, Group Name, Station Names, Network provider and Province

Group Name	Stations	Network	Province
Pretoria (PR)	Booysens (Boo)	Tshwane Air Quality	Gauteng
2009-2013	Mamelodi (Mam)	Tshwane Air Quality	Gauteng
	Olievenhoutbosch (Oli)	Tshwane Air Quality	Gauteng
	Pretoria West (Pre)	Tshwane Air Quality	Gauteng
	Rosslyn (Ros)	Tshwane Air Quality	Gauteng
Johannesburg (J1)	Diepsloot (Die)	City of Johannesburg	Gauteng
2009-2011	Ivory Park (Ivo)	City of Johannesburg	Gauteng
Highveld (HV)	Ermelo (Erm)	DEA	Mpumalanga
2008-2013	Hendrina (Hen)	DEA	Mpumalanga
	Middleburg (Mid)	DEA	Mpumalanga
	Secunda (Sec)	DEA	Mpumalanga

	Witbank (Wit)	DEA	Mpumalanga
Vaal Triangle (VT)	Diepkloof (Dpk)	DEA	Gauteng
2007-2013	Kliprivier (Kli)	DEA	Gauteng
	Sebokeng (Seb)	DEA	Gauteng
	Sharpeville (Sha)	DEA	Gauteng
	Three Rivers (Thr)	DEA	Gauteng
	Zamdela (Zam)	DEA	Free State
Johannesburg (J2)	Alexandra (Ale)	City of Johannesburg	Gauteng
2004-2010	Buccleuch (Buc)	City of Johannesburg	Gauteng
	Jabavu (Jab)	City of Johannesburg	Gauteng
	Orange Farm (Ora)	City of Johannesburg	Gauteng
Mpumalanga power stations (MP)	Camden (Cam)	ESKOM	Mpumalanga
2011-2013	Elandsfontein (Ela)	ESKOM	Mpumalanga
	Grootdraaidam (Gtd)	ESKOM	Mpumalanga
	Komati (Kom)	ESKOM	Mpumalanga
	Leandra (Lea)	ESKOM	Mpumalanga
	Majuba (Maj)	ESKOM	Mpumalanga
	Phola (Pho)	ESKOM	Mpumalanga
	Verkykkop (Ver)	ESKOM	Mpumalanga
Miscellaneous group (MG)	Grootvlei (Gtv)	ESKOM	Mpumalanga
2012-2013	Randwater (Rdw)	ESKOM	Gauteng
	Bodibeng (Bod)	Tshwane Air Quality	Gauteng
	Ekandustria (Eka)	Tshwane Air Quality	Gauteng

West Rand (WR)	Mogale city (Mog)	West Rand District Municipality	Gauteng
2013	Randfontein (Rnf)	West Rand District Municipality	Gauteng

4.3. Results

4.3.1. Ground Based SO_2 Temporal variations

4.3.1.1. Diurnal variation

4.3.1.1a Mean diurnal variation: In accordance with the results from Figure 4.2, it can be seen that Pretoria west of Pretoria group, showed both high SO_2 levels and standard deviation up to even $\sim 14 \pm \sim 15$ ppbv as the site was impacted by both industrial and residential sources. Similar to this, the stations in the Highveld group especially Witbank, Secunda that were representative of both type of emissions, showed double peaks although not prominently and also high SO_2 levels were maintained all throughout the entire day starting from morning until late evening (10 am - 7 pm). Stations like Witbank, Hendrina in this group even reached above 20 ppbv. An exclusive industrial signature was shown by Mpumalanga power stations group with constant high levels from morning until evening (local time from 10 am to 5 pm) where high SO_2 levels of $\sim$ 20 ppbv were seen in some stations like Komati and Grootdraaidam. This could be a combination of both industrial sources and the mixing of pollutants after the inversion layer breakage in the morning hours (Sundström et al., 2015; Vakkari et al., 2013; Venter et al., 2012).

Groups such as Johannesburg 1 & 2, Vaal Triangle (both industrial and household combustion) and stations like Mamelodi and Olievenhoubosch in the Pretoria group with predominance of domestic fuel burning, showed double peaks. However, stations like Alexandra, Jabavu and Orange farm of Johannesburg 2 group could also associated with traffic, as they peaked at 7 am and 6-7 pm, which correlated better with expected large road transportation during the time. It should be noted that the Buccleuch (Johannesburg 2) is impacted by vehicular emissions (DEA, 2012 SOUTH AFRICA ENVIRONMENT OUTLOOK, 2012) also had higher values ($\sim$ 12.5 ppbv) comparable to industrial group, as it lies in close proximity to the road transportations of national highway (N1) and metroway (M1) (Kgabi and Sehloho, 2012). Johannesburg 1 and the West Rand showed

the lowest SO_2 value of all groups. Miscellaneous group stations like Rand water and Grootvlei, showed high SO_2 levels only in the midday (11am-3pm), where Rand water had higher standard deviations than Pretoria west (~ 22 ppbv) during that hours. West Rand group comprising of Randfontein and Mogale city did not show any prominent diurnal variation, as their SO_2 levels were stable throughout the entire period.

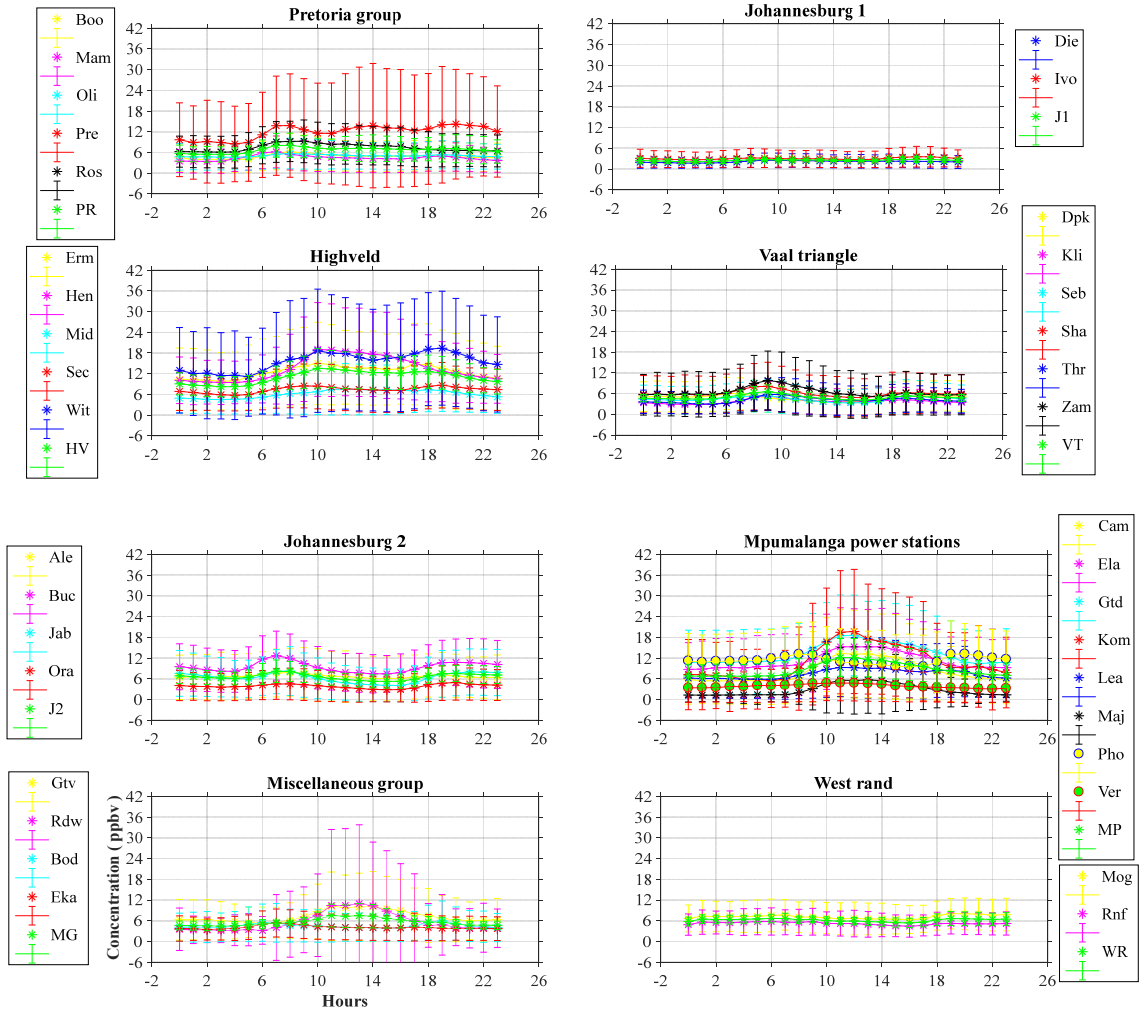

Figure 4.2: Diurnal variation of each group and their respective stations.

4.3.1.1b Seasonal diurnal variations

Winter: The winter diurnal variation of each group and their stations are shown in Figure 4.3. It can be deduced from the Figure that a single peak was seen in Pretoria (morning) except Pretoria west which had 3 peaks. The West Rand group showed an evening peak, whereas Johannesburg 1 & 2, Vaal Triangle, Highveld groups, Bodibeng station of Miscellaneous group showed double peaks which might be due to domestic burning of coal products for space heating in winter. Industrial signature was shown in Mpumalanga power stations group, where high values were maintained from late morning until evening due to the tall stack industrial emissions (Mugabo, 2011). In addition, some stations like Komati and Elandsfontein showed minor night peaks around 8 pm, which might be due to the anti-cyclonic stability over the Highveld which played a useful part in the accumulation of pollutants (Collett et al., 2010). The SO_2 levels of these Mpumalanga power stations, Highveld groups and the Pretoria west station were the highest as they rose up to ~ 18 ppbv, especially Witbank, which was ~ 29 ppbv in the evening. This high SO_2 peak values in winter could be the influence of more prominent multi-inversion layers when compared to other seasons (Venter et al., 2012). Similar to the average diurnal variation, here also the standard deviations of Pretoria west and Rand water stations were more ~ 20 ppbv. Zamdela showed higher values when compared to other stations in the Vaal Triangle group and this could be due to the neighbouring industrial emissions from the north of the site (Feig et al., 2014) like Sasolburg, NATREF and domestic fuel burning.

Summer: The summer diurnal variation of each group and their stations are depicted in Figure 4.4 and where, Pretoria and Johannesburg 1 groups did not show any peak values, especially Johannesburg 1 where the lowest SO_2 levels of ~2 ppbv were recorded. Johannesburg 2, Vaal Triangle, Miscellaneous, West Rand groups showed single peak in the morning after that the SO_2 levels got reduced. This might be due to the increase in the mixing height of the pollutants in summer (Korhonen et al., 2014) as the frequency of occurrence (40 %) of subsidence inversion layer was lower (Thomas and Scorgie, 2006) and thus enabling dispersion of pollutants (Lourens et al., 2011). Although the SO_2 levels of Highveld and Mpumalanga power stations group were within 12 ppbv, few stations like Witbank, Hendrina, Elandsfontein, Grootdraaidam and Komati showed high values ~18 ppbv during the operating hours of the industries.

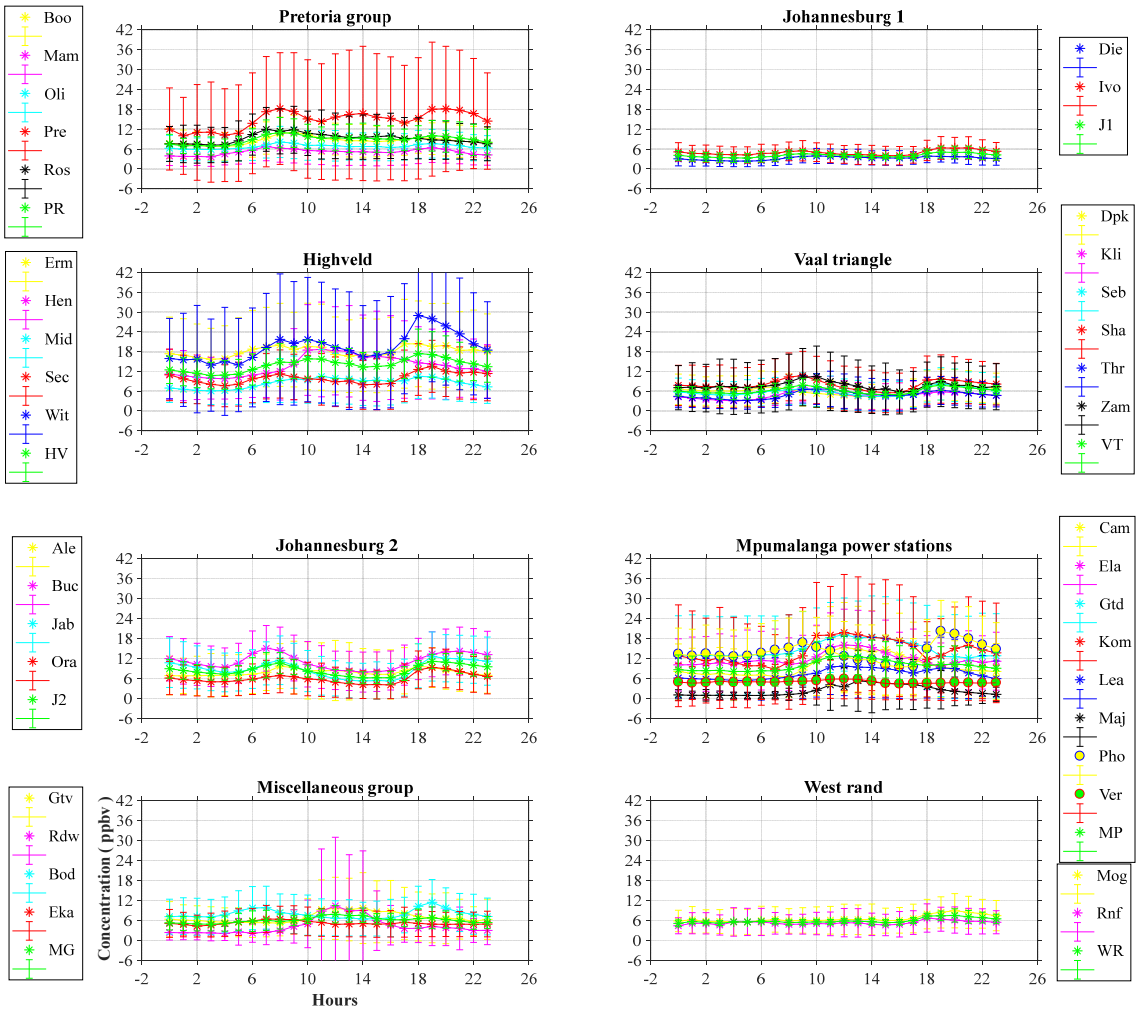

Figure 4.3: Winter diurnal variation of each group and their respective stations.

Spring and autumn: The variations in spring were almost similar to those exhibited in summer in all the groups (Figure 4.5). A remarkable difference was that Witbank and Pretoria west showed lower SO_2 levels in spring compared to other seasons, when Ermelo and Hendrina SO_2 values were higher than that of Witbank and similarly Rosslyn's SO_2 concentration was more than Pretoria west. It could be assumed that the westerly disturbances and anticyclonic circulations that were the dominant features in spring (Garstang et al., 1996; Tyson et al., 1996b) that could favour for the dispersion of pollutants away from the source region. In autumn, similar trends were seen in all the groups as in summer, however the SO_2 levels and standard deviations of Witbank ($\sim 24 \pm 20$ ppbv), Rand water ($\sim 20 \pm 20$ ppbv) and Komati ($\sim 21 \pm 17$ ppbv) were as high as in winter (see. Figure 4.6).

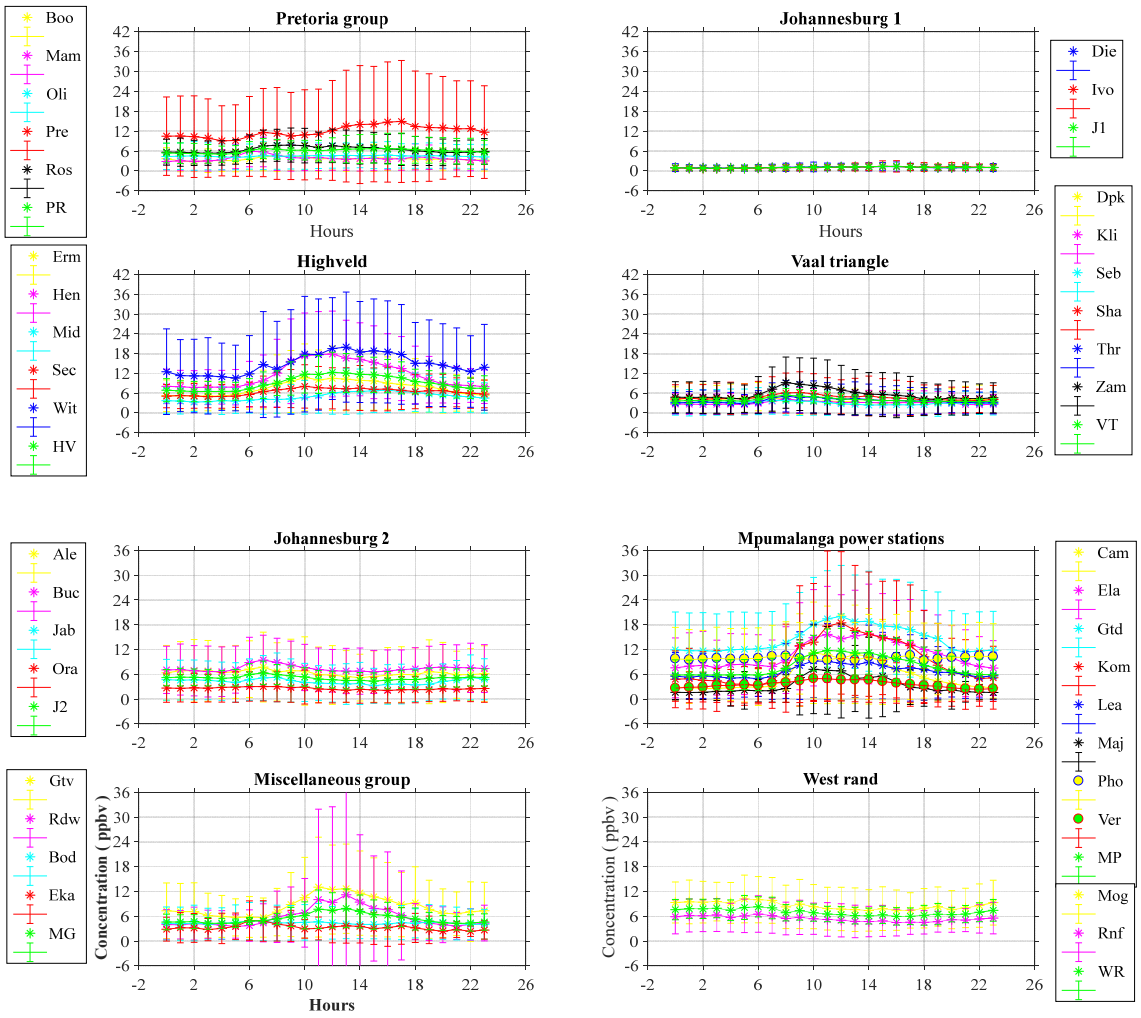

Figure 4.4: Summer diurnal variation of each group and their respective stations.

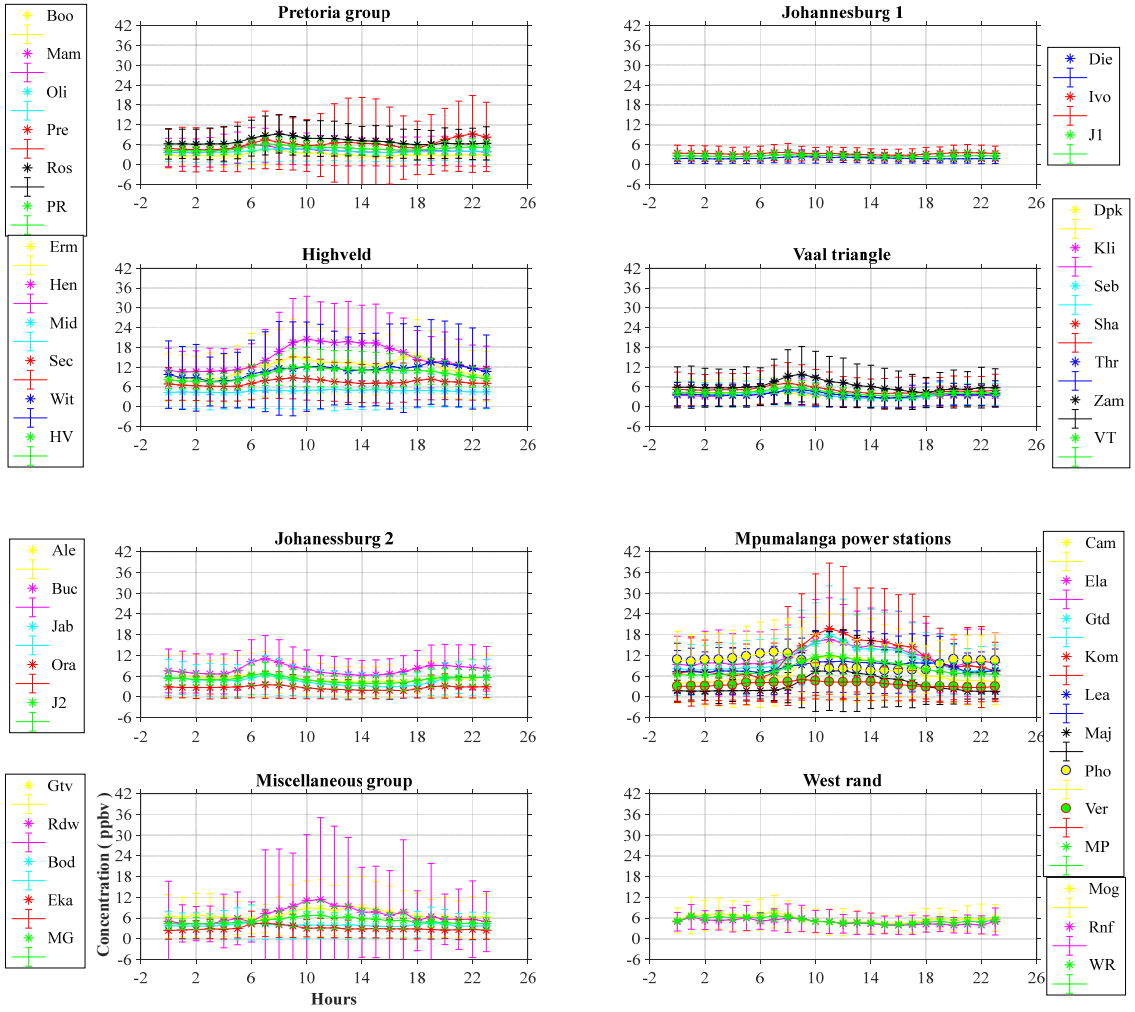

Figure 4.5: Spring diurnal variation of each group and their respective stations

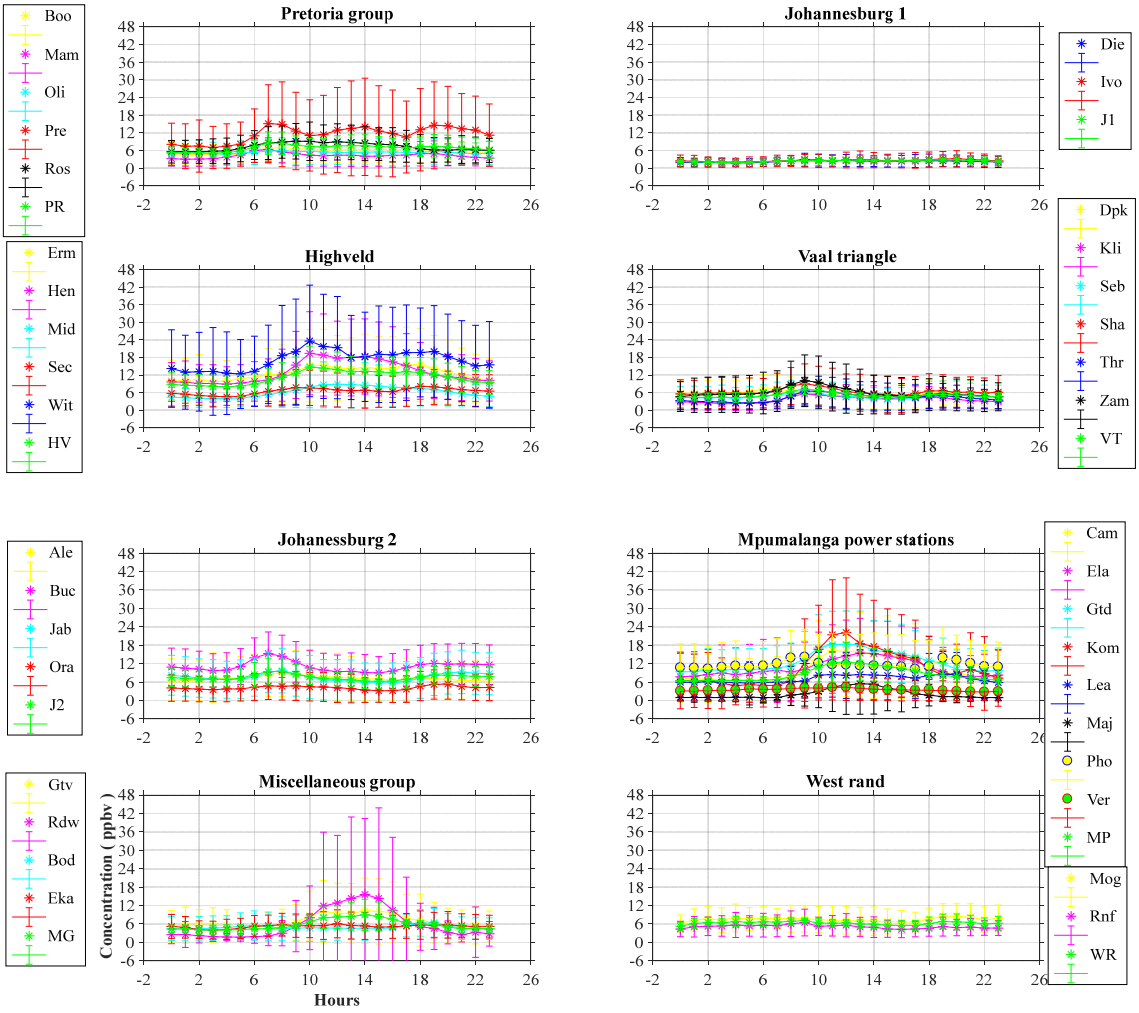

Figure 4.6: Autumn diurnal variation of each group and their respective stations

4.3.1.2. Daily mean variations

The daily mean variations (figures are not shown) proved that until 2011, only Pretoria west from the Pretoria group, showed higher levels when the SO_2 values exceeded slightly than the National Ambient Air Quality Standards (NAAQS) of 48 ppbv. From 2012, almost all the stations in that group including Pretoria west were below 20 ppbv. The Vaal Triangle (0.5-15 ppbv), Miscellaneous (0.5-18 ppbv), Johannesburg 2 (0.5- 20 ppbv) and West Rand (1-13 ppbv) groups generally showed similar ranges, whereas the ranges of the Highveld and Mpumalanga power stations groups were double that of these groups. Sharpeville and Zamdela (Vaal Triangle) were at higher levels up to ~ 22 ppbv with no sign of declination from 2007 to 2013.

Alexandra, Buccleuch from Johannesburg 2 group was sometimes above 20 ppbv in the beginning and after 2008, there was a slight decrease in the values in these stations. Rand water had higher value ~ 48 ppbv only once in November 2013, whereas the Mogale city from the West Rand group exceeded 15 ppbv during the beginning of 2013. It was found that Johannesburg 1 had the lowest SO_2 values of all the groups where Diepsloot and Ivory Park stations did not exceed 9 ppbv in all three years (2009 to 2011). The Highveld group showed stable high SO_2 values where the stations exceeded 18 ppbv throughout the entire period. Especially Witbank, Ermelo and Hendrina stations had consistent high values of above 30 ppbv in the middle of each year (nearly two times that of the Vaal Triangle group), which again proved the dominance of coal based industries in this group. Similarly, all the stations in Mpumalanga power stations were at higher levels (0.5 to 20 ppbv), which were comparable to those of the Highveld group. Camden, Grootdraaidam, Komati and Leandra exceeded 30 ppbv frequently, especially Grootdraaidam when it almost reached the daily limit of NAAQS in the later part of the time period.

Thus, the daily mean variations confirmed that the Highveld and the Mpumalanga power stations group had the highest SO_2 level. This was consistent with the study conducted on major sources of air pollution in South Africa using air borne instruments between 2003 and 2006, where it was proved that the plumes from coal fired power plants and petrochemical facilities typically have higher SO_2 levels (Burger, 2016). Secondly, the SO_2 levels of some stations near Johannesburg and Pretoria like Jabavu, Orange farm, Alexandra and Pretoria west were comparable with that of major industrial based regions of the Highveld and Vaal Triangle groups. This could be that the cities were impacted by the air masses from the Highveld region rich in SO_2 (Beukes et al., 2013). Additionally, other activities like burning of low-grade coal for cooking and heating purposes and vehicular emissions could contribute to the pollution episodes in the megacities (Lourens et al., 2012).

4.3.1.3. Seasonal variations

The seasonal variations of each group and their stations were broadly categorised into intra-seasonal (Figure 4.7) and inter-seasonal variations (Figure 4.8). It should be noted that since the West Rand group had only 2013 data, its Inter-seasonal variations were discussed only.

4.3.1.3a Intra-seasonal variations: In the beginning of the time period i.e., from 2009-2010, concentrations at all the stations in the Pretoria group, except Pretoria west, ranged from 1.5 ppbv to 15 ppbv, while Pretoria west had a few higher SO_2 values and standard deviations $\sim$ 20 ppbv $\pm$ 10 ppbv both in winter and summer of these years. From 2012, all the stations in this group were below 10 ppbv. The reason for such high SO_2 peaks between 2009 and 2010 might be due to point source emissions from Pretoria west and Rooiwal power stations. After 2011, there were maintenance problems, where all six units in Pretoria west station and four units were out of service in Rooiwal power station, thus led to a decline in their performance and output (NERSA, 2013). It was found that the Johannesburg 1 group had low SO_2 values. Both Diepsloot and Ivory Park stations started increasing from autumn, however Diepsloot remained below 5 ppbv even in winter of all the years (2009-2012), while Ivory Park were slightly higher than 5 ppbv in winter. Similarly, the miscellaneous group had low ranges, where they were below 10 ppbv. Nonetheless, the standard deviation for Rand water was sometimes higher than 5 ppbv even reaching up to 11 ppbv. It could be seen that prominent winter peaks were shown in all the stations in the Vaal Triangle for the entire period (2007-2013) and ranged from 1.5 to 10 ppbv in all the seasons. Sharpeville and Zamdela, on the other hand, slightly exceeded 10 ppbv in winter. This was in agreement with the study conducted on air pollutant concentrations where it was found that only the Vaal Triangle area showed unique winter extremities when compared to other hot spot regions, which could be due to the presence of inversion layers at 750-700 hpa and expected.

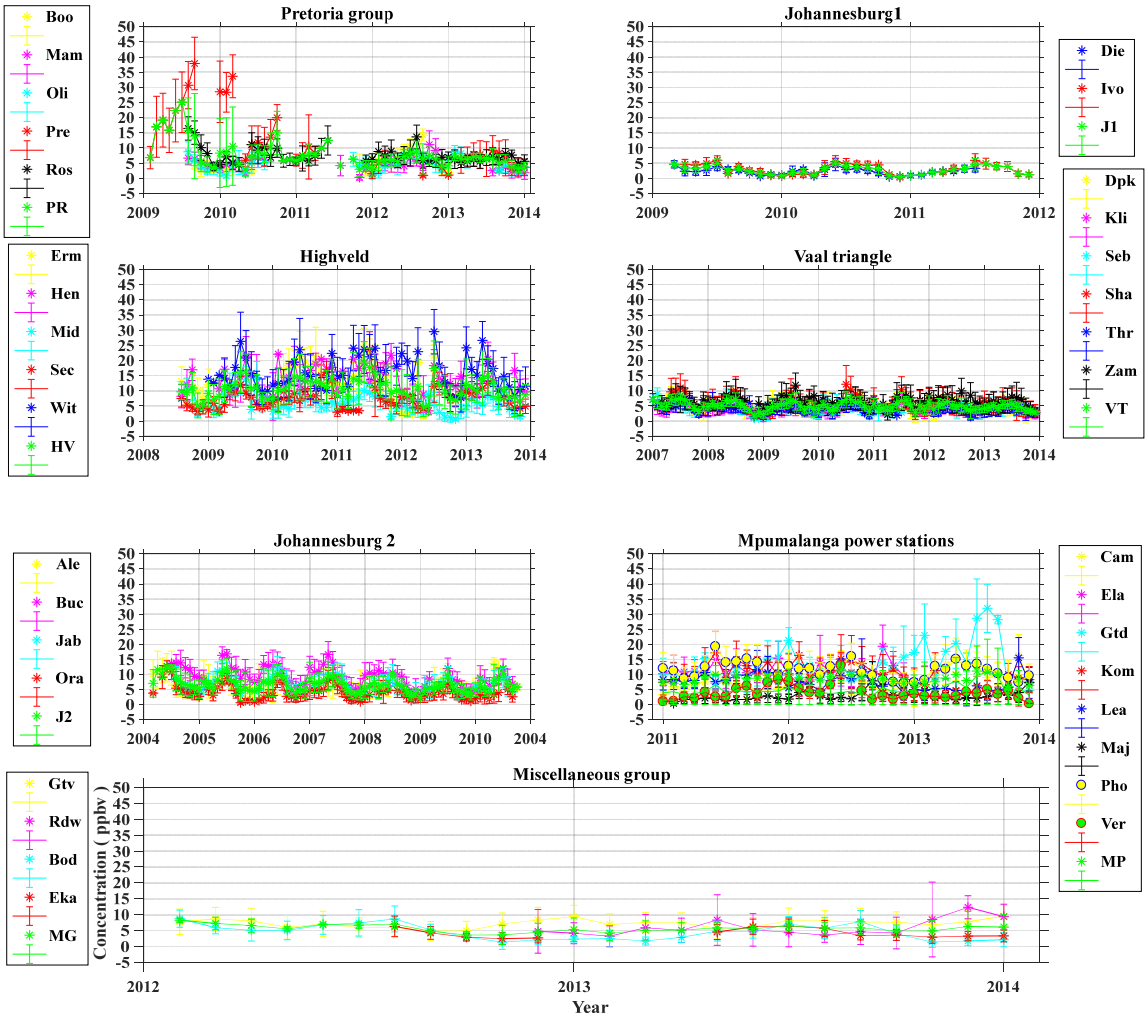

Figure 4.7: Intra-seasonal variation of each group and their respective stations.

less wind speed (Ncipha 2011). The Highveld and Mpumalanga power stations groups showed slightly higher ranges than other groups as Middleburg and Secunda stations in the Highveld group ranged between 2 ppbv and 15 ppbv, while Hendrina, Ermelo and Witbank showed even higher values (>15 ppbv) irrespective of the seasons, sometimes even 20 ppbv. The standard deviations of Witbank and Ermelo were high ~ 10 ppbv, while Middleburg had the lowest value (below 15 ppbv even in winter). There was no decrease seen in the Highveld group. The Johannesburg 2 group resembled the Vaal Triangle group for its ranges and prominent winter peaks. The ranges were from 2 to 12.5 ppbv, but Buccleuch had slightly higher ranges from 3 to 17 ppbv. Winter peaks were seen for all the stations, especially Buccleuch, where the SO_2 values exceeded 15 ppbv, however from 2008 the peak values started to decrease for all the stations. Mpumalanga power stations as said earlier had high ranges (from 2.5 ppbv to 15 ppbv), in spite of the fact that Majuba and Verkykkop stations had the lowest values (below 10 ppbv). Grootdraaidam had the highest

range especially in 2013, when it had high SO_2 values and a high standard deviations of $>$ 20 $\pm$ 10 ppbv irrespective of all the seasons. Leandra had an intermediate range and other stations like Camden, Komati, Elandsfontein and Phola occasionally exceeded 15 ppbv. Some stations in this group did not show any seasonal variations except that they show occasionally a high values even in summer period.

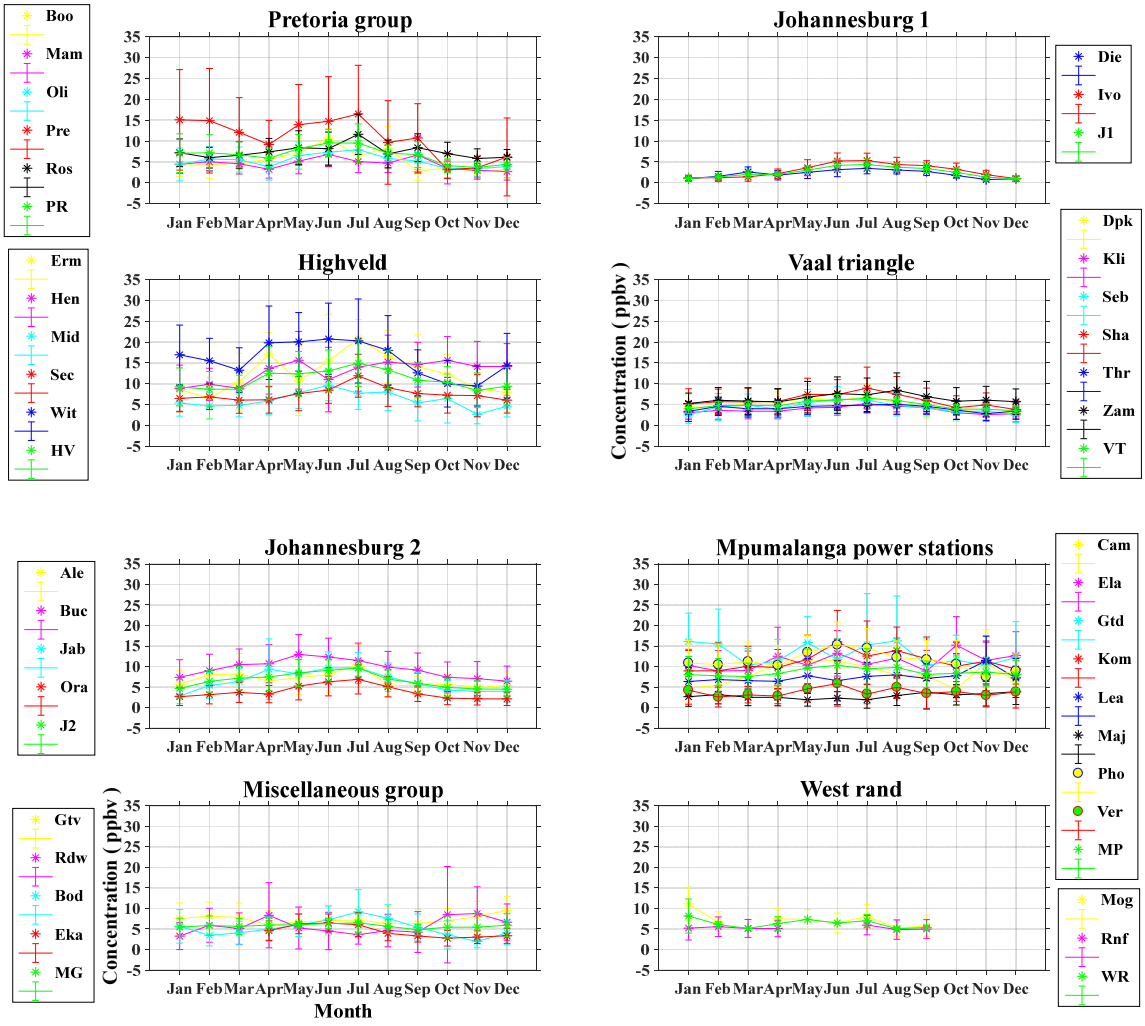

Figure 4.8: Inter-seasonal variation of each group and their respective stations.

4.3.1.3b Inter-seasonal variations: Almost all the groups followed a general seasonal pattern of increasing trend from autumn, reached their maximum level in winter, and later on decreased slowly from spring. Lourens et al. (2011) and Martins et al. (2007) also found such homogenous seasonal patterns, where the SO_2 values show peak in winter, which were probably related to the increase in electricity demand and trapping of pollutants near the surface due to surface inversion during winter. Pretoria West (Pretoria group), showed

regular higher SO_2 levels and deviations of ~16 ±12 ppbv even in summer. A probable explanation could be because of the low stack emission height of the Pretoria west power station, owned by the Tshwane municipality (Spalding-Fecher and Matibe, 2003). The SO_2 must have been released well below the mixing height and thus led to downwash (Thomas, Carpenter and Gartrell, 1963). Witbank in the Highveld group had the highest SO_2 value of all 36 stations, especially in winter, when it reached up to ~ 20 ppbv. Likewise, Hendrina in the same group had SO_2 values of 14 ± 2 ppbv maintained even in spring, apart from autumn and winter, whereas the Middleburg and Secunda stations had low values (below 10 ppbv) except in June and July. Ermelo station exhibited two peak values, one in April and the other in July (~ 20 ppbv). The Johannesburg 1 group had low SO_2 values, even in winter, as the SO_2 levels were maintained below 5 ppbv, which could because a resultant of two main reasons. Firstly, the stations were at urban location where the consumption of electricity was preferred over coal. Secondly, the use of Basa-njengo-Magogo techniques, which is a top down fire lightening procedure, introduced in the low income settlements of Diepsloot and Ivory Park (2012-2013 National Air Quality Officer's Annual Report on Air Quality Management, 2014). Moderate levels were seen in the Vaal Triangle group as their SO_2 values were below 8 ppbv during all seasons, except Sharpeville and Zamdela, which were ~ 8.5 ppbv in July and August. Buccleuch, Orange farm and Jabavu from the Johannesburg 2 group, showed a gradual increasing trend in autumn and winter and a gradual decreasing trend in spring, whereas Alexandra increased sharply in July to reach a maximum value of 10.5 ppbv. All the stations in this group, except Buccleuch, maintained concentration below 11 ppbv, even in winter. The stations in the Mpumalanga power stations group did not show a steady trend, as they increased or decreased suddenly, especially Komati, Grootdraaidam and Elandsfontein, but Majuba showed the lowest value. Rand water in the Miscellaneous group, had unusually low values in winter and increased in spring when it had a higher standard deviation of 11.7 ppbv in October and to a less extent in November and April. Even Grootvlei had lower values in winter and higher values in spring and summer. The West Rand group was similar to that of the Johannesburg 1 group, where Randfontein had smaller ranges (from 4.8 to 5.9 ppbv) and Mogale city was below 7 ppbv, except in January where it increased to 11.2 ppbv.

Overall, from the seasonal variations, it can be concluded that all the groups followed a general seasonal pattern, but Mpumalanga power stations did not show any consistency in their trends, as they were dominated by power stations. Secondly, the Johannesburg 1 group

had the lowest (~ 5 ppbv) and Highveld group had the highest SO_2 values followed by Mpumalanga power stations group (17 ppbv). Pretoria west, Witbank and Rand water (in spring) had high standard deviations (greater than 10 ppbv).

4.3.1.4. Inter-annual variation

The inter-annual averages of the groups and the stations are depicted in Figure 4.9. It should be noted that the annual variations for the Miscellaneous and West Rand groups were not included due to few number of years of data in these stations. It is clear that there was a sharp decline in the SO_2 value of Pretoria west from 2009-2011, where ~ 89% decrease was seen between 2009 and 2013. However, other stations in the Pretoria group did not show any distinct variation, especially Olivenhoubosch and Booysens where there was a decline of only ~10%. The Highveld group had higher ranges, exceeding 10 ppbv, in almost all the years. This was equivalent to the ambient SO_2 concentration inferred from the multi-scale atmospheric transport and chemistry (MATCH) model which was based on an emission inventory provided by the South African Department of Environmental Affairs and Tourism (DEAT), where the mean SO_2 levels were higher than 10 ppbv near the industrial sources (Zunckel et al., 2000). Witbank in the Highveld group almost reached the limit value of 19 ppbv in 2011 and showed high standard deviation of ~ 8 ppbv, which was almost equivalent to the study conducted by Lourens et al. (2011) on spatial and temporal variations of trace gases during 2007-2008, where they have used a passive sampling method. In their study, they found that Witbank had the highest SO_2 annual average of 13.3 ppbv with a standard deviation of ~ 6 ppbv, which might be due to the presence of several local sources like metallurgical and coal based industries, besides domestic fuel burning activities in this area. The other stations like Ermelo, Middleburg and Hendrina declined from 2011 (except 2013) and Secunda showed a decreasing trend from 2010 (but with high value in 2012). The Highveld group showed a decreasing trend from 2011. The Vaal Triangle group overall decreased from 2010, where Sebokeng, Sharpeville, Three Rivers and Diepkloof showed a decrease. Sharpeville and Diepkloof decreased sharply (~ 35%) and Zamdela increased slightly in 2012. Jabavu and Alexendra in the Johannesburg 2 showed a gradual decrease from 2005, Buccleuch and Orange farm almost showed a similar declining trend from 2004, but increased suddenly in 2007. This was more or less similar to that seen in the Department of Environmental Affairs report on annual ambient SO_2 concentrations where these stations

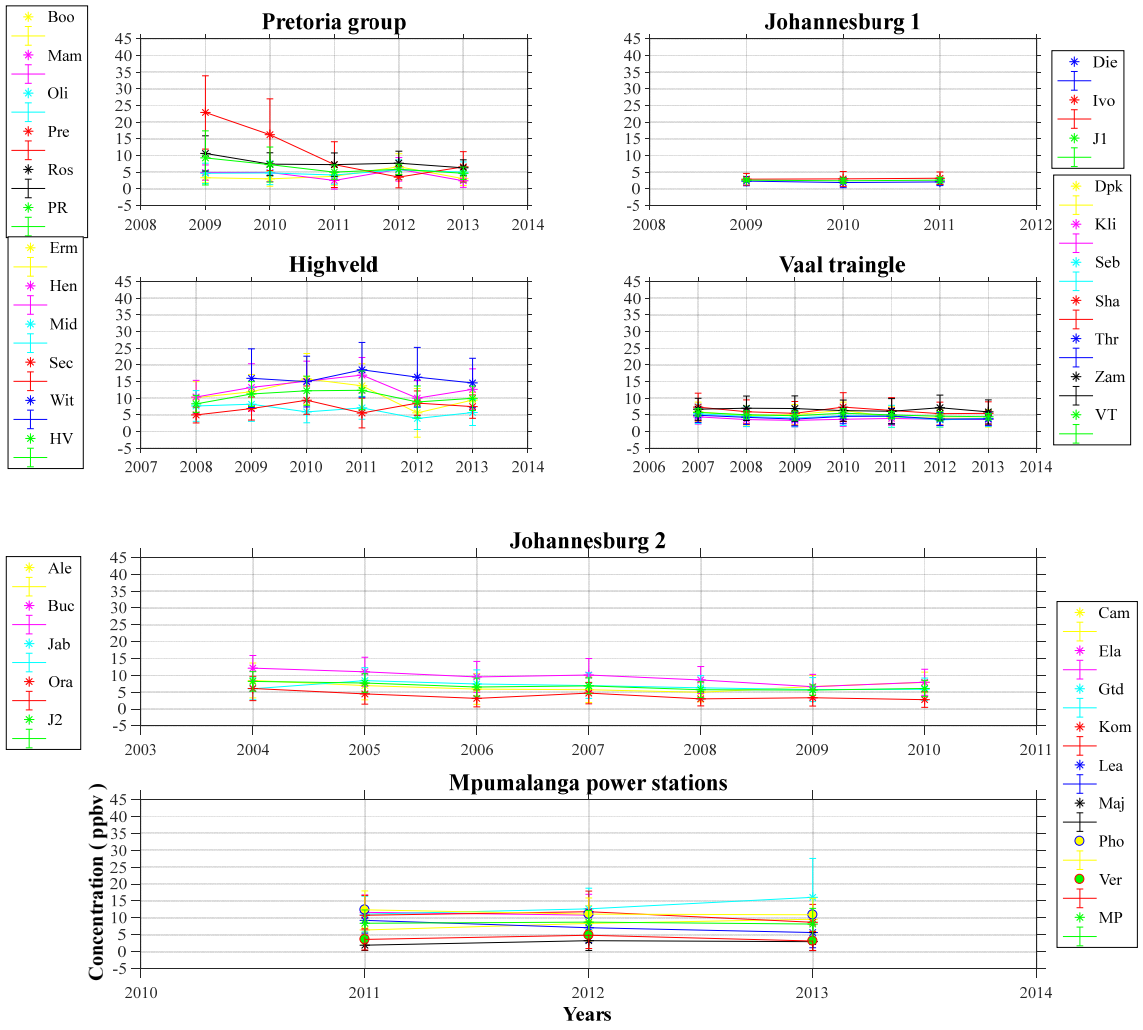

Figure 4.9: Inter-annual variation of each group and their respective stations.

had declined in the last few years of study (DEA, 2012 SOUTH AFRICA ENVIRONMENT OUTLOOK, 2012). The declining trend in SO_2 annual averages in the Johannesburg 2 group, could be attributed to the tremendous improvement (~ 16%) in electricity supply to houses between 2001 and 2011, which led to reduction in the use of coal for cooking (Turok and Borel-Saladin, 2014). The SO_2 levels of Mpumalanga power stations group were maintained below the NAAQS standards (19 ppbv), although this group was dominated by power stations. This might be due to the tall stack emission, which disperse the pollutants above the inversion layer (Lloyd, 1987; Spalding-Fecher and Matibe, 2003). Nonetheless, Grootdraaidam showed high SO_2 values and higher spatial variability in 2013 of 16 ppbv $\pm$ 11.5 ppbv. The Mpumalanga power stations group did not show any uniform variationsas some stations like Camden and Grootdraaidam increased by 45%, whereas Leandra decreased by 40% during 2011-2013 time period, whereas the

other stations in this group showed mixed up trend. The Johannesburg 1 group did not show any distinct variation, as Ivory Park increased slightly (∼10%) and Diepsloot decreased by only (∼11%).

It can be deduced from the inter-annual variations that the stations, which were dominated by the industrial sources, showed a mixed trend; however, the stations like Leandra dominated by human settlements showed a consistent decrease due to the replacement of coal burning with the electrification of the houses.

4.3.2. Spatial interpolation of SO_2 between the GB stations

The spatial interpolation of SO_2 by means of Kriging in each season using the GB data from 36 monitoring stations (Figure 4.10a-d) had been studied, which are as follows:

Autumn: In autumn, the regions located near the power stations like Witbank, Komati and Elandsfontein, had the highest SO_2 levels (∼ 10 ppbv to 12.5 ppbv ranges), whereas their outskirts had 7.5 ppbv to10 ppbv. However, the major portion of the Gauteng province, which covers mega cities such as Pretoria and Johannesburg and the southern part of the Mpumalanga Province, with Verkykkop, Majuba and Grootvlei stations, had a low SO_2 range of 2.5 ppbv - 5 ppbv.

Winter: The seasonal variation in winter was more or less similar to that in autumn, except high ranges were seen in the regions near to power stations like Komati, Elandsfontein etc., (12.5 ppbv to 15 ppbv) and the northern part of Gauteng covering Booysens, Rosebank, Pretoria west (7.5 ppbv to 10 ppbv) when compared to that in autumn. This could be the high SO_2 emissions because of energy demand in winter from the power plants like Hendrina, Komati, Kendal and Pretoria west, Rooiwal power stations in Mpumalanga and Gauteng provinces respectively. However, other factors like persistence of stable inversion layers, low wind speed and low mixing depth also play a vital role, thereby hindering the dispersion of pollutants in winter.

(a) Autumn

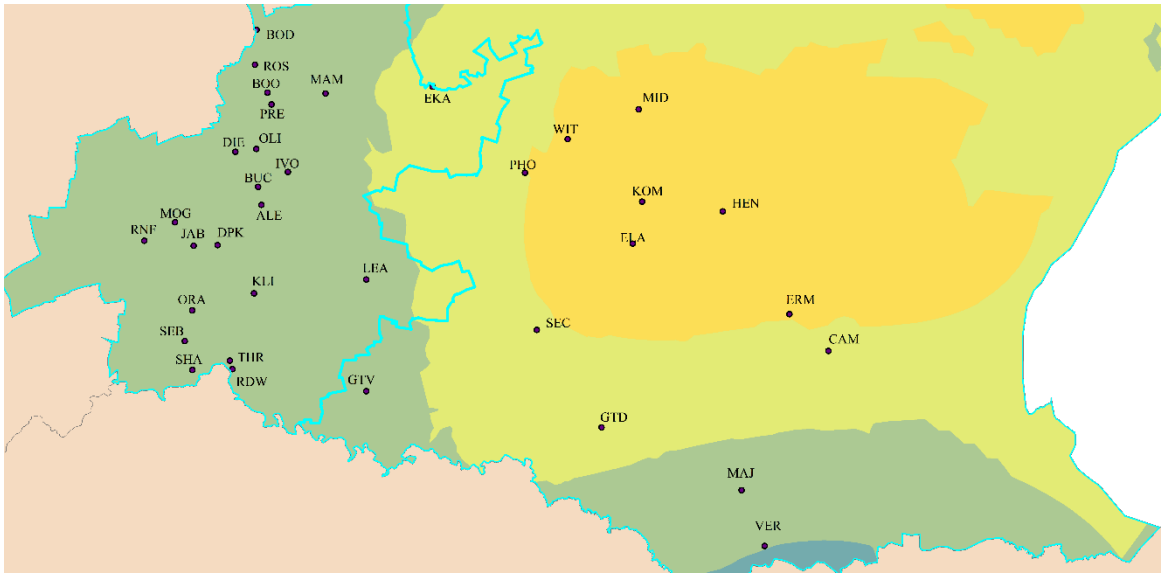

(b) Winter

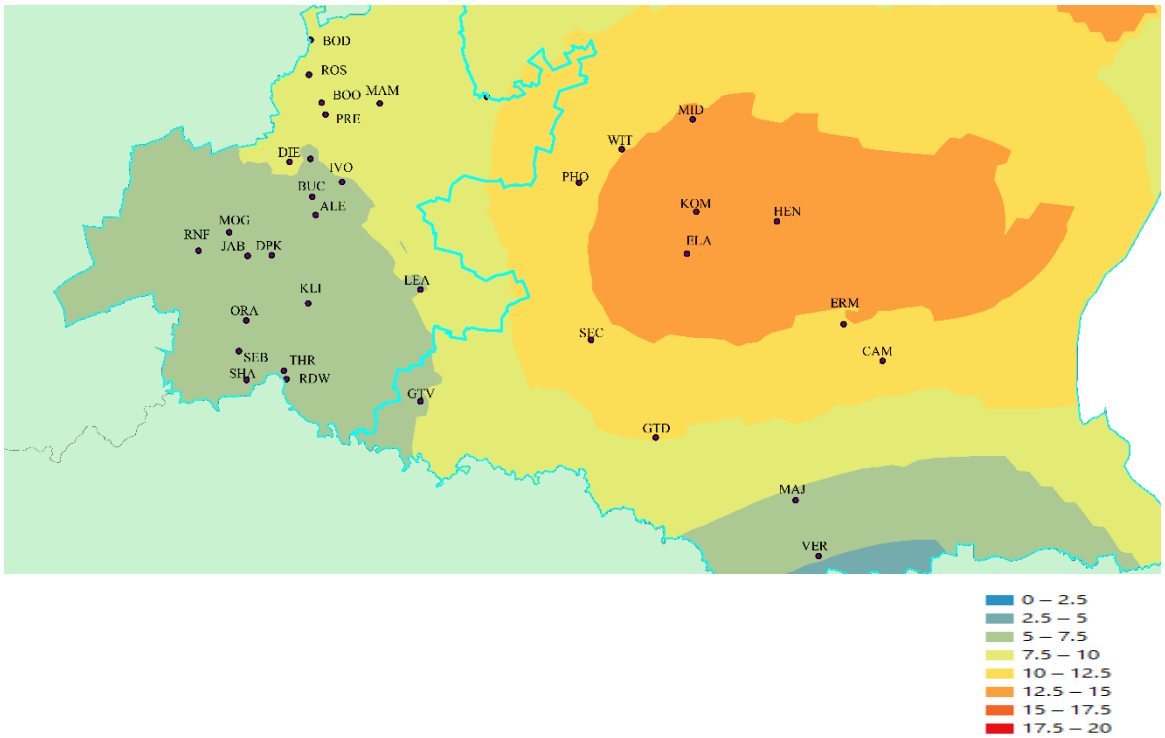

Figure 4.10 (a,b): Spatial interpolation of SO_2 over 36 monitoring stations during Autumn and Winter season.

(c) Spring

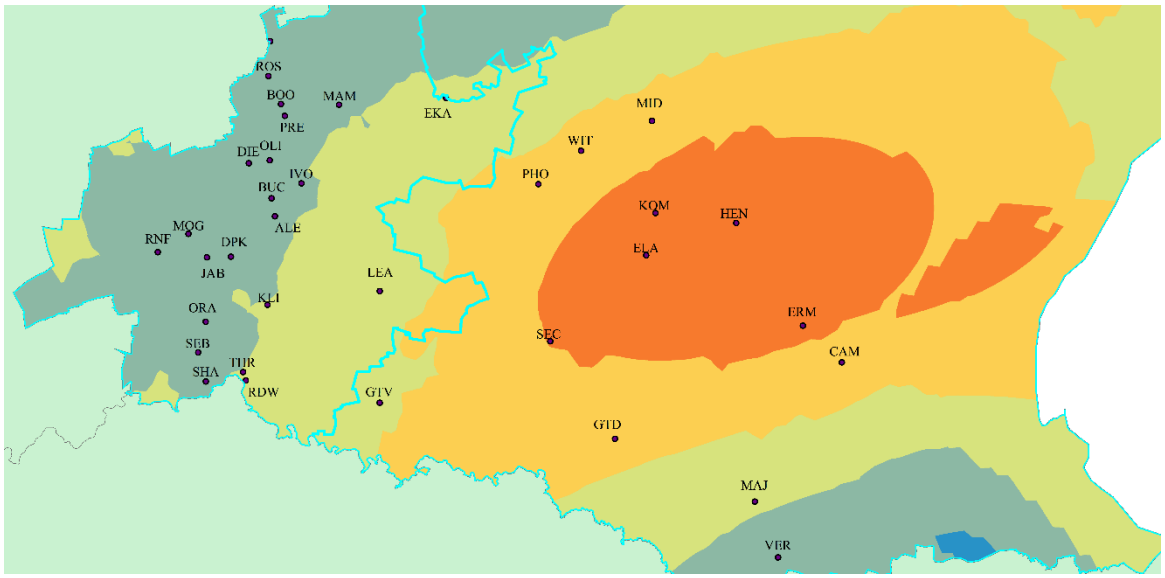

(d) Summer

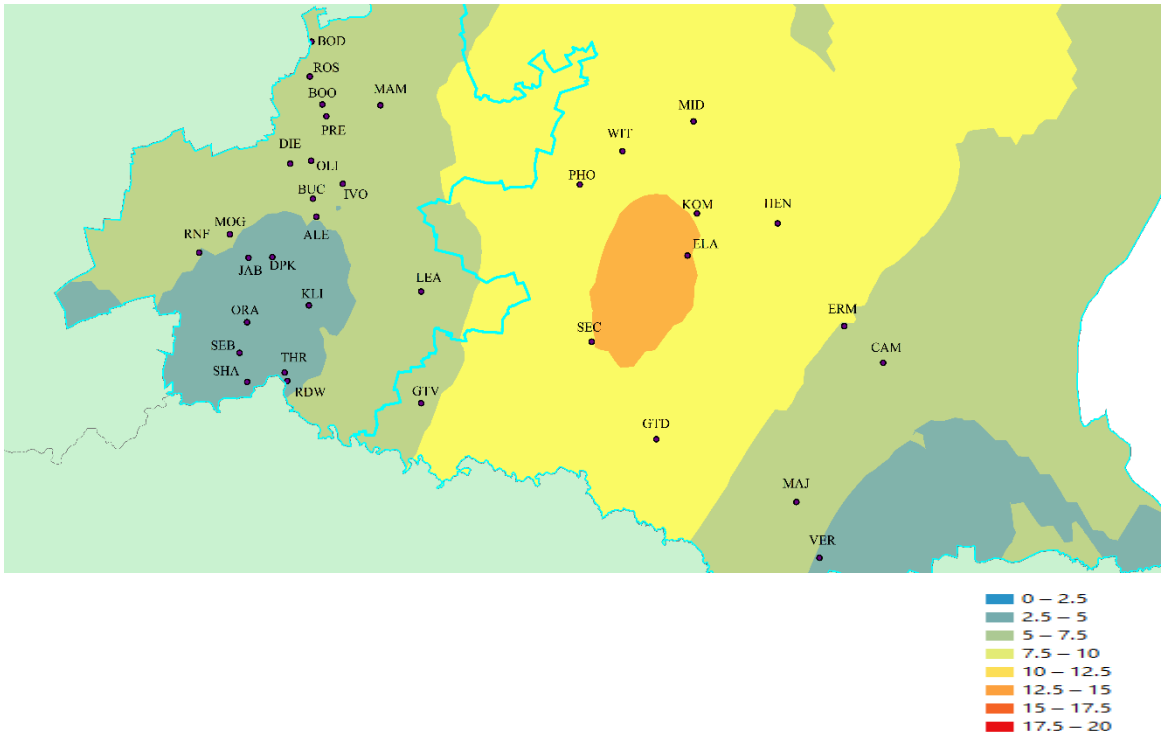

Figure 4.10 (c,d): Spatial interpolation of SO_2 over 36 monitoring stations during Spring and Summer season.

Spring: The interior parts of Mpumalanga and the western part of Gauteng were predicted to have slightly lower levels (of ~ 2.0 ppbv to 2.5 ppbv) of SO_2 in spring, when compared to the winter period. It was found that the wind speed in the northern part of South Africa was the highest in spring, with a maximum value occurring in October (Tesfaye et al., 2011). This might be the main causative agent for long range transport of pollutants, thus resulting in dissipation of SO_2 over the source regions. Another point, which was noticed, that the movement of air parcels were more inclined towards an eastward direction. This feature was seen in all the parts including the central and peripheral regions of the selected provinces. It could be a result of the westerly wave disturbances, which is a spring phenomenon with a frequency of 41% occurrence in October (Tyson et al., 1996a).

Summer: The prominent industrial source regions including Witbank and Hendrina, except the central most of the Highveld plateau and the southern part of Gauteng covering Sharpeville, Three Rivers and Sebokeng, had the lowest SO_2 values of all the seasons thus confirming the dispersion potential of pollutants due to the mixing height increase in summer. In addition, the maximum rainfall in summer (Davis, 2011), could have led to a large scale wet deposition of SO_2 in the summer season. Nevertheless, the western parts of Gauteng experienced higher SO_2 values in summer than spring, which might be due to the plumes from the central industrialised zones moving towards the northwest.

4.3.3. Seasonal vertical variation in SO_2 over South Africa as observed by the OMI

The behaviour of SO_2 differs in the troposphere (it is reactive with a short residence time of a few days) compared to the stratosphere (residence time of approximately a month). The main aim of this study is therefore to investigate the seasonal variations of SO_2 over South Africa based on data from 2004 to 2013 for different altitude levels namely, Planetary Boundary Layer (PBL - centred at 0.9 km), Lower Tropospheric Layer (TRL - centred at 2.5 km), Middle Tropospheric Layer (TRM - centred at 7.5 km), Upper Tropospheric and Stratospheric Layer (STL - centred at 17 km).

As described previously, 10 years of recorded OMI data were used to investigate seasonal variations of SO_2. The seasonal measurements were separated and corresponding mean values were calculated. The spatial mapping of SO_2 vertical columns over South Africa for each season and for different vertical levels (PBL, TRL, TRM and STL) are plotted in Figures 4.11,4.12,4.13 & 4.14. The results are as follows:

***PBL*:** Figure 4.11 shows SO_2 concentration in the PBL layer for different seasons. It is apparent from the figure that a distinctive pattern of high SO_2 levels was located over the central hub of Mpumalanga and its neighbouring regions. By comparison, remote parts of South Africa recorded negligible amounts of SO_2. In spring, SO_2 levels equivalent to 2 DU and slightly dispersed around the location of power stations and the Highveld region were observed. A small amount of 1-1.5 DU (1 DU ~ 5 ppbv) near northern KwaZulu-Natal (KZN) and the adjacent Indian Ocean was seen. A similar seasonality was observed in summer. However, the PBL were more localized around the Highveld region in the vicinity of electrical power plants in Mpumalanga province and the major portion of Gauteng covering the Johannesburg, Pretoria megacities, Sasolburg and part of the Vaal Triangle region. More specifically, the movement of air masses towards the north-west was visible in summer. This could be due to the effect of easterly waves that occur ~55% of the time exclusively in summer (Tyson et al., 1996a; Tyson et al., 1996b). Autumn and winter followed a similar pattern where the SO_2 air masses ranged from 1.5 DU to 2 DU and were more dispersed in Mpumalanga and Gauteng provinces compared to summer and spring. Furthermore, the movement of air masses from north west to south east towards the Indian ocean was clearly apparent in Figure 4.11. This could be due to direct transport from the Highveld region towards the central Indian Ocean as observed by Freiman and Piketh (2003). In their study, they specified the transport pathways from the Highveld only in the lower troposphere at 800-700 hpa. However, in the present study, movement was seen exclusively in the PBL column, which might be due to the low SO_2 levels in the TRL. Winter had the largest number of scattered plumes. This might be due to the existence of prominent anti-cyclonic conditions in this period. Subtropical anticyclones (which are the predominant phenomenon in winter with 70% occurrence in mid-winter) along with the transient ridging anticyclones, contribute 80% of anti-cyclonic circulation in June and July (Tyson 1996b). The occurrence of low SO_2 levels in the outskirts of the Mpumalanga region could be the resultant of ageing of plume masses as they move out from the source region.

***TRL, TRM & STL*:** Seasonal variations of TRL, TRM and STL are shown in Figures 4.12, 4.13 and 4.14. A similar trend was observed to that seen in PBL. The major difference was that overall SO_2 levels were lower namely, the industrialised Highveld region recorded 0.75DU to 0.5 DU, 0.3 DU to 0.5 DU and 0.3 DU for TRL, TRM and STL respectively. The three layers had an identical pattern in spring, where parts of eastern, western and northern cape had slightly higher SO_2 values (TRL 0.4 DU, TRM 0.2 DU to 0.3 DU, STL

0.2 DU). In winter, the SO_2 levels in these three layers showed a scattered and different mixed trend similar to PBL. Both TRL and TRM showed minimum SO_2 concentrations in remote areas in all seasons. However, the STL layer resembled PBL in that respect where the outlying regions from the industrial hub recorded negligible SO_2 values irrespective of season. It was seen that TRM in the vicinity of the Highveld region showed slightly higher SO_2 values in summer. This was consistent with a study by Höpfner et al. (2015) based on Michelson Interferometer for Passive Atmospheric Sounding (MIPAS) measurements. They observed a high mixing ratio of SO_2 in summer over northern (mid to high latitudes) and southern (mid latitudes) at an altitude ~10 km and negligible global SO_2 variations at an altitude ~18 km irrespective of all seasons, except over Antarctica in austral winter. Another interesting feature was that significant high SO_2 columnar amounts equivalent to that of the Highveld region was observed in western Limpopo at all height levels irrespective of any season. This could be the resultant of emissions from Matimba power station and coalmines, located in Lephalale region, Waterberg district municipality (DEA, Waterberg- Bojanala Priority Area Air Quality Management Plan, 2014). Of this, power generation accounted for a major part of nearly 90% of total SO_2 emissions in that province (DEDET, Limpopo Provincial Air Quality Management Plan, 2013).

The seasonal spatial maps of SO_2 data revealed some major findings: Firstly, very low seasonal variation was seen in the vicinity of the highly industrialised region. Here SO_2 levels were 1.5 DU at the PBL in almost all the seasons in this area. Lee et al., (2011) showed similar results in their study on global SO_2 emissions in 2006 using OMI and SCIAMACHY data. They found that there was not much appreciable seasonal variation over high SO_2 point source regions in the world. Secondly, the results of this study showed that the transport of SO_2 plumes from neighbouring South African regions and the recirculation of air over the industrial plateau occurred in all seasons and at all the altitude regions (but more clearly seen in the PBL maps due to high SO_2 columns) except summer. This observation was in accordance with the results studied by Freiman and Piketh (2003), in their seasonal variation of transport pathways to the Highveld region, where these two types of transport occur in combination ~ 35% in winter, spring and autumn, except in summer where they were less than ~ 12% at lower troposphere. Finally, the spatial distribution of SO_2 exhibited differently in winter at all altitudes, where the climatology of the wind clearly plays a vital role. This needs to be investigated further in detail and will be the subject of future work.

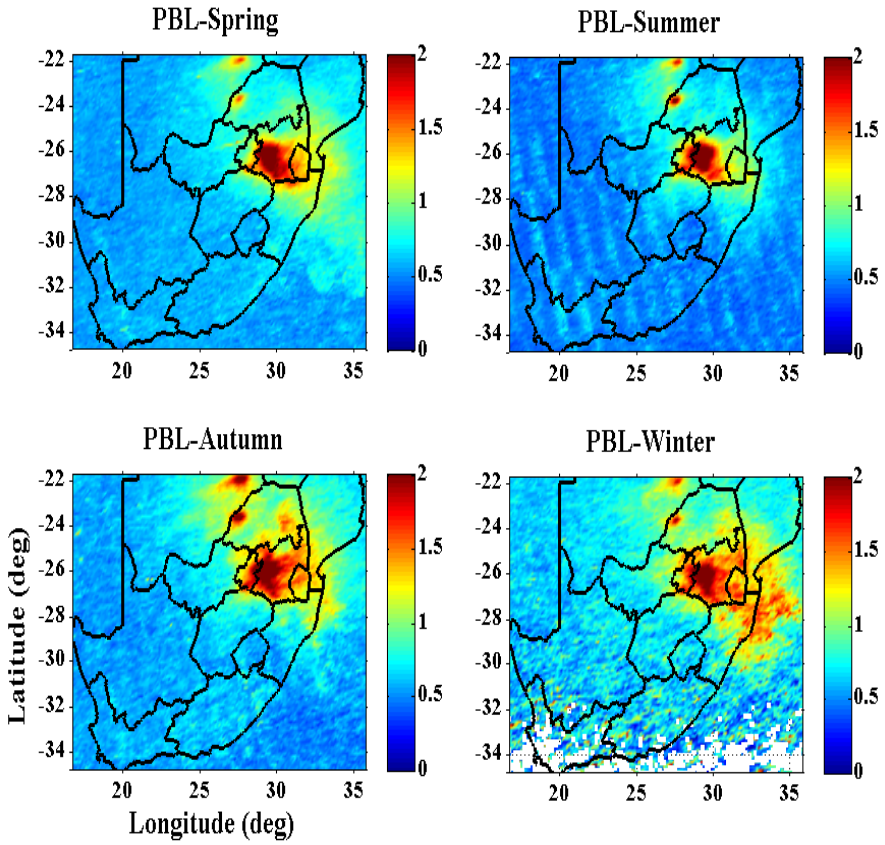

Figure 4.11: Seasonal variation of SO_2 for PBL over South Africa.

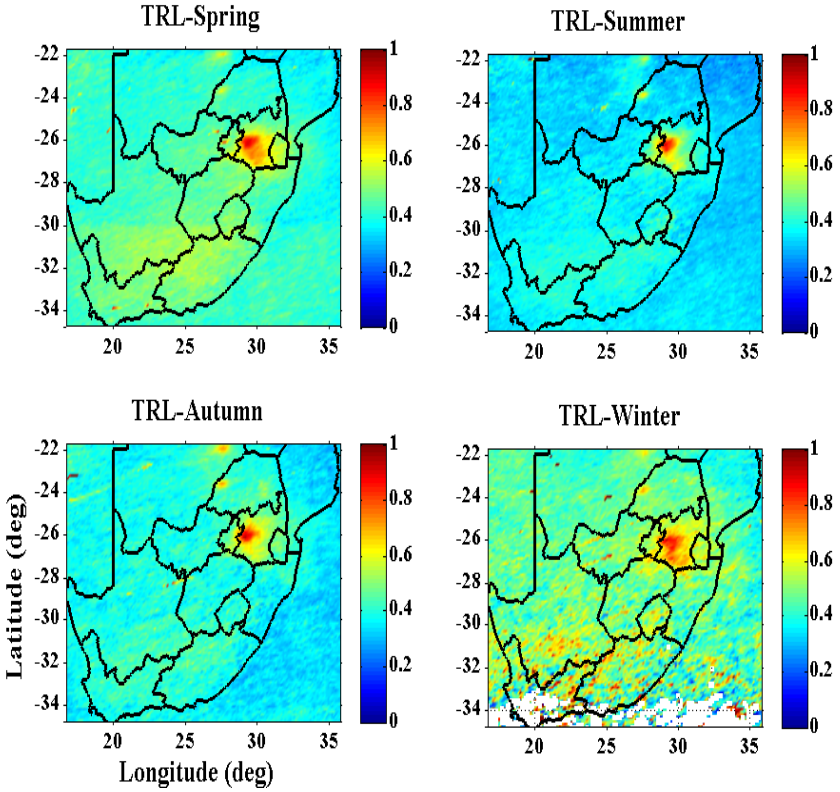

Figure 4.12: Seasonal variation of SO_2 for TRL.

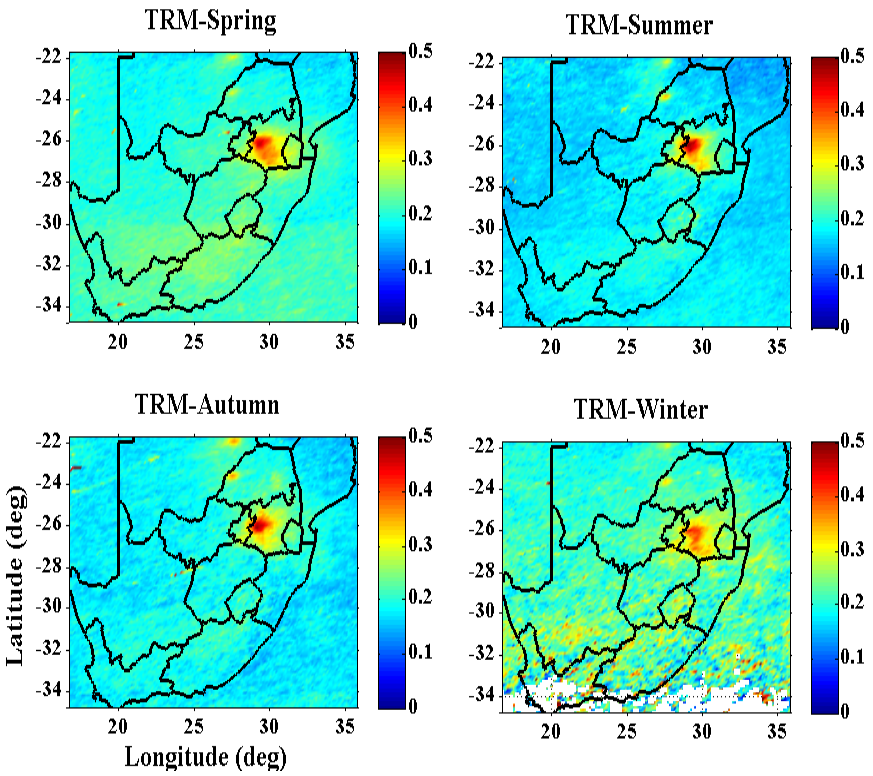

Figure 4.13: Seasonal variation of SO_2 for TRM.

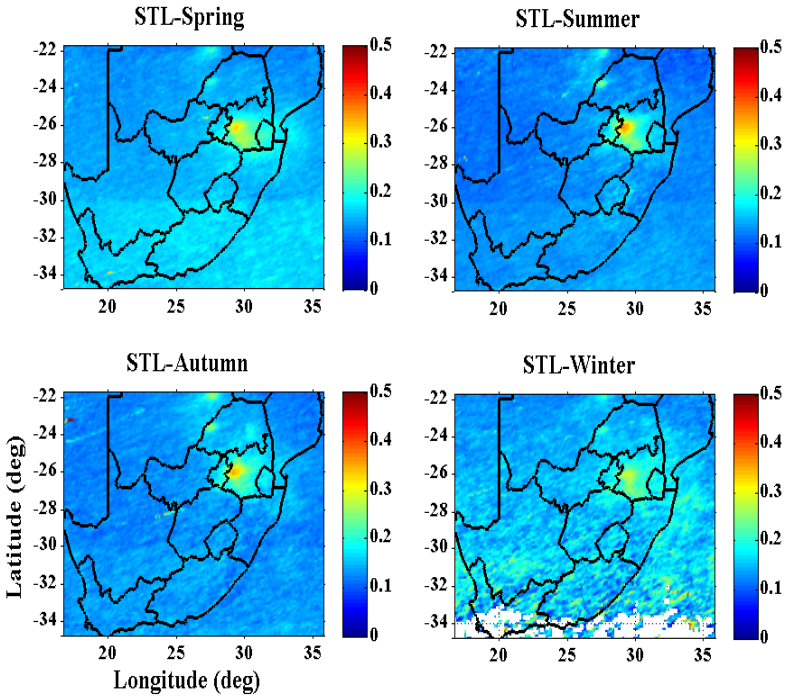

Figure 4.14: Seasonal variation of SO_2 for STL.

4.4 Summary

In this chapter, we have investigated the temporal and spatial variations of SO_2 by utilising GB instruments. The temporal variations showed that Pretoria west, Witbank and Rand water had both consistent high SO_2 and high standard deviations based on diurnal, daily and seasonal analysis. The seasonal diurnal variations inferred that double peaks were shown in most of the groups in winter, except the Mpumalanga power stations group and during spring, the SO_2 values of Witbank and Pretoria west had been underscored by other stations in their respective group. The overall temporal based analysis showed that the Mpumalanga power stations group had the highest SO_2 values followed by the Highveld group, whereas the Johannesburg 1 group had the lowest SO_2 values. The seasonal variations proved that all the groups except Mpumalanga power stations, followed a general seasonal variation except Mpumalanga power stations group, as they were at high levels even in summer. Rand water had a peculiar low level in winter and showed high SO_2 levels and standard deviations in October (spring).

The spatial analysis based on the kriging method, showed that high SO_2 levels were found in the major industrial areas of the Highveld, irrespective of the season. Thus from both the temporal and spatial based analysis, it was shown that the highest SO_2 levels were centralised in the industrial zones of the Mpumalanga province. However, it was found that the SO_2 plumes were under the influence of wind speed and direction, which was in agreement with the previous studies on wind climatology, which proved that the SO_2 level not only depend on the emission sources, but also on the meteorological conditions, which need to be explored further in future studies.

The seasonal variation of SO_2 at different height levels indicated that most of the SO_2 was confined to the Planetary Boundary Layer (PBL) layer with relatively high SO_2 plumes observed near industrial regions in Mpumalanga irrespective of all the vertical columns. Besides this, the spatial maps confirmed that, there was not much seasonal variation in their ranges as PBL had ~2 DU, followed by Lower Tropospheric Layer (TRL) (0.5 DU to 0.75 DU), whereas the Middle Tropospheric Layer (TRM) and Upper Tropospheric and Stratospheric Layer (STL) had smaller amounts of SO_2 (nearly 0.4 DU). The seasonal variations illustrated that winter was characterized by the most dispersed SO_2 plumes. This was in direct contrast to summer, which had the most confined plumes. In spring, relatively small amounts of SO_2 were seen in TRL, TRM and STL over the southern parts of the

country. PBL and STL showed negligible SO_2 concentrations in all seasons over the regions except those falling inside the industrial Highveld.

4.5 References

Bayraktar, H. and Turalioglu, F.S. 2005. A Kriging-based approach for locating a sampling site—in the assessment of air quality. *Stochastic Environmental Research and Risk Assessment*, *19*(4), pg.301-305.

Beukes, J.P., Van Zyl, P.G., Venteric, A.D., Josipov, M., Jaars, K., Tiitta, P. and Worsnop, D. 2013. Source region plume characterisation of the interior of South Africa as observed at Welgegund. *Clean Air Journal= Tydskrif vir Skoon Lug*, 23(1), pg.7-10.

Burger, R.P. 2016. The distribution of aerosol and trace gases in the lower troposphere over South Africa Ph.D thesis, Faculty of Science, University of the Witwatersrand, Johannesburg.

Clark, N.A., Demers, P.A., Karr, C.J., Koehoorn, M., Lencar, C., Tamburic, L. and Brauer, M., 2015. Effect of early life exposure to air pollution on development of childhood asthma. *Environmental health perspectives*, *118*(2), pg.284.

Collett, K.S., Piketh, S.J. and Ross, K.E., 2010. An assessment of the atmospheric nitrogen budget on the South African Highveld. *South African Journal of Science*, *106*(5-6), pg.35-43.

Davis, C. L., 2011. Climate Risk and Vulnerability: A Handbook for Southern Africa. *Council for Scientific and Industrial Research, Pretoria, South Africa*, ISBN 978-0-620-50627-4, pg.1-92.

Department of Environmental Affairs (DEA), REPUBLIC OF SOUTH AFRICA, 2012 SOUTH AFRICA ENVIRONMENT OUTLOOK, Chapter 5: Air Quality, Draft 2 Version 2, (April 2012)., from http://soer.deat.gov.za/dm_documents/Chapter_5__Air_Quality_ 4kp8X.pdf. (accessed on 15 February 2017).

Department of Environmental Affairs (DEA), REPUBLIC OF SOUTH AFRICA, 2014 Part 2, Waterberg- Bojanala Priority Area Air Quality Management Plan: Threat Assessment, (December 2014). (accessed on 8 May 2015).

Department of economic development, environment and tourism, (DEDET), REPUBLIC OF SOUTH AFRICA, Limpopo Provincial Air Quality Management Plan, (October 2013). http://www.saaqis.org.za/documents/LIMPOPO%20PROVINCIAL%20AQMP.pdf. (accessed on 06 March 2018).Feig, G., Ncipha, X., Vertue, B., Naidoo, S.,

Mabaso, D., Ngcukana, N. and Masuku, N., 2014. Analysis of a period of elevated ozone concentration reported over the Vaal Triangle on 2 June 2013. *Clean Air Journal, 24*(1), pg.10-16.

Feng, X., Li, Q., Zhu, Y., Wang, J., Liang, H. and Xu, R., 2014. Formation and dominant factors of haze pollution over Beijing and its peripheral areas in winter. *Atmospheric Pollution Research*, *5*(3), pg.528-538.

Freiman, M. T. and S. J. Piketh., 2003. Air transport into and out of the industrial Highveld region of South Africa. *Journal of Applied Meteorology, 42*(7), pg.994-1002.

Garstang, M., Tyson, P.D., Swap, R., Edwards, M., Kållberg, P. and Lindesay, J.A., 1996. Horizontal and vertical transport of air over southern Africa. *Journal of Geophysical Research: Atmospheres*, *101*(D19), pg.23721-23736.

Ghozikali, M.G., Mosaferi, M., Safari, G.H. and Jaafari, J., 2015. Effect of exposure to O_3, NO_2, and SO_2 on chronic obstructive pulmonary disease hospitalizations in Tabriz, Iran. *Environmental Science and Pollution Research*, *22*(4), pg.2817-2823.

Hamm, N.A.S., Finley, A.O., Schaap, M. and Stein, A., 2015. A spatially varying coefficient model for mapping PM10 air quality at the European scale. *Atmospheric Environment*, *102*, pg.393-405.

Höpfner, M., Boone, C.D, Funke, B, Glatthor, N, Grabowski, U, Günther, A, Kellmann, S, Kiefer, M, Linden, A, Lossow, S. and Pumphrey, H.C., 2015. Sulfur dioxide (SO_2) from MIPAS in the upper troposphere and lower stratosphere 2002–2012. *Atmospheric Chemistry and Physics*,*15*(12), pg.7017-7037.

Hörmann, C., Sihler, H, Bobrowski, N, Beirle, S, de Vries, M.P, Platt, U. and Wagner, T., 2013. Systematic investigation of bromine monoxide in volcanic plumes from space by using the GOME-2 instrument. *Atmospheric Chemistry and Physics, 13*(9), pg.4749.

Kgabi, N.A. and Sehloho, R.M., 2012. Seasonal Variations of Tropospheric Ozone Concentrations. *Global Journal of Science Frontier Research*, *12*(5-B).

Klimont, Z., Smith, S.J. and Cofala, J., 2013. The last decade of global anthropogenic sulfur dioxide:2000–2011 emissions. *Environmental Research Letters*, *8*(1): 014003. DOI:10.1088/1748-9326/8/1/014003.

Korhonen, K., Giannakaki, E., Mielonen, T., Pfüller, A., Laakso, L., Vakkari, V. and Ramandh, A., 2014. Atmospheric boundary layer top height in South Africa: measurements with lidar and radiosonde compared to three atmospheric models. *Atmospheric Chemistry and Physics*, *14*(8), pg.4263-4278.

Lee, C., Martin, R.V, van Donkelaar, A, Lee, H, Dickerson, R.R, Hains, J.C, Krotkov, N, Richter, A, Vinnikov, K. and Schwab, J.J., 2011. SO_2 emissions and lifetimes: Estimates from inverse modeling using in situ and global, space-based (SCIAMACHY and OMI) observations. *Journal of Geophysical Research: Atmospheres*, *116*(D6),DOI: 10.1029/2010JD014758.

Levelt, P.F., van den Oord, G.H, Dobber, M.R, Malkki, A, Visser, H, de Vries, J, Stammes, P, Lundell, J.O. and Saari, H., 2006. The ozone monitoring instrument. *IEEE Transactions on geoscience and remote sensing*, *44*(5): pg. 1093-1101. *DOI:10.1109/TGRS.2006.872333.*

Liousse, C., Assamoi, E., Criqui, P., Granier, C. and Rosset, R., 2014. Explosive growth in African combustion emissions from 2005 to 2030. *Environmental Research Letters*, *9*(3), 035003.

Lloyd, S.M., 1987. The control of air pollution at South African coal-fired power stations. *The Clean Air Journal*, 20-24. ISSN 0379-4709.

Lloyd, P.J., 2002. Coal mining and the environment. *Energy Research Institute*, University of Cape Town.

Lourens, A.S., Beukes, J.P., Van Zyl, P.G., Fourie, G.D., Burger, J.W., Pienaar, J.J. and Jordaan, J.H., 2011. Spatial and temporal assessment of gaseous pollutants in the Highveld of South Africa. *South African Journal of Science*, *107*(1-2), pg.1-8.

Lourens, A.S., Butler, T.M., Beukes, J.P., Van Zyl, P.G., Beirle, S., Wagner, T.K. and Lawrence, M.G., 2012. Re-evaluating the NO2 hotspot over the South African Highveld. *South African Journal of Science*, *108*(11-12), pg.83-91.

Macpherson, A.J., Simon, H., Langdon, R. and Misenheimer, D., 2017. A mixed integer programming model for National Ambient Air Quality Standards (NAAQS) attainment strategy analysis. *Environmental Modelling and Software*, *91*, pg.13-27.

Martins, J.J., Dhammapala, R.S., Lachmann, G., Galy-Lacaux, C. and Pienaar, J.J., 2007. Long-term measurements of sulphur dioxide, nitrogen dioxide, ammonia, nitric acid

and ozone in southern Africa using passive samplers. *South African journal of science*, *103*(7-8), pg.336-342.

Menyah, K. and Wolde-Rufael, Y., 2010. Energy consumption, pollutant emissions and economic growth in South Africa. *Energy Economics*, *32*(6), pg.1374-1382.

Mugabo, C., 2011. Ambient air quality in a low income urban area on the South African Highveld: A case study of Leandra township (Doctoral dissertation). Faculty of Science, University of the Witwatersrand, Johannesburg.

National Air Quality Officer's Annual Report on Air Quality Management - 2012-2013, March 2014, Department: Environmental Affairs, Republic of South Africa.

National Energy Regulator of South Africa (NERSA), Consolidated Report on the Audit Findings of the Electricity Generation Industry Compliance Audits Conducted in 2013, 2013,http://www.nersa.org.za/Admin/Document/Editor/file/Electricity/Compliance%20Monitoring/Consolidated%20Report%20on%20Audit%20findings%20of%20the%20Electricity%20Generation%20Industry%20Compliance%20Audits%20Conducted%20in%202013.pdf. (accessed on 28 February 2018).

Ncipha, X.G., 2011. Comparison of air pollution hotspots in the Highveld using airborne data.Master degree thesis.. University of the Witwatersrand, Johannesburg.

Pretorius, I., Piketh, S., Burger, R. and Neomagus, H., 2015. A perspective on South African coal fired power station emissions. *Journal of Energy in Southern Africa*, *26*(3), pg.27-40.

Qu, W.J., Arimoto, R., Zhang, X.Y., Zhao, C.H., Wang, Y.Q., Sheng, L.F. and Fu, G., 2010. Spatial distribution and interannual variation of surface PM 10 concentrations over eighty-six Chinese cities. *Atmospheric Chemistry and Physics*, *10*(12), pg.5641-5662.

Richter, A., Wittrock, F. and Burrows, J.P., 2006. SO2 measurements with SCIAMACHY, In Proceedings of the first Atmospheric Science Conference 2006, The European Space Agency, ESRIN, Frascati, Italy, 8/5/2006 -12/5/2006, ISBN 92-9092-939-1.

Smith, S. J., Aardenne, J. V., Klimont, Z., Andres, R. J., Volke, A. and Delgado Arias, S., 2011. Anthropogenic sulfur dioxide emissions: 1850–2005. *Atmospheric Chemistry and Physics*, *11*(3), pg.1101-1116.

Spalding-Fecher, R. and Matibe, D.K., 2003. Electricity and externalities in South Africa. *Energy policy*, *31*(8), pg.721-734.

Sundström, A.M., Nikandrova, A., Atlaskina, K., Nieminen, T., Vakkari, V., Laakso, L. and Venter, A.D., 2015. Characterization of satellite-based proxies for estimating nucleation mode particles over South Africa. *Atmospheric Chemistry and Physics*, *15*(9), pg.4983-4996.

Tesfaye, M., Sivakumar, V., Botai, J. and Mengistu Tsidu, G., 2011. Aerosol climatology over South Africa based on 10 years of Multiangle Imaging Spectroradiometer (MISR) data. *Journal of Geophysical Research: Atmospheres*, *116*(D20). doi: 10.1029/2011JD016023

Thomas, F.W., Carpenter, S.B. and Gartrell, F.E., 1963. Stacks—How High?. *Journal of the Air Pollution Control Association*, *13*(5), pg.198-204. doi:10.1080/00022470.1963.10468165

Thomas, R. and Scorgie, Y., 2006. Air quality impact assessment for the proposed new coal-fired power station (Kendal North) in the Witbank area (Report No.: APP/06/NMS-01 Rev 0.3) Airshed Planning Professionals (Pty) Ltd.

Turok, I. and Borel-Saladin, J., 2014. Is urbanisation in South Africa on a sustainable trajectory?. *Development Southern Africa*, *31*(5), pg.675-691.

Tyson, P.D., Garstang, M., Swap, R., Kallberg, P. and Edwards, M., 1996a. An air transport climatology for subtropical southern Africa. *International journal of climatology*, *16*(3), pg.265-291.

Tyson, P.D., Garstang, M. and Swap, R., 1996b. Large-scale recirculation of air over southern Africa. *Journal of applied meteorology*, *35*(12), pg.2218-2236.

Theys, N., De Smedt, I, Gent, J, Danckaert, T, Wang, T, Hendrick, F, Stavrakou, T, Bauduin, S, Clarisse, L, Li, C. and Krotkov, N., 2015. Sulfur dioxide vertical column DOAS retrievals from the Ozone Monitoring Instrument: Global observations and comparison to ground-based and satellite data. *Journal of Geophysical Research: Atmospheres*. *120*(6), pg.2470-2491.

Vakkari, V., Beukes, J.P., Laakso, H., Mabaso, D., Pienaar, J.J., Kulmala, M. and Laakso, L., 2013. Long-term observations of aerosol size distributions in semi-clean and

polluted savannah in South Africa. *Atmospheric Chemistry and Physics*, *13*(4), pg.1751-1770.

Venter, A.D., Vakkari, V., Beukes, J.P., Van Zyl, P.G., Laakso, H., Mabaso, D. and Laakso, L., 2012. An air quality assessment in the industrialised western Bushveld Igneous Complex, South Africa. *South African Journal of Science*, *108*(9-10), pg.1-10.

Wang, Y., Ying, Q., Hu, J. and Zhang, H., 2014. Spatial and temporal variations of six criteria air pollutants in 31 provincial capital cities in China during 2013–2014. *Environment international*, *73*, pg.413-422.

Xia, X., Qi, Q., Liang, H., Zhang, A., Jiang, L., Ye, Y.and Huang, Y., 2016. Pattern of Spatial Distribution and Temporal Variation of Atmospheric Pollutants during 2013 in Shenzhen, China. *ISPRS International Journal of Geo-Information*, *6*(1), 2. doi:10.3390/ijgi6010002

Zou, B., Wilson, J.G., Zhan, F.B., Zeng, Y. and Wu, K., 2011. Spatial-temporal variations in regional ambient sulfur dioxide concentration and source-contribution analysis: A dispersion modeling approach. *Atmospheric environment*, *45*(28), pg.4977-4985.

Zunckel, M., Robertson, L., Tyson, P.D. and Rodhe, H., 2000. Modelled transport and deposition of sulphur over Southern Africa. *Atmospheric Environment*, *34*(17), pg.2797-2808.

Chapter 5

Long-range transport of SO_2 over South Africa: A case study of the Calbuco volcanic eruption in April 2015

This chapter is based upon

S.K. Sangeetha, V. Sivakumar and M. Gebreslasie, Long-range transport of SO2 over South Africa: A case study of the Calbuco volcanic eruption in April 2015, Revised and Submitted to *Atmos. Environment* (2018).

Abstract

South Africa (SA) is influenced by anthropogenic SO_2 emissions, however, no studies exist detailing the atmospheric or climatic effects resulting from volcanic eruptions at this location. In this work, the Calbuco volcano situated in southern Chile, was used as a case study to investigate the transport of volcanic SO_2 plumes over SA in 2015. The Calbuco volcano underwent a series of eruptive phases starting from 22 April 2015. In this study, HYSPLIT forward trajectories and cluster analysis were carried out in order to estimate the altitude level of air parcels entering the Southern Africa. This analysis confirmed that trajectories beginning in Calbuco arrived in SA during the last few days of April and the 1st week of May 2015. In order to estimate the rise in SO_2 columnar concentrations at various altitudes and surface SO_2 levels, Ozone Monitoring Instrument (OMI) data and 19 ground-based (GB) monitoring stations (situated throughout SA) were utilised. A comparative analysis employing SO_2 data from pre (2014) and post (2016) volcanic eruption periods was also included in this study. Results showed that a major increase in SO_2 concentration was observed at the Planetary Boundary Layer (~ 2 DU) when compared to its upper layers during April and May 2015. However, no significant increase was seen by GB stations, thereby proving that SA was not affected by volcanic plumes at the surface or ground level.

5.1 Introduction

Volcanic eruptions are a natural emission source of SO_2 and can inject SO_2 deep into the atmosphere, sometimes reaching stratospheric altitudes (Prata et al., 2015). Although volcanic gases and particles in the troposphere and stratosphere do not influence human health directly, they may still exhibit significant, adverse environmental impacts. It has been shown that even limited interaction between volcanic clouds (in the mid and upper troposphere) and aircraft, can result in major damage or interruption of air traffic (Prata, 2009). This damage can span the range from a sulphur smell or light dust in the cabin to major consequences including heavy dust, electrical and computer systems failure and temporary engine malfunction (Guffanti et al., 2010). Aircraft using North Atlantic and trans-Pacific air routes are more susceptible to traffic disturbances due to volcanoes in Iceland and Japan (Prata, 2009). Between 1953 and 2009, volcanoes were responsible for significant damage to aircraft included Augustine (USA), Mount St. Helens (USA),

Redoubt (USA), Sakura-jima (Japan) and Pinatubo (Philippines) (Guffanti et al., 2010). In the stratosphere, the residence time of SO_2 is longer than that in the troposphere. This is because surface SO_2 reacts with aerosol particles to form sulphate aerosols. Furthermore, the measurement of volcanic SO_2 emissions is challenging due to the aperiodic and unpredictable nature of eruptions (Khokhar et al., 2005). It has been estimated that nearly 11.9 Tg of SO_2 is released into the atmosphere every year as a result of active volcanoes together with 6.8 Tg contributed by passive degassing of volcanoes (Stoiber et al., 1987). Of the six, routinely monitored volcanic gases measured by remote sensors, SO_2 is the dominant species. This is due to the large amounts emitted, short residence time and simple structure of its absorption bands in the UV and IR. The result affirms that it is easily measured by both UV and IR spectral- based sensors (Carn et al., 2016).

Satellite-based instruments can provide valuable information on volcanic emission sources by tracking the path of plumes released and reaction of gases in the upper atmosphere remotely. They have good spatial, spectral and temporal resolution and are therefore able to provide continuous global coverage. As a result, they may help in mitigating damage caused to aircraft by unexpected volcanic emissions. Infrared (IR) and ultraviolet (UV) based techniques are capable of measuring increased gas column levels due to volcanic eruptions (Prata et al., 2007). IR satellite sensors such as Moderate Resolution Imaging Spectroradiometer (MODIS), Atmospheric Infrared Sounder (AIRS) and Advanced Very High Resolution Radiometer (AVHRR) have captured near real-time images of plumes rising from the Kasatochi volcano (Corradini et al., 2010). On 8 August 2008, the second Global Ozone Monitoring Experiment (GOME-2), a UV based instrument, detected SO_2 plumes from the same volcano and traced their path across North America until they reached Spain one week after the eruption. Additionally, GOME-2 daily SO_2 data has been used to investigate variations in degassing volcanoes (Rix et al., 2009). On 30 September 2007, the Infrared Atmospheric Sounding Interferometer (IASI) was the first instrument to record an image of volcanic plumes rising from the Jebel volcano at Tair (located in the Red sea, Republic of Yemen) a few hours after a major eruption. The IASI maps showed SO_2 plumes passing from Sudan, travelling through the Gulf countries and west Asia and finally reaching India on 11 October 2007 (Clarisse et al., 2008).

The Ozone Monitoring Instrument (OMI), a sensor employing UV/Visible wavelengths, is currently the best satellite-based monitoring instrument in terms of its spatial resolution, sample rate and sensitivity. As a result, OMI is able to detect and differentiate multiple,

densely packed sources (Fioletov et al., 2013). During September 2004 – September 2006, OMI was able to discriminate SO_2 loadings between multi-volcanic sources in Eucador and South Colombia and showed that the major portion of SO_2 emissions resulted from the Tungurahua volcano. For the same volcano, OMI observed increasing SO_2 levels prior to a major eruptive phase in July and August 2006 (Carn et al., 2008). OMI satellite images also identified SO_2 emissions from the Nyamuragira volcano in the Eastern Congo as a result of the eruption on 8 November 2011. It was shown that emissions increased to 9 times that of its counterpart, the Nyiragongo volcano. This geological activity produced a deep lava lake which is now considered the largest lava lake on the planet (Campion., 2014). During November 2011, good agreement was found between daily SO_2 fluxes derived from OMI and GOME-2 data for the Nyamuragira volcano (Theys et al., 2013). An inventory of continuously emitting global SO_2 point sources was completed by OMI for the period from 2005 to 2014. In this list, SO_2 sources were classified into 4 main categories. Of the total number of SO_2 sources identified, 76 volcanic sources accounted for 30% of global SO_2 emissions. It should be noted that explosive volcanic emissions were excluded from this list and that this may have the effect of increasing the overall total if included (Fioletov et al., 2016). Such eruptions can play an important role in increasing SO_2 levels at locations distant from the site of the volcanic activity. The above studies therefore illustrate the capacity of OMI to effectively detect volcanic SO_2 sources.

The main aim of this study was to explore any potential increase in tropospheric SO_2 levels over South Africa as a result of the Calbuco volcanic eruption in Chile (22 - 23 April 2015). This analysis was undertaken through the use of OMI and ground-based (GB) SO_2 data sets for the period from 2014 to 2016. Hybrid Single Particle Lagrangian Integrated Trajectory (HYSPLIT) analysis for various altitudes was completed in order to compute air parcel trajectories from the source location and to confirm South Africa as their final location. The SO_2 columnar amounts at 4 vertical levels over entire South Africa during the pre- and post-volcanic periods were investigated through the application of OMI data. This was done to determine prime locations where SO_2 levels had increased. The rise in SO_2 at these locations was verified with the help of 19 GB monitoring stations located throughout South Africa.

This chapter is organized as follows: Section 5.2 describes the selected study regions and section 5.3 outlines the instruments employed. The obtained results are described in section 5.4 and the measured conclusions are given at the end.

5.2 Study regions

In this study, two regions were defined namely, the source (Calbuco volcano) and destination (South Africa). Calbuco volcano is an active stratovolcano located in Southern Chile (Figure 1). The first eruptive pulse occurred on 22 April 2015 at 18:08 local time (21:08 UTC) and lasted for 2 hours. This was followed by a second strong eruption on 23 April at 01:00 local time (04:00 UTC) which lasted for approximately six hours and produced eruptive columns up to an altitude of 15 km. A third phase of seismic activity was seen on the same day at 23:30 local time (2:30 UTC). This resulted in plumes, which reached an altitude of 2 km and travelled towards the northeast (https://www.volcanodiscovery.com/calbuco/news/22april2015/major-eruption.html).
Figure 5.1 shows the location of the Calbuco volcano, South Africa and the distance between them (~ 8250 km).

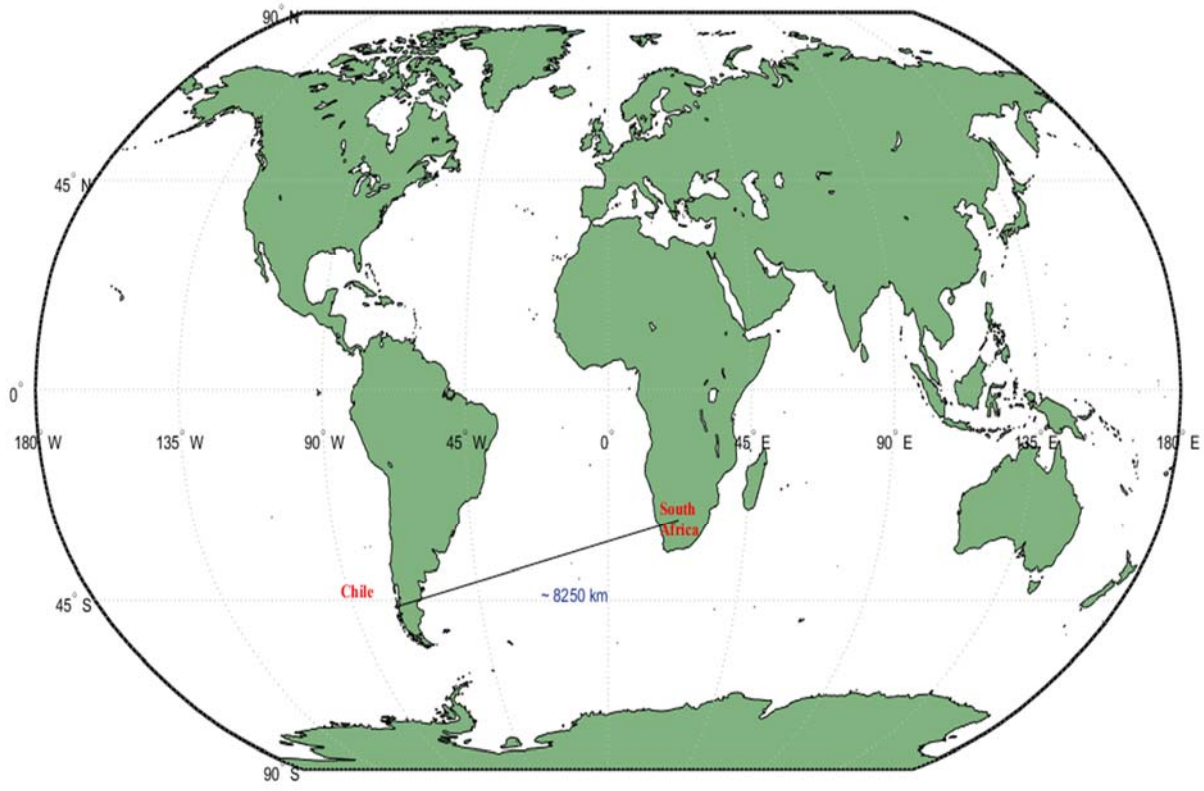

Figure 5.1: Location of Calbuco volcano, Chile and South Africa and distance between these locations.

5.3. Data and Instrumentation

5. 3.1. HYSPLIT trajectory model

In order to estimate the path of air parcels arriving in South Africa, forward trajectory and clustering analysis was performed based on the National Oceanic and Atmospheric Administration (NOAA) HYSPLIT4 meteorological input data. The HYSPLIT model is designed to assess air parcel trajectories arising from atmospheric and climatological phenomena (Draxler and Hess, 1998) and is based on the combination of Lagrangian and Eulerian approaches. The Lagrangian approach employs a moving frame of reference that traces the path of air parcels from their initial point through the calculation of advection, deposition and diffusion. By comparison, the Eulerian based technique uses a fixed three-dimensional grid as a reference frame for calculating pollutant concentration (Rolph et al., 2017).

In this study, 315-hour forward trajectories at various altitudes between 1 km and 21 km were calculated at a frequency of 6 hours, starting at 18:00 UTC 22 April and continuing to 6 May 2015. The meteorological data files for April and May 2015 were downloaded from the NCAR/NCEP global reanalysis archive from the ARL server. From the results of forward trajectory analysis, only selected altitudes were chosen to perform the cluster analysis. The concept of clustering results from merging the trajectories that are closer to each other and separate them into separate groups. This ensures a minimum variation between trajectories within the same group and a maximum variation between different clusters (HYSPLIT Basic Tutorial Contents). The clustering based approach therefore gives a better idea of the number or percentage of trajectories that will reach the selected destination. For this study, a total run time of 315 hours was selected to perform clustering and the number of clusters was chosen based upon the plot on percentage change in total spatial variance (TSV) and the combined clusters. The final number of clusters are those after which there was a large increase in percentage of TSV. After selecting the cluster numbers, cluster mean was estimated and this gave the percentage of each cluster. The final step was to plot individual trajectories associated with each cluster.

5.3.2 OMI data

OMI is a nadir viewing spectrometer that employs a two-dimensional charged-coupled detector (CCD) to measure trace gases in the sunlit portion of the earth. It flies on NASA's

EOS-AURA satellite. This is a sun synchronous satellite with 13:45 local equator passing time in the ascending node (Krotkov et al., 2016). In this study, OMI level 2 daily data product named OMSO2G, Version 003 from 2014 to 2016 was employed to detect the spatial variation of SO_2 over South Africa at four altitude levels. These levels are as follows: Planetary Boundary Layer (PBL-centered at 0.9 km), Lower Tropospheric Layer (TRL-centered at 2.5 km), Middle Tropospheric Layer (TRM- centered at 7.5 km) and Upper Tropospheric and Stratospheric Layer (STL-centered at 17 km). A newly developed algorithm based on Principal Component Analysis (PCA) applied to radiance data and developed in October 2014, was used to extract SO_2 data. This algorithm has a retrieval noise which is less than a factor of two compared to the previous version (Li et al., 2013).

5.3.3 Ground-based (GB) data

In order to study whether volcanic SO_2 plumes originating from the Calbuco volcano affects surface SO_2 levels in South Africa, GB SO_2 data were collected from 19 monitoring stations (of different network providers) for the period from 2014 to 2016. These stations were located mostly in the north western and central part of the country. The respective networks that were under the South African Weather Service (SAWS) provided the raw data for this study. Figure 5.2 shows the location of South African GB stations. In order to improve data quality, 70% data completeness was carried out. In this process, data with negative, missing or zero values were filtered out in a similar manner to that reported in an earlier study (Sangeetha et al., 2017a, 2018). Secondly, it was found that some stations had different time resolution. All the data sets were therefore converted into hourly averaged data to ensure uniformity. The stations were grouped according to their respective networks to represent a better consolidation of the results section. This methodology was followed in previous research (Sangeetha et al., 2018). Table 5.1 summarizes the details of each station with their groups, network providers and provinces. It should be noted that Rand Water station was not included in any group and is therefore considered as a single station.

Table 5.1: Grouping of stations according to the classification group name, station name, network provider and province.

Group Name	Stations	Network	Province
North West	Khuma (Khu)	North West Provincial Government (NWPG)	North West
	Damonsville (Dam)	NWPG	North West
	Jouberton (Jou)	NWPG	North West
	Mmabatho (Mma)	NWPG	North West
	Phokeng (Pho)	NWPG	North West
Highveld (HV)	Ermelo (Erm)	DEA	Mpumalanga
	Hendrina (Hen)	DEA	Mpumalanga
	Middleburg (Mid)	DEA	Mpumalanga
	Secunda (Sec)	DEA	Mpumalanga
	Witbank (Wit)	DEA	Mpumalanga
Vaal Triangle (VT)	Diepkloof (Dpk)	DEA	Gauteng
	Kliprivier (Kli)	DEA	Gauteng
	Sebokeng (Seb)	DEA	Gauteng
	Sharpeville (Sha)	DEA	Gauteng
	Three Rivers (Thr)	DEA	Gauteng
	Zamdela (Zam)	DEA	Free State
West Rand (WR)	Mogale City (Mog)	West Rand District Municipality	Gauteng
	Randfontein (Rnf)	West Rand District Municipality	Gauteng
Rand Water	Rand Water (Rdw)	ESKOM	Gauteng

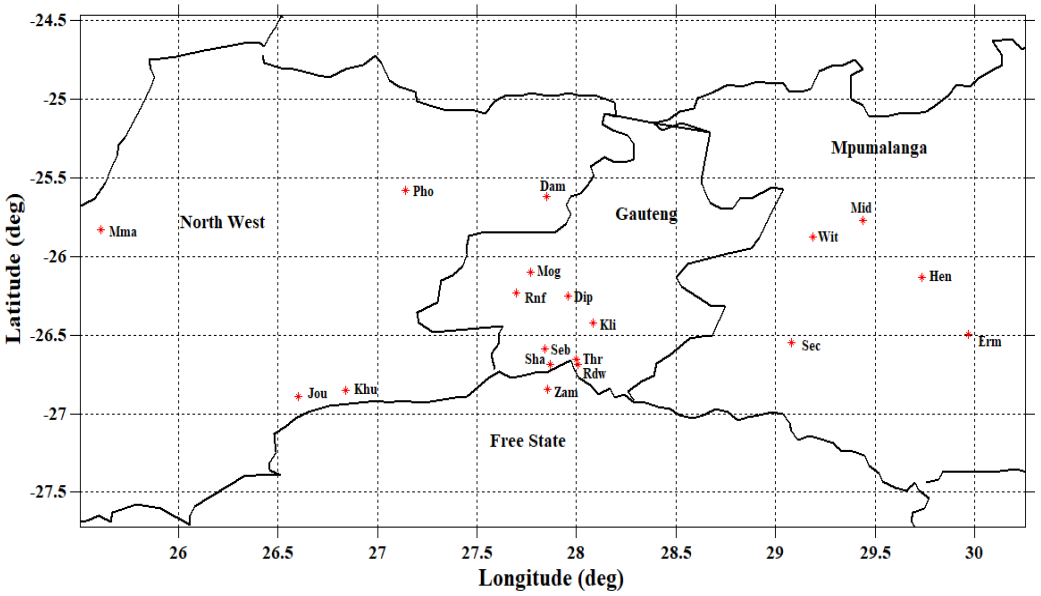

Figure 5.2: Location of ground-based monitoring stations in South Africa.

5.4 Results

5.4.1. HYSPLIT trajectory model

5.4.1a *Forward trajectory analysis*

The 315-hour forward trajectory at various altitudes and originating at the Calbuco volcano are shown in Figure 5.3. Consideration of Figure 5.3 shows that trajectories at altitudes 10 km, 12-15 km, 17 km and 18 km reached South Africa. Table 5.2 contains trajectory details and their arrival date. Air parcels at an altitude of 2 km did not enter South Africa but were observed circulating along the west coast of South Africa from 29th of April. They moved in an anti-clockwise direction until the last day of trajectory analysis. The altitude of these air volumes reduced and reached the surface by the end of the analysis period. This effect is similar to that observed by Hayer et al. (2016). They reported that such plumes were caught in a cyclonic stream in the Atlantic coast off South Africa and remained there for more than a week. Trajectories at altitudes of 17 km and 18 km had a travel time of 3-4 days while air parcels in the altitude range from 13 km to 15 km arrived simultaneously at South Africa. Plumes at an altitude of 10 km showed a significant reduction in altitude of about 6 km, while air masses at an altitude of 12 km had a corresponding reduction in altitude of 5 km. However, the remaining altitudes under study did not experience much variation.

Table 5.2: Details of trajectory analysis showing entry date into South Africa, duration of stay and altitude levels within the country

Trajectory altitude (km)	Date of entry into SA	Duration in SA	Altitude in SA (km)
10	1/5/2015	Until 2/5/2015	~ 4
12	30/4/2015	Until 1/5/2015	~ 7
13	26/4/2015	Until 27/4/2015	~ 10.5
14	26/4/2015	Until 27/4/2015	~ 13.5
15	26/4/2015	Until 27/4/2015	~ 15
17	28/4/2015	Until 30/4/2015	~ 18
18	30/4/2015	3/5/2015	~ 18

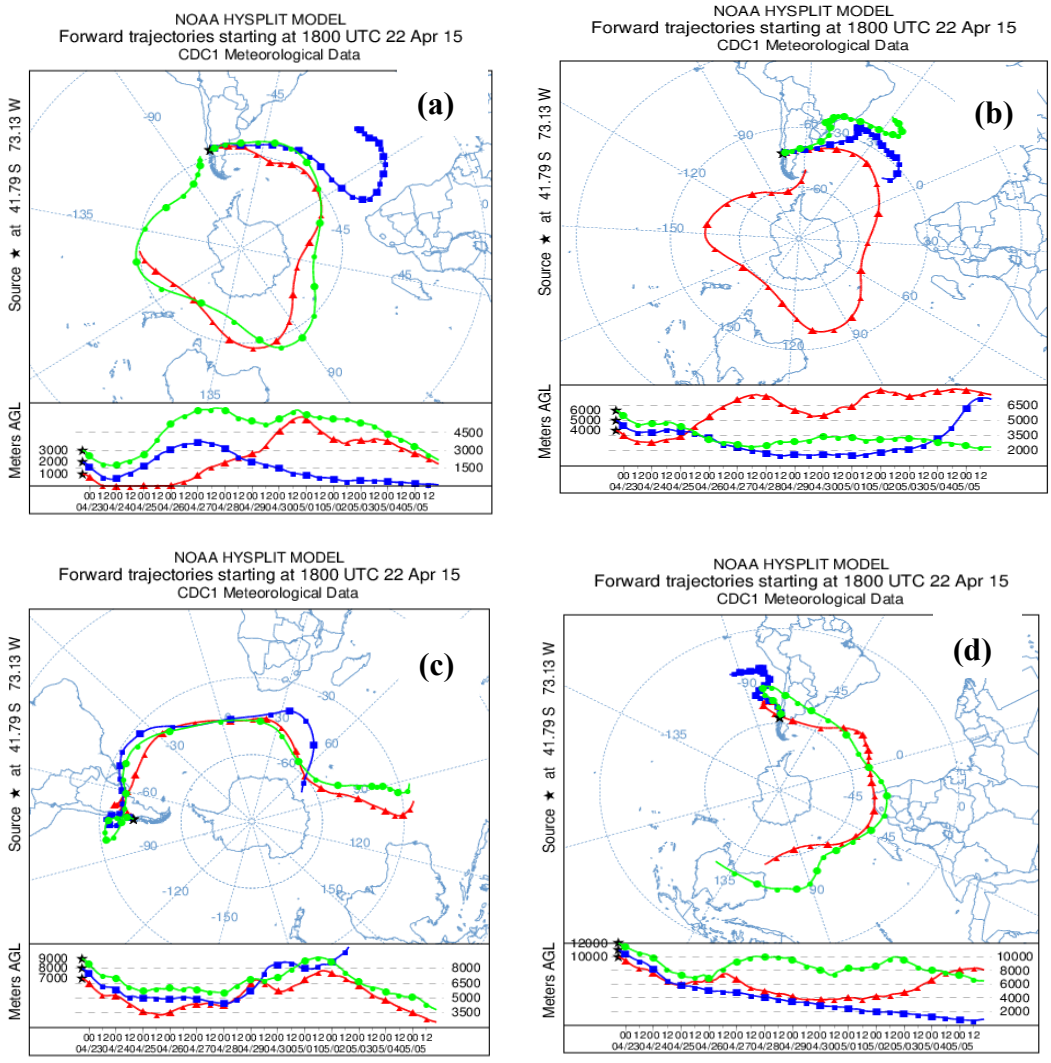

Figure 5.3: Forward trajectories originating from the Calbuco volcano on 22 April 2015 at 18:00 UTC for altitude ranges: (a) 1000 - 3000 m, (b) 4000 - 6000 m, (c) 7000 - 9000 m, (d) 10000 – 12000 m

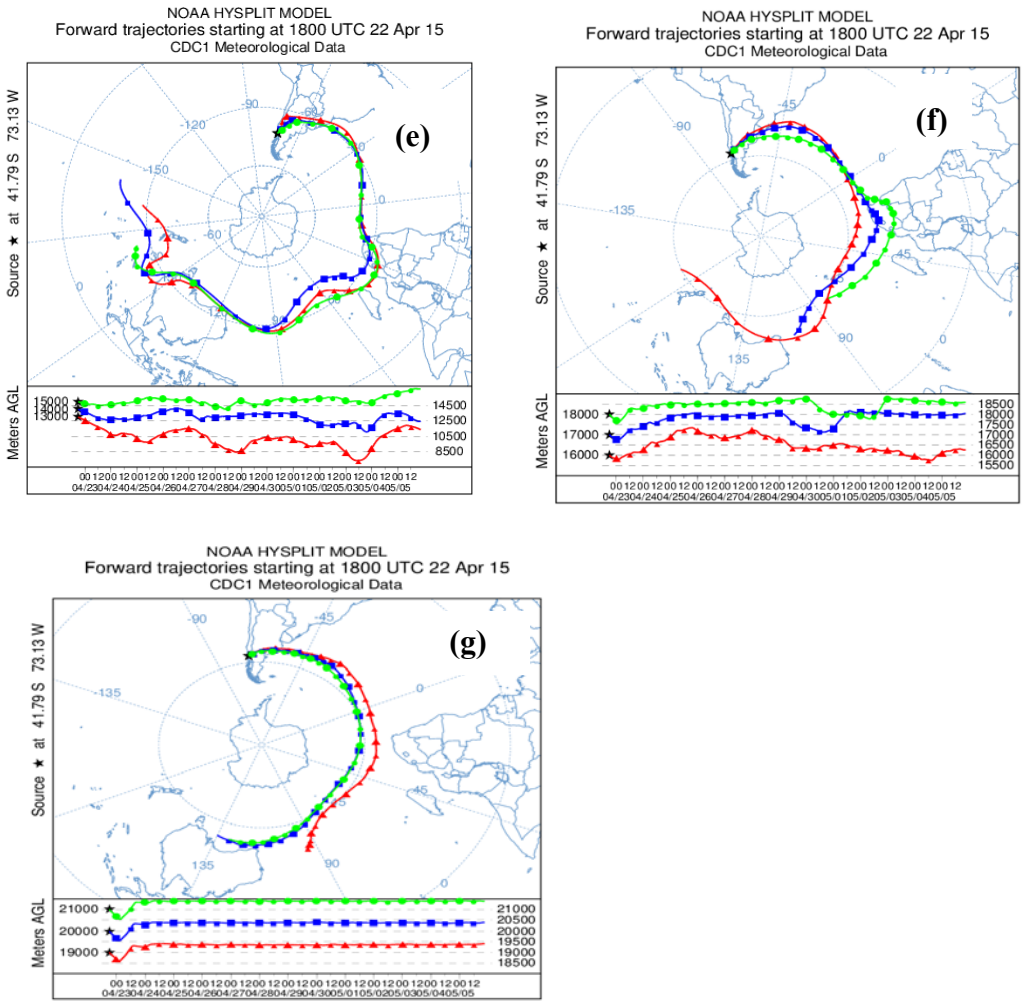

Figure 5.3: Forward trajectories originating from the Calbuco volcano on 22 April 2015 at 18:00 UTC for altitude ranges: (e) 13000 – 15000 m, (f) 16000 – 18000 m, (g) 19000 – 21000 m.

5.4.1b *Clustering of trajectory analysis*

The clustering of trajectories was done based on selected altitudes from the forward trajectory analysis. In order to avoid discrepancies in the results, the same starting time and the total run and clustering time (315 hours) as that of forward trajectories was selected. Figures 5.4 - 5.7 show the cluster means and selected clusters at selected altitudes while Table 5.3 gives details of each cluster at various altitudes. Based on the percentage of trajectories that travelled to South Africa, it can be inferred that clusters at 10 km, 12 km to 14 km had higher trajectories inside the country. These were equivalent to TRL and TRM layers. Low percentage values were seen at altitudes from 17 km, where at 19 km and 20 km (not shown in the table) the value was below 10%.

Table 5.3: Details of clusters at each altitude with their numbers, their total percentage and percentage travelled inside SA

Altitude (km)	Cluster number with associated percentage of trajectories	No of trajectories & percentage that only passed SA
8	Cluster 1 (29%)	4 (9%)
10	Cluster 1 (60%)	9 (36%)
12	Cluster 1 (22%)	8 (22.2%)
	Cluster 2 (6%)	2 (5.6%)
	Cluster 4 (11%)	2 (5.6%)
13	Cluster 1 (23%)	4 (10%)
	Cluster 3 (15%)	5 (12.5%)
14	Cluster 1 (25%)	5 (10.4%)
	Cluster 2 (27%)	7 (14.5%)
17	Cluster 2 (6%)	2 (4%)
	Cluster 3 (14%)	4 (8%)

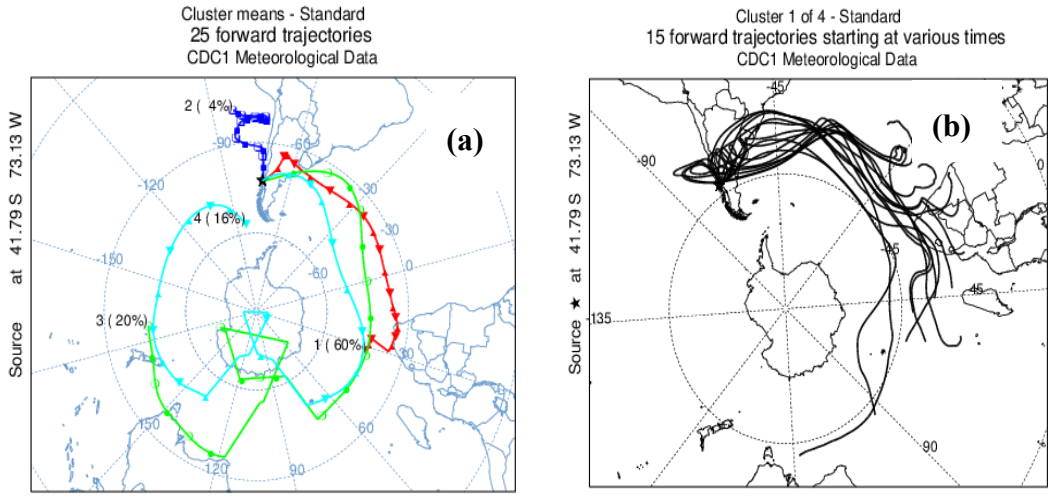

Figure 5.4: Clusters at 10 km (a) Cluster means at 10 km, (b) Cluster 1 at 10 km.

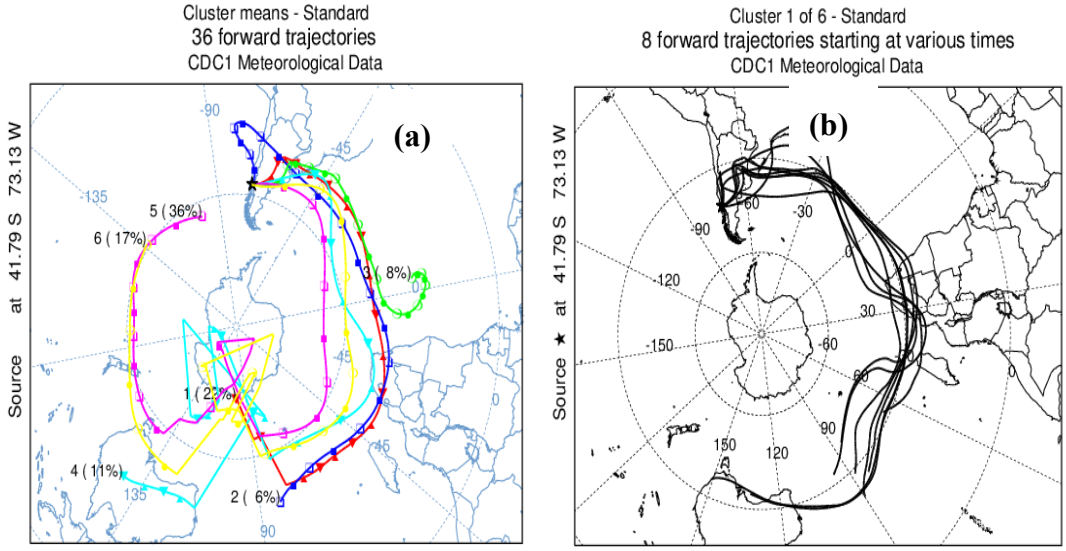

Figure 5.5: Clusters at 12 km (a) Cluster means at 12 km, (b) Cluster 1 at 12 km.

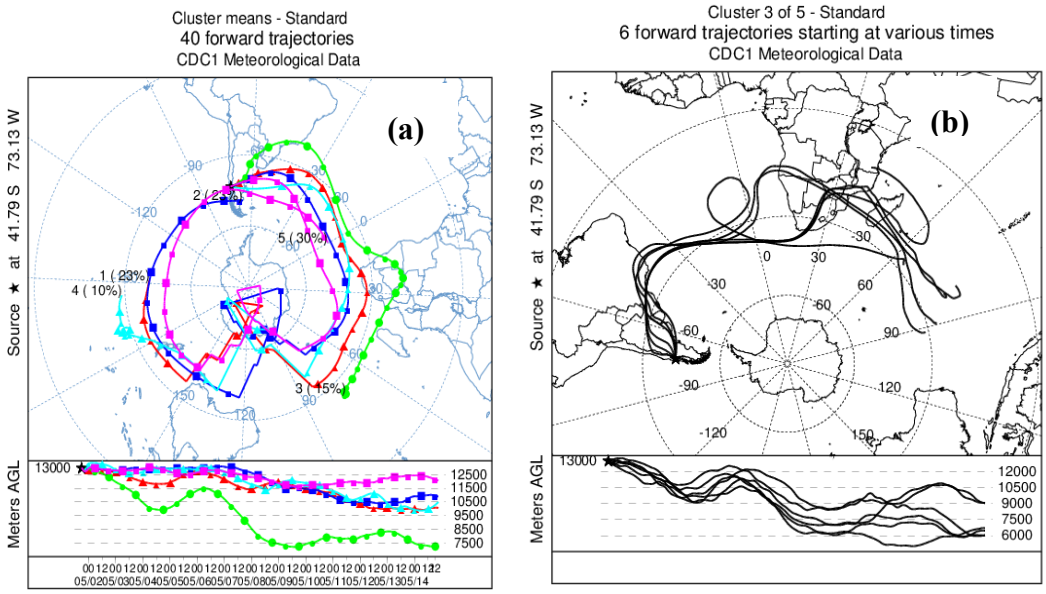

Figure 5.6: Clusters at 13 km (a) Cluster means at 13 km, (b) Cluster 3 at 13 km.

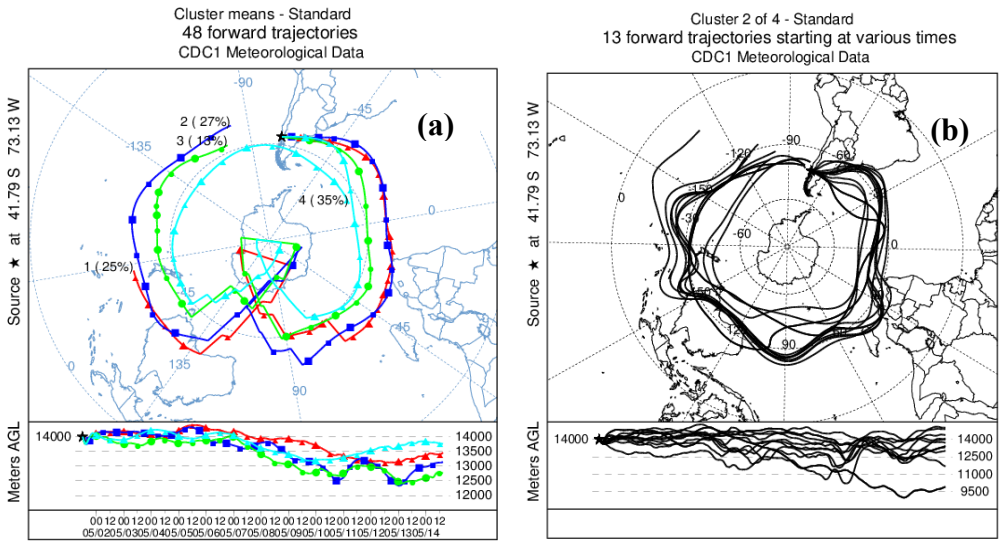

Figure 5.7: Clusters at 14 km (a) Cluster means at 14 km, (b) Cluster 2 at 14 km.

5.4.2 *OMI SO_2 observations*

Monthly mean variations for the year from 2014 to 2016 and for the four altitudes, were calculated using OMI daily SO_2 values. The results are discussed below:

The following figures show the SO_2 variations of PBL for each year (Figures 5.8 (a to c) TRL (Figure 5.9), TRM (Figure 5.10) and STL (Figure 5.11) for 2015. Analysis presented in these figures illustrates that the provinces North West, Gauteng, Limpopo and Mpumalanga were the most affected in May 2015 and Free State in April of the same year. Furthermore, in these locations during April and May 2015, there was a steep rise in SO_2 levels. This is particularly noticeable in May 2015 for all altitudes, however, the difference was observed only in the ranges as seen in Tables 5.4 and 5.5. Table 5.4 shows SO_2 values at various altitudes and their difference with that of SO_2 in PBL. Table 5.5 shows SO_2 values at specific altitudes in different years and their differences with that of their corresponding values in 2015 at the same altitudes. It can be seen from Table 5.4 that PBL had the highest columnar value during April and May 2015 and the difference between it and values for the other layers increases from TRL, TRM and STL, i.e., STL had the smallest SO_2 value. Table 5.5 further illustrates this effect. Here, PBL had the highest elevation in 2015 when compared to pre (2014) and post (2016) volcanic years. The measurement difference between the year was found to be ~ 2 DU. TRL had a moderate deviation of ~ 0.75 DU while TRM and STL the smallest deviations of ~ 0.2 DU. This observation has been previously reported in an OMI based study of seasonal vertical variation in SO_2 over South Africa, during a time period from 2004 to 2013. In this investigation, the SO_2 columnar amount for PBL, TRL, TRM and STL was 1 DU, 0.5 DU, 0.2 DU to 0.3 DU and 0.1DU to 0.2 DU respectively (Sangeetha et al., 2017b). This was lower than the values in 2015 for all altitudes. Therefore, through this analysis and together with previous work, it is shown that the rise in SO_2 columnar values can be directly attributed to the action of the Calbuco volcano with the PBL exhibiting the most significant impact.

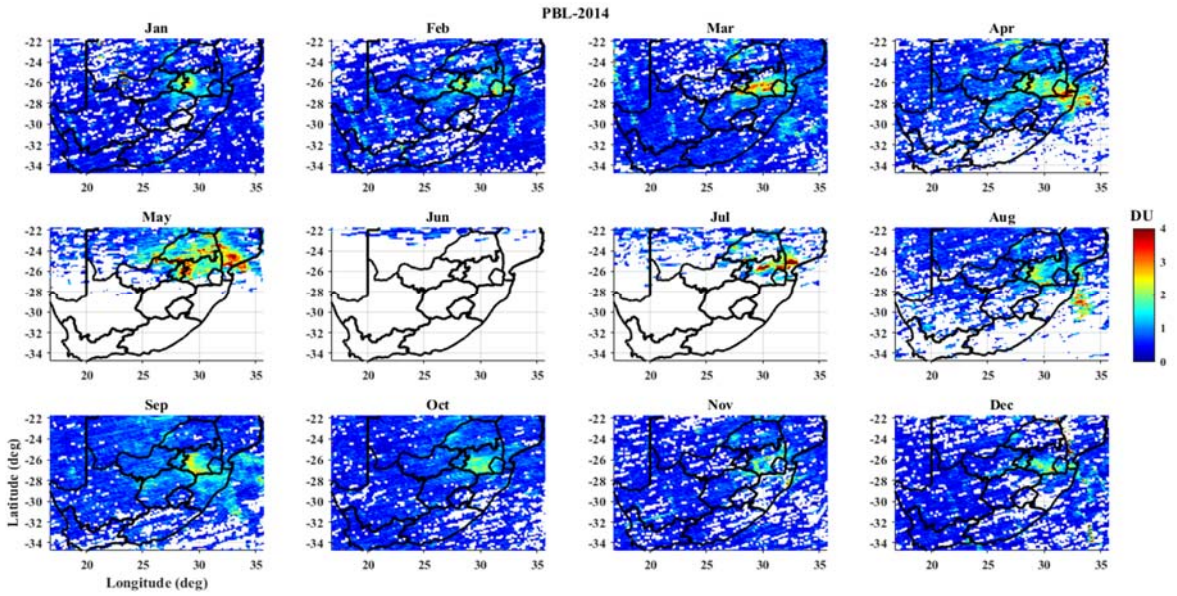

Figure 5.8a: OMI SO_2 variations over South Africa at PBL during 2014.

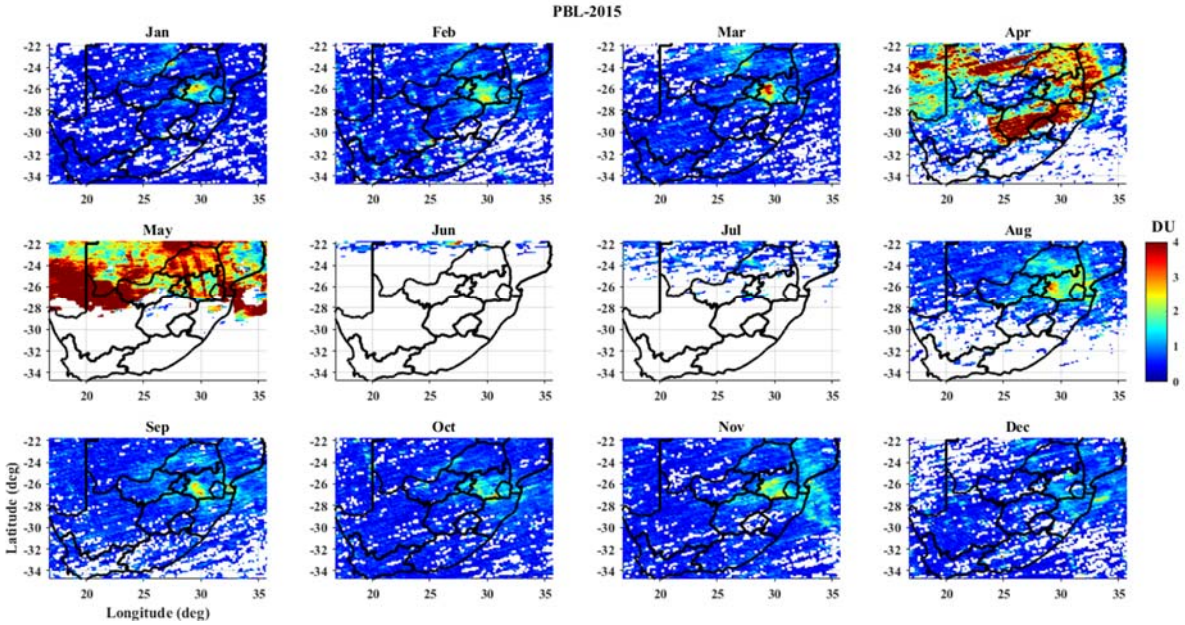

Figure 5.8b: OMI SO_2 variations over South Africa at PBL during 2015.

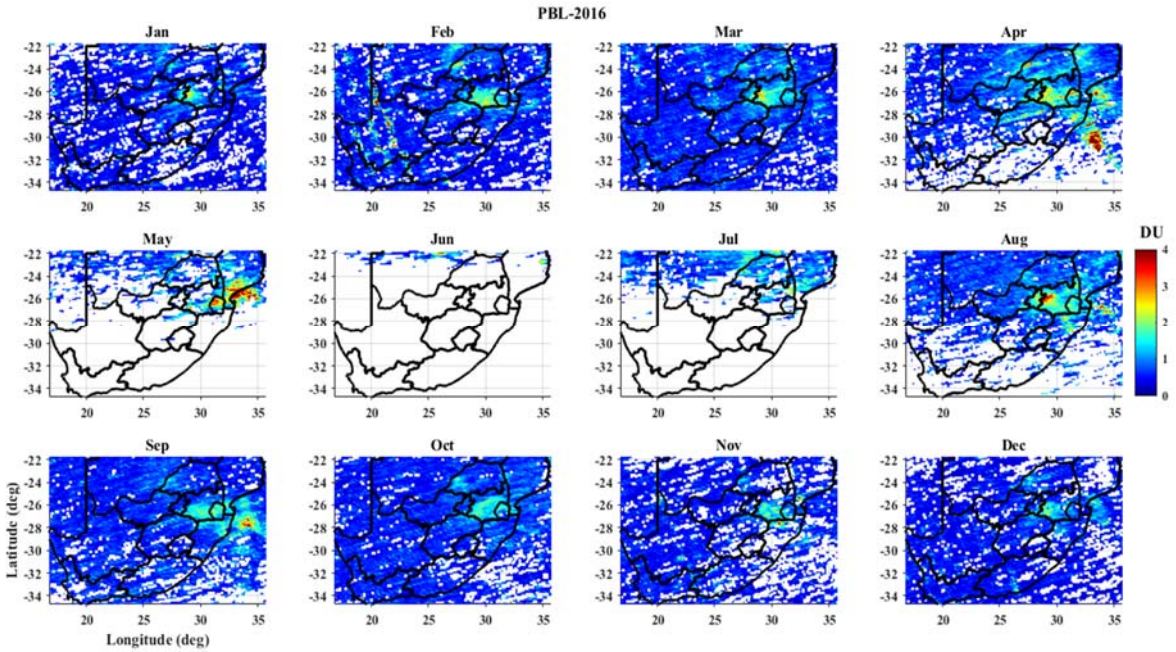

Figure 5.8c: OMI SO_2 variations over South Africa at PBL during 2016.

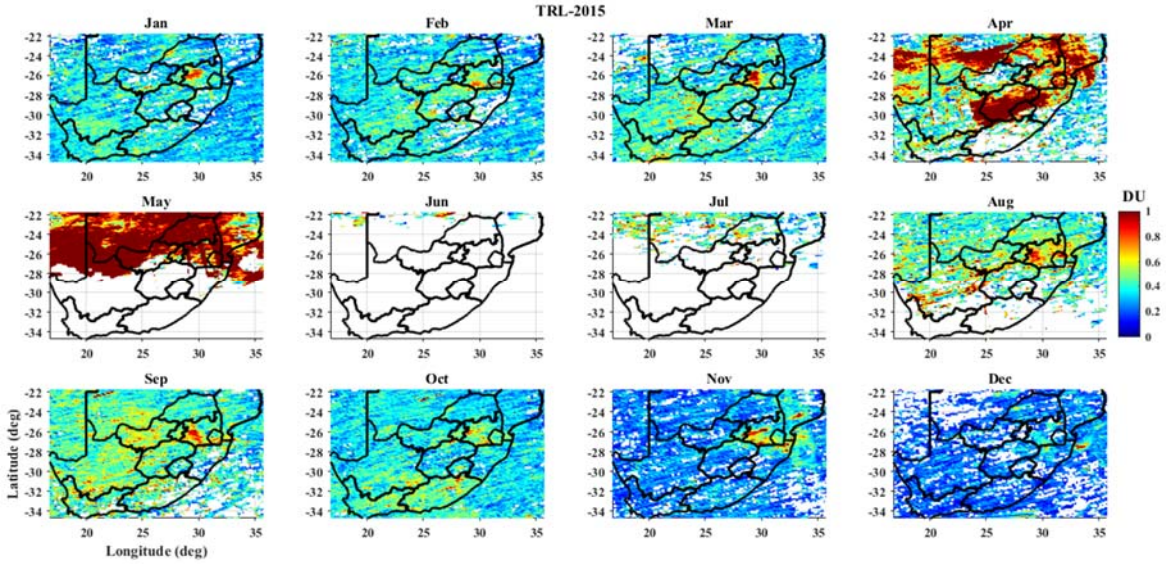

Figure 5.9: OMI SO_2 variations over South Africa at TRL during 2015.

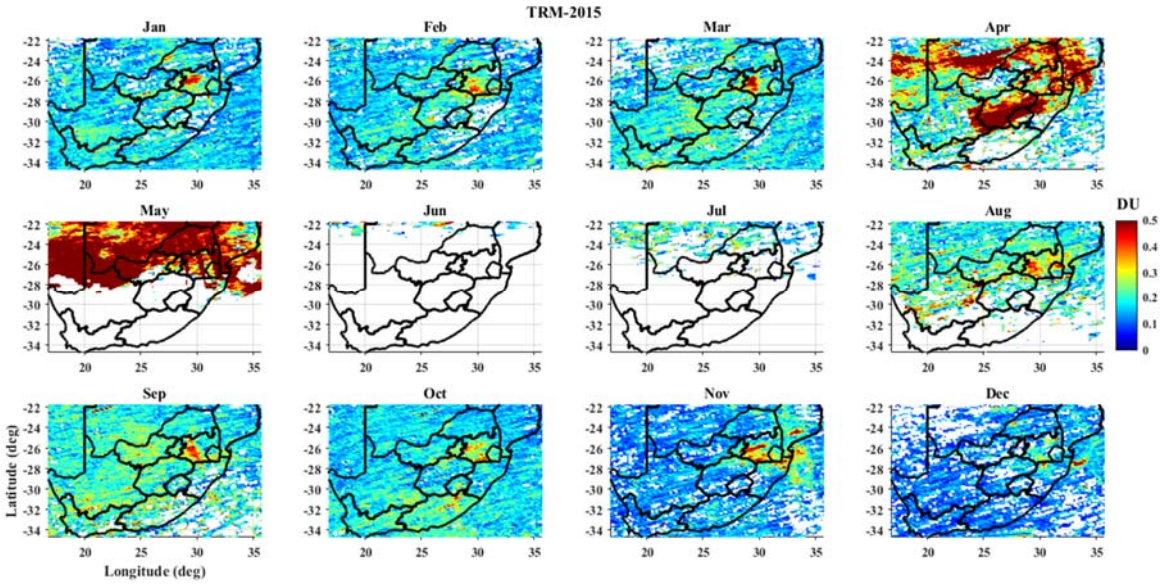

Figure 5.10: OMI SO_2 variations over South Africa at TRM during 2015.

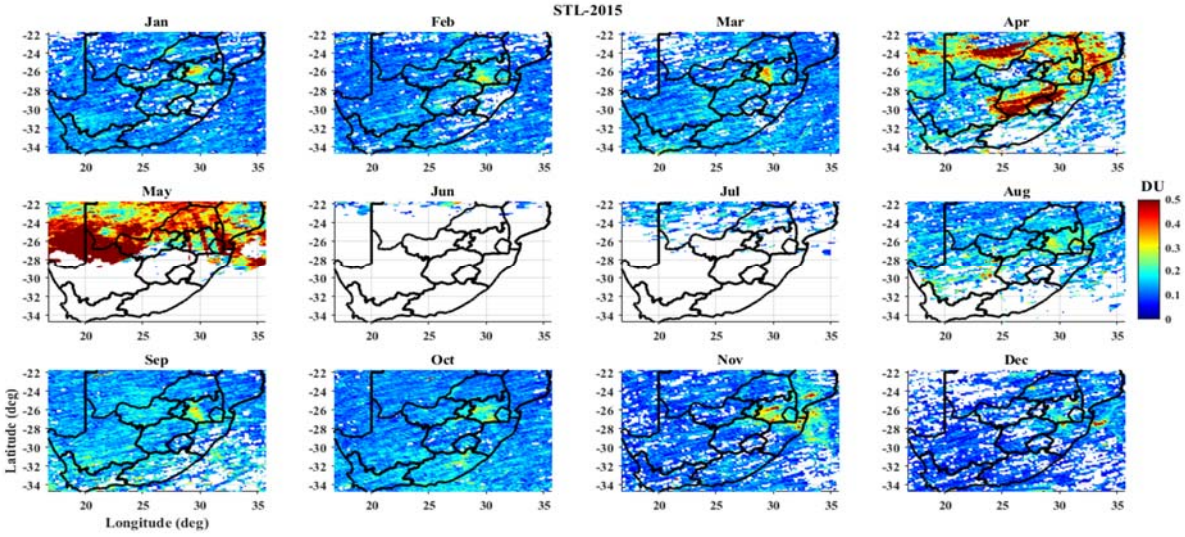

Figure 5.11: OMI SO_2 variations over South Africa at STL during 2015.

Table 5.4: SO_2 columnar values during April & May 2015 at various altitude levels over Calbuco volcano affected regions. Values in brackets indicate differences from PBL SO_2 values (Δ)

Altitude levels	SO_2 columnar values & differences (Δ) in DU
PBL	3
TRL	1 (2)
TRM	0.5 (2.5)
STL	0.2-0.5 (2.5-2.8)

Table 5.5: SO_2 columnar values at various years & altitude levels over Calbuco volcano affected regions. Values in brackets show the differences from their SO_2 values in 2015 (Δ)

Altitude levels	Years with SO_2 columnar values & differences (Δ) in DU		
	2014	2015	2016
PBL	1.5-2.5 (0.5-1.5)	3	~ 1 (2)
TRL	0.5 (0.5)	1	0.25 (0.75)
TRM	0.4 (0.1)	0.5	0.3-0.4 (0.1-0.2)
STL	0.1-0.2 (0.1-0.3)	0.2-0.5	0.1-0.2 (0.1-0.3)

5.4.3 *Ground Based measurements*

5.4.3.1 *Daily mean variations*

The daily mean variation for each group and their stations (figure not shown) proved that the stations in the North West group showed a well-marked increment in SO_2 values during April and May 2015, especially Damonsville and Phola stations. In a study conducted at Marikana in the North West province, it was found that daily mean SO_2 variations ranged between 0.1 ppbv and 20.8 ppbv (Venter et al., 2012). This is similar to results presented in this study for the stations at Damonsville and Phola. For the Vaal Triangle and Highveld groups, no clear rise in SO_2 values were seen as these stations usually have high peak values from autumn until to winter. However, the number of extreme values increased during April-May 2015 at stations such as Witbank.

The frequency plots based upon the daily mean variations for the years 2014, 2015 and 2016 are shown in Figure 5.12. It is noticed that Sharpeville, Sebokeng, Diepkloof, Zamdela and Rand Water showed an excessive number of high levels in 2015 when compared to those recorded in 2014 and 2016. Figures 5.12a, 5.12b, 5.12c show the frequency plots of Diepkloof, Sebokeng and Rand Water in 2014, 2015 and 2016. In Diepkloof during 2015, there were 116 values that ranged between 1.8 - 3.3 ppbv, however only 78 values were in the range 1.69- 2.9 ppbv in 2016. Similarly, in Sebokeng, there were 77 values in the range 1.7 - 3.07 ppbv and 73 values that ranged between 3.07 - 4.3 ppbv in 2015. Rand Water also showed slight elevations in 2015.

5.4.3.2 *Monthly mean variations*

In a similar manner to daily mean variations, monthly mean variations (Figure 5.13) showed a substantial rise in SO_2 values in the North West group especially in the stations of Phola, Mmabatho and Damonsville. An increment increase in SO_2 level was also seen in the Highveld group at the stations of Witbank, Middleburg and Hendrina. In order to quantify the increase in SO_2 levels in each month, a monthly mean difference between 2015 and 2014 (Figure 5.14 a), 2015 and 2016 (Figure 5.14 b) was calculated. It should be noted that monthly differences were calculated only for specific groups due to the limitation of non availability of monthly data for other groups.

.

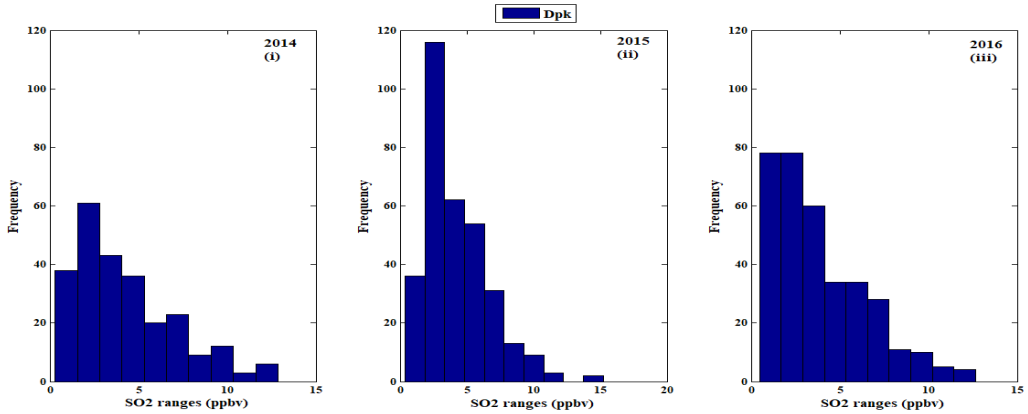

Figure 5.12a: Frequency plots of daily mean SO_2 values of Diepkloof in (i) 2014, (ii) 2015, (iii) 2016.

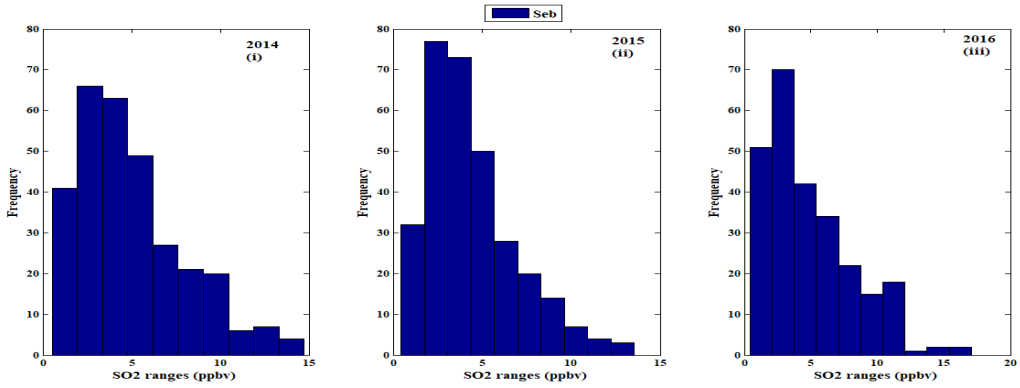

Figure 5.12b: Frequency plots of daily mean SO_2 values of Sebokeng in (i) 2014, (ii) 2015, (iii) 2016.

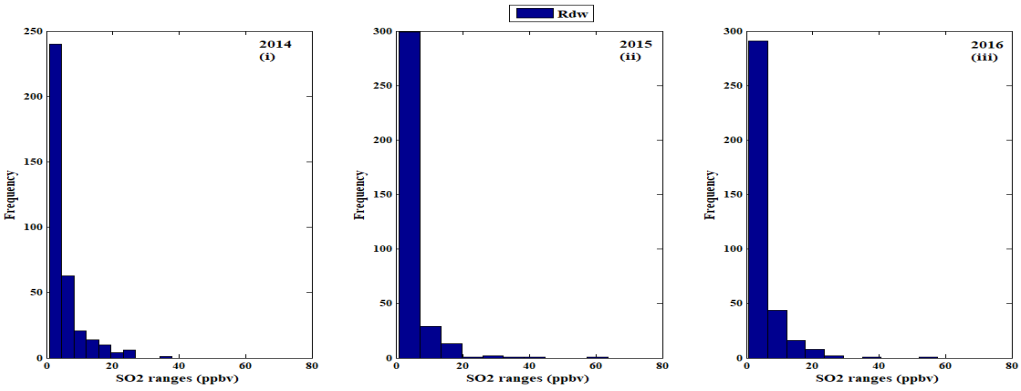

Figure 5.12c: Frequency plots of daily mean SO_2 values of Rand Water in (i) 2014, (ii) 2015, (iii) 2016.

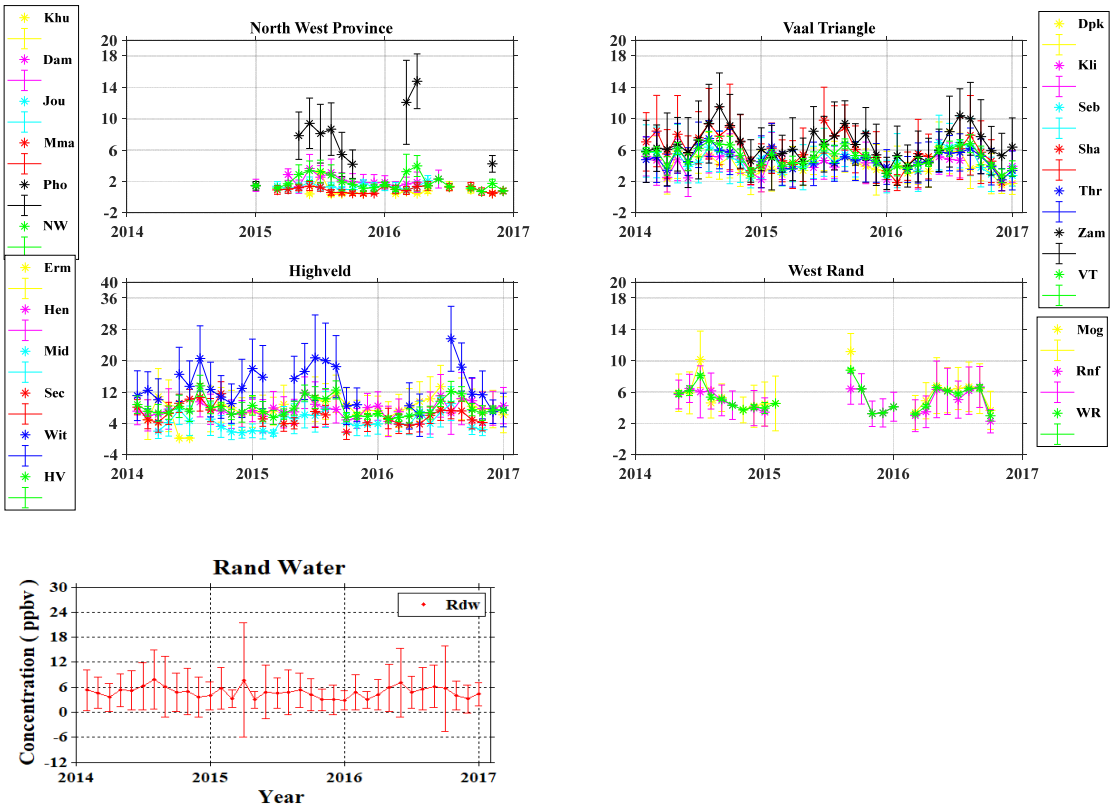

Figure 5.13: Monthly mean variations of each group and their respective stations.

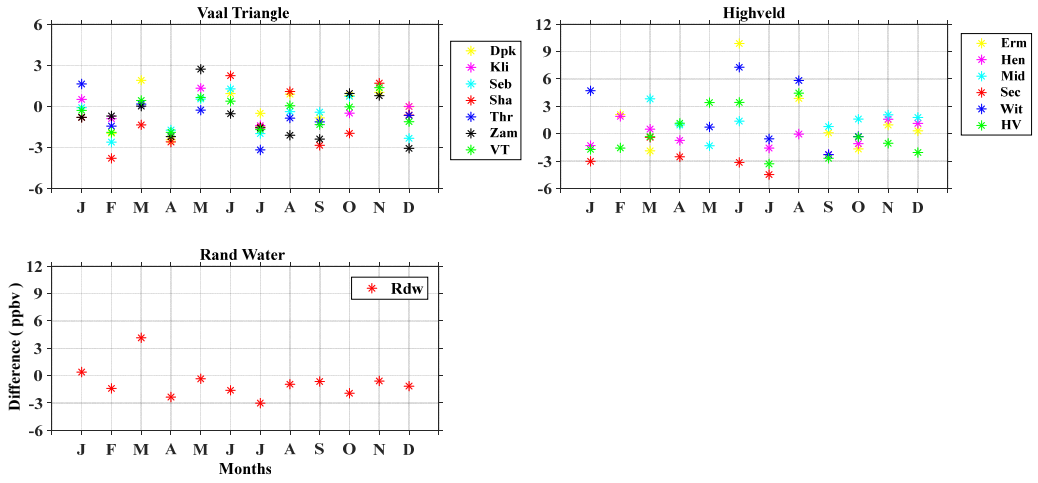

Figure 5.14a: Monthly mean differences between 2015 and 2014 for specific groups and their respective stations.

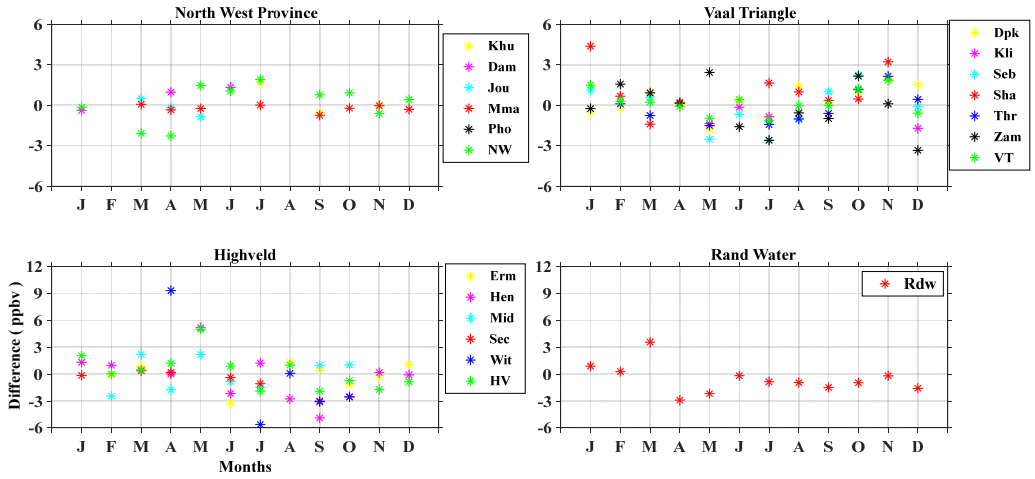

Figure 5.14b: Monthly mean differences between 2015 and 2016 for specific groups and their respective stations.

It can be inferred from the monthly mean differences, that Zamdela showed a difference of 2.5 ppbv in May for both 2014 and 2016. Sharpeville from the same Vaal Triangle group also showed a rise of 2.3 ppbv in June and 1.7 ppbv in July 2015, when compared to 2014 and 2016. There were also visible differences seen in the Highveld stations Hendrina, Ermelo, Witbank and Middleburg. Witbank had the highest difference of 9.3 ppbv in April 2016 and similarly in June and July 2014 of 7.3 ppbv and 5.8 ppbv. Middleburg had a variation of 4 ppbv in March 2014 and 3 ppbv in May 2016, while that of Hendrina was 5.18 ppbv in May 2016. Ermelo also showed a deviation of 3.8 ppbv in August 2014. The North West stations of Damonsville and Khuma reported a minor difference of ~ 1.5 ppbv in June and July.

5.4.3.3 *Yearly mean variations*

For the period from 2014 to 2016, overall yearly averages together with standard deviations were calculated and shown in Table 5.6. Witbank showed the highest elevation of about ~ 2 ppbv, where the SO_2 value was 14.7 ppbv in 2015. This value is significantly larger than that reported in a study on spatial and temporal variations of SO_2 in the Highveld region during August 2007- August 2008. In this work, the annual SO_2 average for Witbank was reported as 13.3 ppbv (Lourens et al., 2011). A further study by Laakso et al. (2012) conducted at Elandsfontein (situated in the Highveld region) found that the overall SO_2

average from 11 February 2009 to 31 January 2011 was 11.5 ppbv and ~10.68 ppbv from September 2005 to August 2007 (Josipovic et al., 2010). These values are comparatively smaller than the average values in the present study. Stations like Damonsville, Diepkloof, Sharpeville and Randfontein had comparatively high SO_2 values in 2015 than 2016. Mogale City and the average of the West Rand group showed high SO_2 levels of 1.5 ppbv to 2 ppbv in 2015 when compared with 2014 and 2016.

Table 5.6: Yearly average SO_2 (ppbv) together with standard deviation for each station and their respective groups. Highlighted in yellow colour represents the increased value during 2015, perhaps due to volcanic activities.

Stations \ Years	2014	2015	2016
Khuma	No Data	0.75 ± 0.86	0.76 ± 0.43
Damonsville	No Data	2.27 ± 1.35	1.87 ± 1.10
Jouberton	No Data	1.33 ± 0.60	1.37 ± 0.66
Mmabatho	No Data	0.85 ± 0.52	1.09 ± 0.57
Phokeng	No Data	6.55 ± 3.84	9.71 ± 5.76
North West Province	No Data	2.35 ± 1.38	2.96 ± 2.27
Diepkloof	4.30 ± 2.79	4.21 ± 2.40	3.91 ± 2.64
Kliprivier	4.17 ± 2.52	3.95 ± 2.11	4.22 ±2.24
Sebokeng	5.02 ± 3.0	4.42 ± 2.51	4.92 ± 3.29
Sharpeville	6.94± 4.14	6.06 ± 3.64	4.86 ± 3.73
Three Rivers	5.30 ± 2.93	4.62 ± 2.61	4.60 ±2.55
Zamdela	6.99 ± 4.24	6.48 ± 3.74	6.58 ±4.05
Vaal Triangle	5.44 ± 0.73	4.96 ± 0.68	4.85 ± 0.71
Ermelo	6.30 ± 5.63	8.43 ±4.59	8.55 ±5.20
Hendrina	7.86 ± 4.68	7.64 ± 4.35	8.01 ±5.09
Middleburg	3.70 ± 3.44	4.45 ±3.42	5.09± 3.64
Secunda	7.63 ± 3.61	4.70 ±2.80	5.48 ±2.68
Witbank	13.80 ±7.34	14.70 ± 8.50	12.35± 8.53
Highveld	7.8±1.60	7.98 ± 2.22	7.90 ± 2.22
Mogale City	5.76 ± 3.12	7.54 ± 4.38	5.36 ± 3.05
Randfontein	5.17 ± 2.42	4.70 ± 2.39	4.68 ± 2.91
West Rand	5.47 ± 0.49	6.12 ± 1.40	5.02 ± 0.10
Rand Water	5.15 ± 5.16	4.40 ± 5.70	4.89 ± 5.37

5.5 Conclusions

The main aim of this study was to verify that volcanic SO_2 plumes originating from the Calbuco volcano reached South Africa during the eruptive periods of 2015. To this end, forward trajectory analysis, clustering of trajectory analysis, OMI SO_2 maps and GB measurements over South Africa were employed. All these methods proved that volcanic plumes impacted South African locations during April and May 2015. In addition, it was shown that SO_2 levels increased at all altitude levels. The trajectory plots showed that maximum number of air parcels reaching the country occurred in the lower and mid tropospheric layers. However, OMI spatial maps illustrated that the largest increase in SO_2 level (corresponding to 2 DU) was confined to the PBL layer and occurred during April and May 2015. This rise in SO_2 level in the PBL can be attributed to volcanic activity apart from the ambient background due to accumulated anthropogenic SO_2 emissions. However, the upper layers such as TRM and STL showed minimal increase. This could be due to the interaction of SO_2 with volcanic aerosols to form a sulphate aerosol layer which acted as a sink for volcanic SO_2 at these altitudes. However, there was no appreciable increase in GB SO_2 measurements. Finally, the HYSPLIT trajectory analysis proved that air parcels entering South Africa were mostly at low and mid tropospheric altitudes and not at the surface. Based on this study, it can be therefore concluded that SO_2 plumes observed over South Africa during April and May 2015, originated from the Calbuco volcano and were mainly confined to the PBL layer and above.

5.6 References

Campion, R., 2014. New lava lake at Nyamuragira volcano revealed by combined ASTER and OMI SO2 measurements. *Geophysical Research Letters*, *41*(21), pg.7485-7492.

Carn, S.A., Krueger, A.J., Arellano, S., Krotkov, N.A. and Yang, K., 2008. Daily monitoring of Ecuadorian volcanic degassing from space. *Journal of Volcanology and Geothermal Research*, *176*(1), pg.141-150.

Carn, S.A., Clarisse, L. and Prata, A.J., 2016. Multi-decadal satellite measurements of global volcanic degassing. *Journal of Volcanology and Geothermal Research*, *311*, pg.99-134.

Clarisse, L., Coheur, P.F., Prata, A.J., Hurtmans, D., Razavi, A., Phulpin, T., Hadji-Lazaro, J. and Clerbaux, C., 2008. Tracking and quantifying volcanic SO 2 with IASI, the September 2007 eruption at Jebel at Tair. *Atmospheric Chemistry and Physics*, *8*(24), pg.7723-7734.

Corradini, S., Merucci, L., Prata, A.J. and Piscini, A., 2010. Volcanic ash and SO2 in the 2008 Kasatochi eruption: Retrievals comparison from different IR satellite sensors. *Journal of Geophysical Research: Atmospheres*, *115*(D2).

Draxler, R.R. and Hess, G.D., 1998. An overview of the HYSPLIT_4 modelling system for trajectories. *Australian meteorological magazine*, *47*(4), pg.295-308.

Fioletov, V.E., McLinden, C.A., Krotkov, N., Li, C., Joiner, J., Theys, N., Carn, S. and Moran, M.D., 2016. A global catalogue of large SO2 sources and emissions derived from the Ozone Monitoring Instrument. *Atmospheric Chemistry and Physics*, *16*(18), pg.1497-11519.

Fioletov, V.E., McLinden, C.A., Krotkov, N., Yang, K., Loyola, D.G., Valks, P., Theys, N., Van Roozendael, M., Nowlan, C.R., Chance, K. and Liu, X., 2013. Application of OMI, SCIAMACHY, and GOME-2 satellite SO2 retrievals for detection of large emission sources. *Journal of Geophysical Research: Atmospheres*, *118*(19), pg.11399-11418, doi:10.1002/jgrd.50826.

Guffanti, M., Casadevall, T.J. and Budding, K.E., 2010. *Encounters of aircraft with volcanic ash clouds: a compilation of known incidents, 1953-2009*. US Department of Interior, US Geological Survey.

Hayer, C., Carboni, E., Ventress, L., Povey, A. and Grainger, R., 2016. Satellite observations of the volcanic plume from the 23rd April 2015 eruption of Calbuco volcano. *EGU General Assembly*, Conference Abstracts, *18*, pg. 17035.

HYSPLIT Basic Tutorial Contents, Last Revised April 2017, Obtained from https://ready.arl.noaa.gov/documents/Tutorial/HYSPLIT_Tutorial.pdf (accessed on 17 July 2017).

Josipovic, M., Annegarn, H.J., Kneen, M.A., Pienaar, J.J. and Piketh, S.J., 2010. Concentrations, distributions and critical level exceedance assessment of SO_2, NO_2 and O_3 in South Africa. *Environmental monitoring and assessment*, *171*(1), pg.181-196.

Khokhar, M.F., Frankenberg, C., Van Roozendael, M., Beirle, S., Kühl, S., Richter, A., Platt, U. and Wagner, T., 2005. Satellite observations of atmospheric SO_2 from volcanic eruptions during the time-period of 1996–2002. *Advances in Space Research*, *36*(5), pg.879-887.

Krotkov, N.A., McLinden, C.A., Li, C., Lamsal, L.N., Celarier, E.A., Marchenko, S.V., Swartz, W.H., Bucsela, E.J., Joiner, J., Duncan, B.N. and Boersma, K.F., 2016. Aura OMI observations of regional SO 2 and NO 2 pollution changes from 2005 to 2015. *Atmospheric Chemistry and Physics*, *16*(7), pg.4605-4629.

Laakso, L., Vakkari, V., Virkkula, A., Laakso, H., Backman, J., Kulmala, M., Beukes, J.P., Van Zyl, P.G., Tiitta, P., Josipovic, M. and Pienaar, J.J., 2012. South African EUCAARI measurements: seasonal variation of trace gases and aerosol optical properties. *Atmospheric Chemistry and Physics*, *12*(4), pg.1847-1864.

Li, C., Joiner, J., Krotkov, N. A. and Bhartia, P. K., 2013. A fast and sensitive new satellite SO_2 retrieval algorithm based on principal component analysis: Application to the ozone monitoring instrument. *Geophysical Research Letters, 40*(23): 6314-6318. doi:10.1002/2013GL058134.

Lourens, A.S., Beukes, J.P., Van Zyl, P.G., Fourie, G.D., Burger, J.W., Pienaar J.J., Read C.E. and Jordaan J.H., 2011. Spatial and temporal assessment of gaseous pollutants in the Highveld of South Africa. *South African Journal of Science*, *107*(1-2), pg.1-8.

Prata, A.J., Carn, S.A., Stohl, A. and Kerkmann, J., 2007. Long range transport and fate of a stratospheric volcanic cloud from Soufriere Hills volcano, Montserrat. *Atmospheric Chemistry and Physics*, *7*(19), pg.5093-5103.

Prata, A.J., 2009. Satellite detection of hazardous volcanic clouds and the risk to global air traffic. *Natural hazards*, *51*(2), pg.303-324.

Prata, F., Bluth, G., Werner, C., Realmuto, V., Carn, S. and Watson, M., 2015. Remote sensing of gas emissions from volcanoes. In *Monitoring Volcanoes in the North Pacific* . Springer Berlin Heidelberg, pg. 145-186.

Rix, M., Valks, P., Hao, N., Van Geffen, J., Clerbaux, C., Clarisse, L., Coheur, P.F., Erbertseder, T., Zimmer, W. and Emmadi, S., 2009. Satellite monitoring of volcanic sulfur dioxide emissions for early warning of volcanic hazards. *IEEE Journal of Selected Topics in Applied Earth Observations and Remote Sensing*, *2*(3), pg.196-206.

Rolph, G., Stein, A. and Stunder, B., 2017. Real-time Environmental Applications and Display sYstem: READY. *Environmental Modelling and Software*, *95*, pg.210-228.

Sangeetha, S. K., Sivakumar, V., Josipovic, M., Gebreslasie, M. and Wright, C.Y., 2017a. SO_2 Climatology and Assessment of Ozone Monitoring Instrument (OMI) measurements at Sharpeville (27.86°E; 26.68°S) a South African ground-based station. *International Journal of Remote Sensing*, *38:23, 6680-6696.*

Sangeetha, S.K., Sivakumar, V., Gebraslasie, M. and Wright, C.Y., 2017b. Seasonal vertical variation in SO2 over South Africa as observed by the Ozone Monitoring Instrument (OMI), *Proc. of 33nd Annual conference of South African society for atmosphere science, Protea Hotel Ranch Resort, Polokwane, (South Africa), ISBN* 978-0-620-77401-7, *pg. 82-85, 21-22 September 2017.*

Sangeetha, S. K. and Gebreslasie, M., 2018. Long-term Temporal and Spatial analysis of SO2 over Gauteng and Mpumalanga monitoring sites of South Africa, *International Journal of Environment and Pollution*, (to be submitted).

Stoiber, R.E., Williams, S.N. and Huebert, B., 1987. Annual contribution of sulfur dioxide to the atmosphere by volcanoes. *Journal of Volcanology and Geothermal Research*, *33*(1-3), pg.1-8.

Theys, N., Campion, R., Clarisse, L., van Gent, J., Dils, B., Corradini, S., Merucci, L., Coheur, P.F., Van Roozendael, M., Hurtmans, D. and Clerbaux, C., 2013. Volcanic SO2 fluxes derived from satellite data: a survey using OMI, GOME-2, IASI and MODIS. *Atmospheric Chemistry and Physics (ACP)*, *13*, pg.5945-5968.

Venter, A.D., Vakkari, V., Beukes, J.P., Van Zyl, P.G., Laakso, H., Mabaso, D., Tiitta, P., Josipovic, M., Kulmala, M., Pienaar, J.J. and Laakso, L., 2012. An air quality assessment in the industrialised western Bushveld Igneous Complex, South Africa. *South African Journal of Science*, *108*(9-10), pg.1-10.

Volcano Discovery. Obtained from https://www.volcanodiscovery.com/calbuco/news/22april2015/major-eruption.html. (accessed on 22 september 2017).

Chapter 6

Summary and Future perspectives

6.1 Summary

In this work, the first part of the study was focused on SO_2 seasonal and/or climatological variations by utilizing Ozone Monitoring Instrument (OMI) measurements from a satellite-derived spectrometer in conjunction with ground-based measurements. They both differed in measurement techniques: the former derived the columnar amounts and the latter gave SO_2 levels only at the surface. Thus, the first step was to perform a comparative analysis between them by converting the columnar values from OMI into volume mixing ratios by applying the pressure difference at the surface and boundary layer and to study their interrelationship in different seasons and years. For this purpose, a study area, namely Sharpeville in Gauteng, was chosen for its long-term GB data availability and its primary location around an industrialized zone. It was found that OMI overestimated GB measurements; however, there were some significant correlation coefficients regardless of various time scales and particularly in winter. Both OMI and GB measurements tended to increase from autumn until late winter, after which their SO_2 values decreased. OMI showed raised SO_2 levels in summer when compared to that of GB values.

The second part of the study considered SO_2 climatology during the years 2004 to 2013 at 36 monitoring stations in Gauteng and Mpumalanga provinces of South Africa, where the industrialized hot spot regions are located. The stations were grouped into eight different groups and their respective temporal variations were analysed. In addition, an ordinary kriging-based approach was performed to study the spatial distributions of SO_2 over the selected GB stations. It was observed that Pretoria West, Witbank and Rand Water stations had high SO_2 levels and standard deviations. Most of the stations had peak SO_2 values in winter, on the other hand in spring, SO_2 values of Witbank and Pretoria west were lower. All of the groups except for the Mpumalanga power (MP) stations group followed a well-marked seasonal variation. This was particularly evident in the Vaal Triangle group. The MP group followed by the Highveld group showed the highest SO_2 values in all of the time scales analysed. The spatial analysis based on the kriging

approach further showed that extreme SO_2 levels were concentrated around major industrial zones of Mpumalanga regardless of the season.

The last part of the study was focused on the long-range transport of SO_2 over South Africa resulting from Calbuco volcanic eruptions, which occurred in 22 April 2015. A case study was carried to identify the increase in SO_2 over South Africa using data from both GB stations and satellite instruments (OMI). The data for the period from 2014 to 2016, i.e., the year before and after the volcanic eruptions were considered. The study illustrated an increase in SO_2 over South Africa during the year of volcanic eruptions based on both GB and satellite data. There is an indication, post-eruptions, of about ~20 % increase in the SO_2 from the previous year (2014). This study was carried out to explain the origin and/or contribution using the Hybrid Single Particle Lagrangian Integrated Trajectory (HYSPLIT) model forward trajectory and revealed air masses leaving Calbuco at a height of 12 000 m and travelling over SA on 28 April 2015 at a height of 8 000 m. However, the study concluded that there were no significant increase in SO_2, which were noticed in the ground or surface level measurements. An increased level of SO_2 were clearly seen at the height PBL and above (TRL, TRM and STL) based on OMI satellite observations.

6.2 Future Perspectives

The present research have addressed only on SO_2 measurements using OMI satellite (mainly). However, in order to understand the air quality of South Africa in depth, the other pollutants such as aerosols ($PM_{2.5}$ and PM_{10}), O_3, CO, CO_2 and NO_2 besides SO_2 need to be emphasised. Therefore, the future work will be focused on the above pollutants employing GB measurements (AERONET, SAAQIS data sets) and satellite-based instruments namely MISR, MODIS, TES, CALIPSO, OMI and other upcoming instruments like TROPOMI. Secondly, if possible the influence of meteorological parameters (PBL height, wind, humidity, pressure, surface temperature) on the satellite measurements and modelling the air quality and health based study are some of the key factors that are aimed for the future research work.